United States
Department of
Agriculture

Agricultural
Research
Service

Channel & Watershed Processes Research Unit
National Sedimentation Laboratory
Oxford, Mississippi 38655

Studies in Suspended Sediment and Turbulence in Open Channel Flows

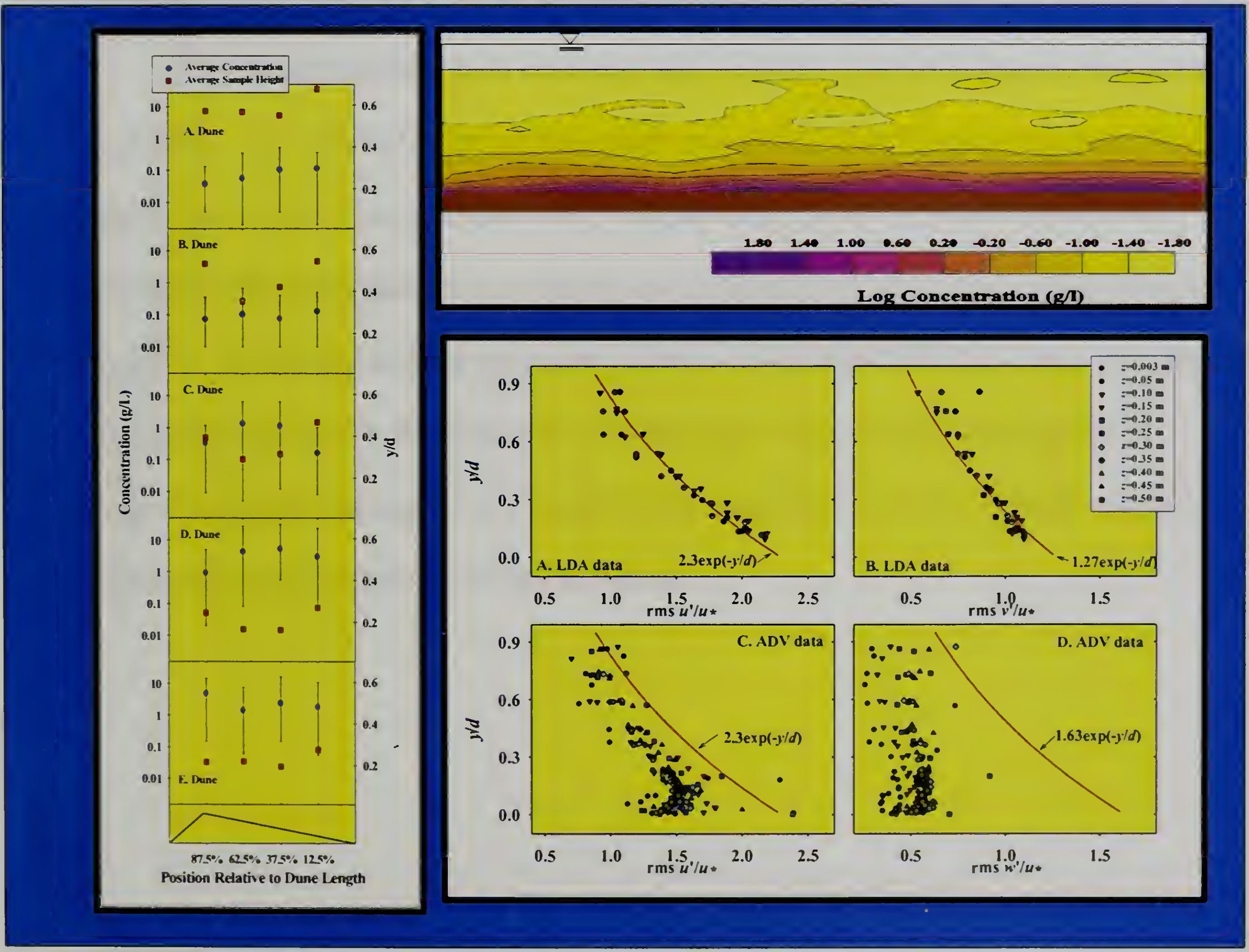

Daniel G. Wren, Sean J. Bennett, Brian D. Barkdoll, and Roger A. Kuhnle

Research Report No. 18

December 2000

NOTE

This report represents the completed Ph.D. thesis of Daniel G. Wren for the Department of Civil Engineering, University of Mississippi. His research was directed by Sean J. Bennett and Roger A. Kuhnle, USDA-ARS, and Brian D. Barkdoll, University of Mississippi. The thesis is reproduced herein.

ACKNOWLEDGMENTS

My family provided both emotional and monetary support during my time at the university. My father provided innumerable motivational talks that never failed to help me move on when I was disillusioned. Sean Bennett provided extensive advice and support in the preparation of experiments and in the analysis and organized reporting of results. I would like to thank my major professor, Brian Barkdoll for his help and support throughout my time at the University of Mississippi. Roger Kuhnle also provided valuable support and expertise. I would like to thank my committee members for their assistance in the preparation of this document.

ABSTRACT

The measurement of suspended-sediment concentrations, the study of the variability of concentration, quantification of lateral mixing in sediment-laden flows, and the effect of suspended sediment on turbulence are important areas in the study of river hydraulics. Suspended-sediment load is a key indicator for assessing the effect of land-use changes and engineering practices in watercourses. In this dissertation, methods for measuring suspended-sediment concentration are reviewed in detail, resulting in the conclusion that acoustic techniques are the most in need of further use and development. The variability of time series of suspended-sediment concentration data taken at a single point and taken simultaneously at two laterally separated positions in both dune and upper-stage plane beds is examined. Concentration was found to vary greatly in both conditions, with no correlation between simultaneous samples. A new method for calculating the transverse diffusion coefficient using turbulent velocity fluctuations and transverse velocity gradients in a sediment-laden flow is described, with results comparable to those measured in natural rivers and in previous flume studies. Velocity profiles, turbulence intensities, and suspended-sediment concentrations obtained in supercritical conditions in a sediment-laden flow were compared to theory. Velocity profiles showed good agreement with the law of the wall, the magnitude of turbulence intensities was found to depend on the measurement technique, and the Rouse equation was modified to better-fit concentration profiles over flat, mobile beds. Throughout this work, sediment refers to non-cohesive particles in the sand-size fraction, 0.062-2 mm.

TABLE OF CONTENTS

CHAPTER PAGE

LIST OF TABLES

LIST OF FIGURES

FIGURE PAGE

LIST OF SYMBOLS AND ABBREVIATIONS

Reference depth	a
y intercept of regression line	b
Acoustic Doppler Velocimeter	ADV
Suspended-sediment concentration	C
Reference concentration	C_a
Coefficient of Variation	CV
Grain Size	D
Water depth	d
Darcy-Weisbach friction factor	f
Froude number	Fr
Acceleration of gravity	g
Hertz	Hz
Dispersion coefficient	k
Equivalent sand roughness	k_s
Laser Doppler Anemometer	LDA
Mixing length	l
Prandtl's mixing length	L_m
Slope of regression line	m
Total number of observations	n
Optical Backscatter	OBS

Probability of incorrect assumption of association between variables	P
Pascal	Pa
Discharge	Q
Exponent in Rouse equation	r
Pearson Product Moment Correlation coefficient	R
Reynolds number	Re
Root mean square downstream instantaneous variation	rms u'
Root mean square vertical instantaneous variation	rms v'
Root mean square cross stream instantaneous variation	rms w'
Water surface slope	S
Standard deviation	s_x
Total Maximum Daily Load	TMDL
Depth-integrated flow velocity	U
Mean flow velocity	$\bar{u}$
Shear velocity	u_*
Turbulent velocity fluctuations in the x direction	u'
Instantaneous downstream velocity	u_i
Upper-Stage Plane Bed	USPB
Turbulent velocity fluctuations in the y direction	v'
Particle fall velocity	w_s
Individual measurement	X
Mean of measurements	$\bar{X}$

Mean cross-stream velocity	$\overline{w}$
Longitudinal distance	x
Vertical distance	y
Transverse distance	z
Mass momentum transfer constant	β
Velocity defect height	δ
Sediment transfer coefficient	ε_s
Vertical diffusivity	ε_y
Transverse diffusion coefficient	ε_z
Eddy viscosity	η
Von Karman Coefficient	κ
Dynamic viscosity	μ
Lateral variance of concentration	σ_z^2
Fluid density	ρ
Mean boundary shear stress	τ_0

CHAPTER I

INTRODUCTION

Proper management of water resources requires knowledge of sediment load and yield. This is a significant problem, particularly when one considers that worldwide sediment yield has been estimated at 20 billion tons per year (Holeman, 1968). There are many situations that require measurement of sediment concentration and particle size. Various industries require large amounts of sediment free water. The planning of hydraulic structures such as dams, canals, etc. is practically impossible without sediment data. Sediment free streams and reservoirs are highly valued for recreation. Sediment deposition in stream or river channels can cause flooding. The movement of contaminants such as radionuclides and pesticides that are often sorbed to sediments can be measured with knowledge of sediment movement. Rates of erosion and the impact of land use on drainage basins can also be estimated (Edwards and Glysson, 1999; Vanoni, 1975).

The movement of sediment is inextricably linked with the turbulence associated with natural flows. Many studies have been dedicated to determining the mechanisms for turbulent suspension of sediments (Clifford et al., 1993; Ashworth et al., 1996; and Nezu and Nakagawa, 1993, among others). The study of sediment movement is not possible without considering the effects of fluid turbulence.

Throughout this work, sediment refers to non-cohesive particles in the sand-size fraction, 0.062-2 mm. Smaller particles are defined as fines, and are generally distributed

homogeneously with depth, greatly lowering the difficulty of measuring their concentration. This work focuses on the behavior and sampling of sand-sized particles because they are more difficult to measure and model. Larger particles than sand will move mainly as bed load, particularly in lowland streams and rivers. In this work, fines and bed load are not considered.

The following chapters each examine topics related to the movement of sediments and the effects of turbulence. Chapter II is a detailed literature review of methods that can be used to measure suspended-sediment concentration in fluvial systems. Chapter III examines the variability of suspended-sediment concentrations over upper-stage plane and dune beds. Chapter IV describes a method for determining the transverse dispersion coefficient in the presence of large sediment concentrations using turbulence data. Chapter V examines vertical profiles of velocity, turbulence intensity, and suspended-sediment concentration in a supercritical flow over a flat, sand bed. Each chapter stands alone as a separate piece of work with its own introductory material, experimental setup, results and conclusions. A small amount of material is repeated in chapters that share equations or come from the same experiments. This repetition aids the reader since pertinent information is all in one place. Chapter VI provides a short summary of the overall conclusions from this work and concludes the dissertation, and Chapter VII lists future work that could expand on the results reported here.

CHAPTER II

FIELD TECHNIQUES FOR SUSPENDED-SEDIMENT MEASUREMENT

Introduction

The present work provides an in-depth comparison of existing suspended-sediment measurement techniques and aims to aid the practitioner and researcher in the selection and use of suspended-sediment measurement equipment. There is considerable difficulty and expense in sediment measurement. Some of the expense is due to the fact that streams carry more than 50% of their total sediment transport during flood events (Nelson & Benedict, 1950). Since these large flows often occur at night and are hard to predict, it is difficult to obtain sediment samples unless some type of automated measurement system is used. Even under good conditions, however, the time and labor inherent in sediment sampling add to its expense. In addition, traditional forms of sediment measurement where sediment samples are taken in the field and analyzed in a laboratory may accumulate errors in sampling and computation as large as 20% (McHenry et al., 1967). These ex-situ techniques also modify the particle size distribution since aggregates are often broken up in sample collection and handling. The importance of measuring particle sizes for fine sediments without disturbing aggregates has been emphasized by other researchers (Walling and Moorhead, 1989; Droppo and Ongley, 1992 & 1994; Walling and Woodward, 1993; Woodward & Walling, 1992). On the other hand, allowing the particles to settle may allow the creation of more aggregates than existed in the original sample. Phillips and Walling (1995a) found that settling for one hour followed by resuspension may cause increases in volume mean particle size of

up to 24%. Based on their findings, they recommended that suspended-sediment measurements for fines be made in-situ.

Suspended fine sediment (<0.062 mm) in streams tends to be well mixed across the cross section and usually does not show sudden large fluctuations with time. Sand transport, however, does show large fluctuations with time (Figure 2.1) and space (Figure 2.2). For 16 sites in five states Burkham (1985) found that coefficients of variation (*CV*= standard deviation/cross sectional mean) for high sand concentrations were as high as 70 percent. This value of the *CV* should not be taken as error in the sampling techniques, but most likely resulted from the variability of the processes of sand transport in streams and rivers. Willis and Bolton (1979) found under steady uniform flow in a laboratory flume with 0.5-mm sand, that the *CV* for sand concentration data was 62 percent on average over a range of flows. Also Kuhnle and Willis (1998) found that *CV* values of sand transport were approximately 100% for data from the Goodwin Creek Watershed in northern Mississippi. An appreciation of the variability associated with the transport processes of suspended sediment needs to be maintained to distinguish between the natural variability of sediment transport and measurement errors.

Ideally, researchers would like to be able to measure the suspended-sediment concentration and size distribution at all points in a given river or stream. The second best procedure would be to measure at all points in a cross section. The third and fourth ranked possibilities are measuring along one vertical or measuring at one point, respectively. Each time the procedure includes a smaller portion of the river or stream, spatial error is introduced. The progression of temporal error can be described in much

the same way as spatial error with sampling at one instant introducing the greatest degree of error. Sediment discharge error results from a combination of spatial and temporal error. Throughout this work, the degree of temporal and spatial error are two criteria used to evaluate suspended-sediment measurement techniques.

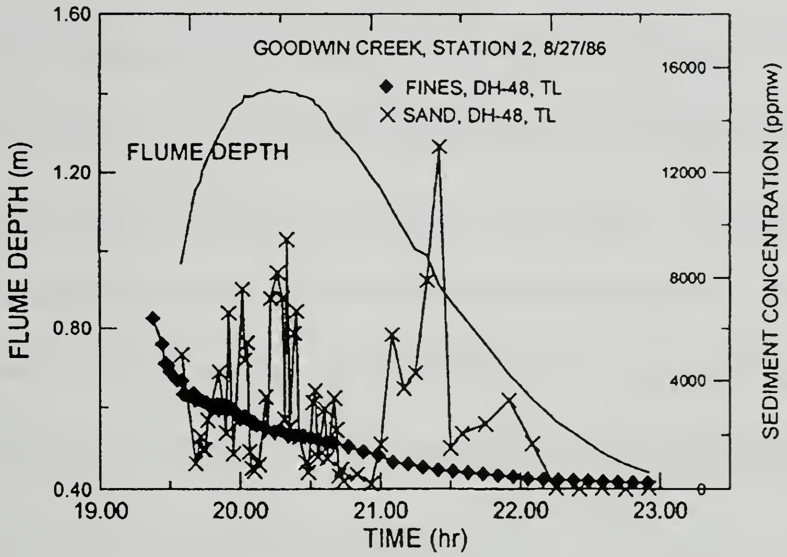

Figure 2.1. Temporal fluctuations in suspended-sediment in Goodwin Creek Watershed in northern Mississippi (ppmw=Parts per Million per Weight).

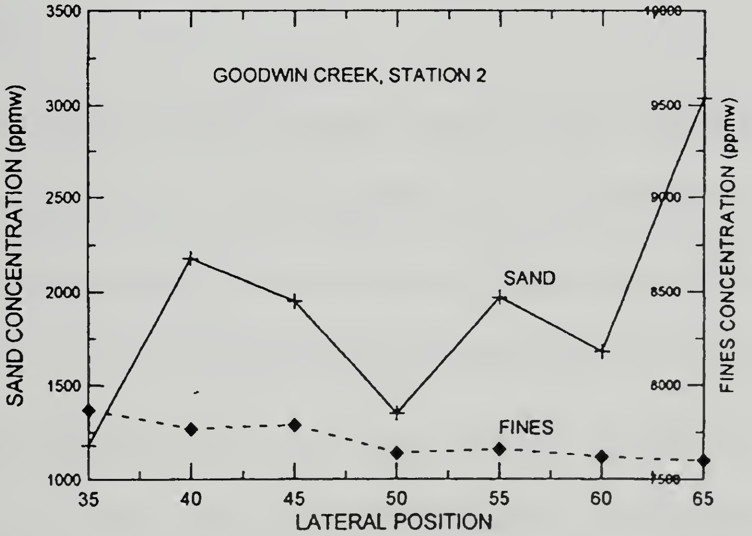

Figure 2.2. Spatial fluctuations in suspended-sediment in Goodwin Creek Watershed northern Mississippi (ppmw=Parts per Million per Weight).

Suspended-sediment Measurement Techniques

The following sections describe methods for measuring suspended-sediment concentration, and in some cases, particle-size distribution. The operating principles, advantages, and disadvantages of the techniques are described. Table 1 contains a summary of this information. References for the summary material in Table 1 may be found in the text of the work. Some methods are covered in more detail than others. In particular, the acoustic method is given more attention because, with further development, it has great potential. More information is presented on instrumented techniques because of their more recent development. Here, instrumented refers to techniques that log data in real time. Of the techniques covered, only pump sampling and bottle sampling are not instrumented techniques.

Acoustic Methods

Operating Principle

Short bursts (≈10μs) of high frequency sound (1-5 MHz) emitted from a transducer are directed towards the measurement volume. Sediment in suspension will direct a portion of this sound back to the transducer (Thorne et al., 1991) (Figure 2.3). When the sediment is of uniform size, the strength of the backscattered signal allows the calculation of sediment concentration. The water column is sampled in discrete increments based on the return time of the echo (Figure 2.4). The backscattered strength is dependent on particle size as well as concentration. This can be exploited by using multiple frequencies for the investigation of both particle size

Table 2.1. Suspended-sediment Measurement Techniques

Technology	Operating Principle	Advantages	Disadvantages
Acoustic	Sound backscattered from sediment is used to determine size distribution and concentration.	good spatial and temporal resolution, measures over wide vertical range, non-intrusive	backscattered acoustic signal is difficult to translate, signal attenuation at high particle concentration
Bottle Sampling	A water-sediment sample is taken isokinetically by submerging a container in the stream flow and later analyzed.	accepted, time-tested technique, allows determination of concentration and size distribution, most other techniques are calibrated against bottle samplers	poor temporal resolution, flow intrusive, requires laboratory analysis to extract data, requires on-site personnel
Pump Sampling	A water-sediment sample is pumped from the stream and later analyzed.	accepted, time-tested technique, allows determination of concentration and size distribution	poor temporal resolution, intrusive, requires laboratory analysis, does not usually sample isokinetically
Focused Beam Reflectance	The time of reflection of a laser incident on sediment particles is measured.	no particle size dependency, wide particle size and concentration measuring range	expensive, flow intrusive, point measurement only
Laser Diffraction	The refraction angle of a laser incident on sediment particles is measured.	no particle size dependency	unreliable, expensive, flow intrusive, point measurement only, limited particle size range
Nuclear	The backscatter or transmission of gamma or x-rays through water-sediment samples is measured.	low power consumption, wide particle size and concentration measuring range	low sensitivity, radioactive source decay, regulations, flow intrusive, point measurement only
Optical	The backscatter or transmission of visible or infrared light through water-sediment sample is measured.	simple, good temporal resolution, allows remote deployment and data logging, relatively inexpensive	exhibits strong particle size dependency, flow intrusive, point measurement only, instrument fouling
Remote Spectral Reflectance	Light reflected and scattered from a body of water is remotely measured.	able to measure over broad areas	poor resolution, poor applicability in fluvial environment, particle size dependency

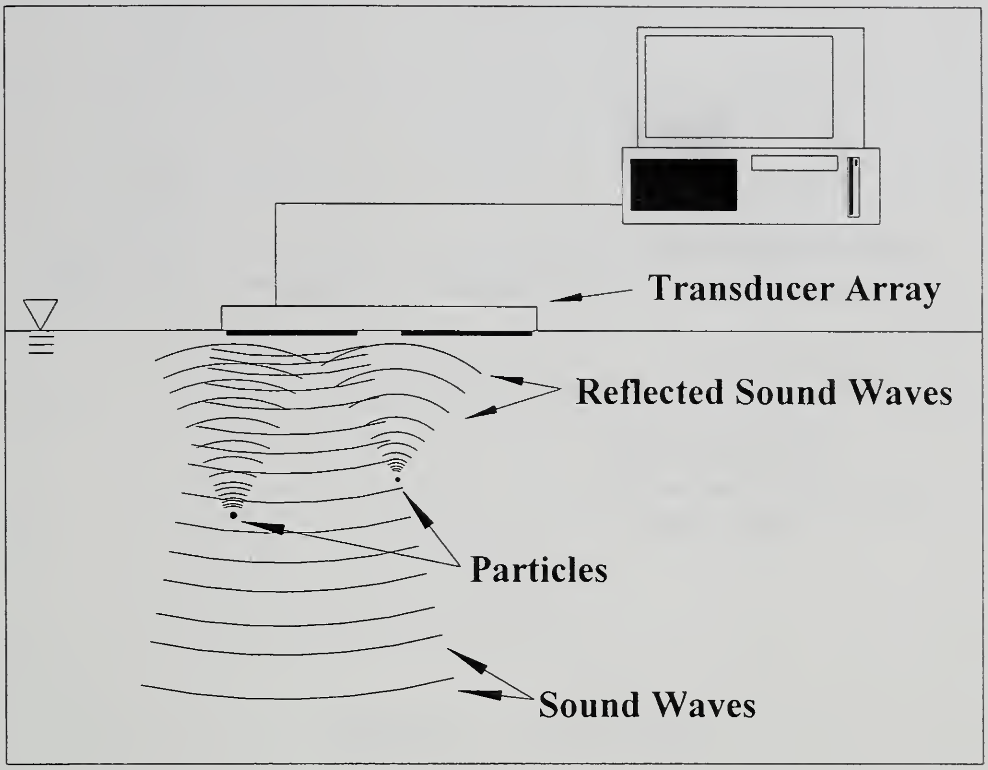

Figure 2.3. Acoustic backscatter.

(Crawford and Hay, 1993) and concentration. Various authors have presented techniques for converting backscatter data into sediment concentration and size distribution. At the high frequencies generally employed, backscatter devices have a range of 1-2 m due to water and sediment attenuation of the signal and the desire for high resolution measurements (Downing et al., 1995). Measurements in water depths greater than 2 m may be taken by submerging the transducer(s) to the desired depth. The validity of the acoustic approach has been established by several researchers (Thorne et al., 1991, 1992 1993, 1994, and 1995; Schat, 1997; Crawford and Hay, 1993; and others). Improvement of the acoustic method has also been encouraged (Van Rijn, 1993, Van Rijn and Schaafsma, 1986).

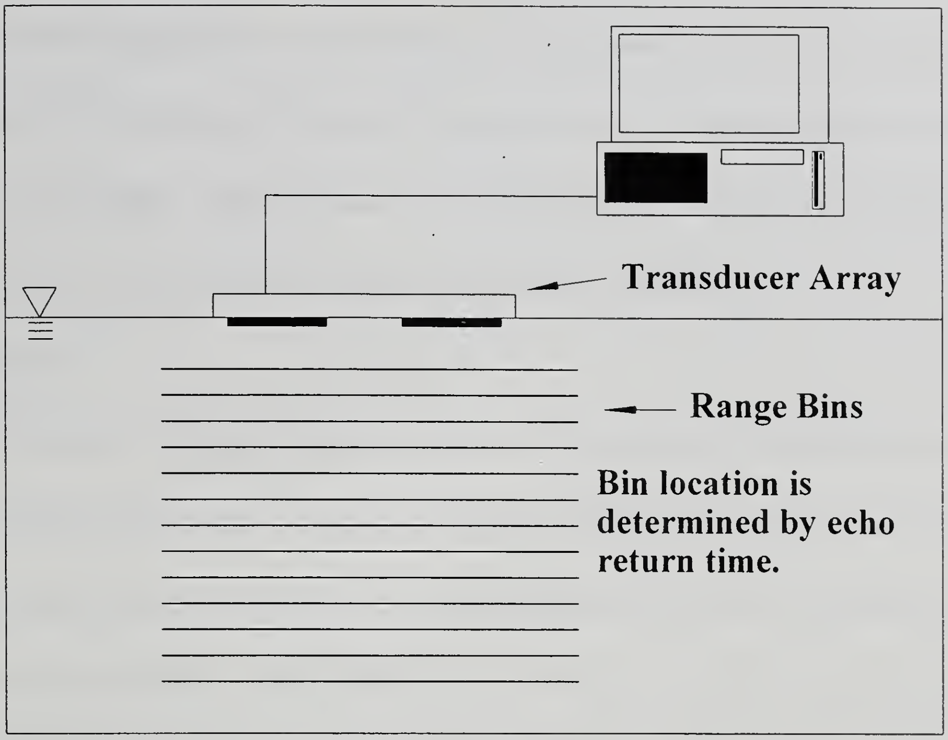

Figure 2.4. Range Gating.

Advantages

Acoustic suspended-sediment measurement offers the ability to non-intrusively measure sediment parameters through a vertical range on the order of several meters. This claim is unique among suspended-sediment measurement techniques (Thorne et al., 1995). The high degree of temporal (≈0.1 s) and spatial (≈1 cm) resolution offer the opportunity to study the mechanics of turbulent sediment transport (Thorne et al., 1994). This technique is well suited for deployment over long periods of time.

Acoustic measurement provides a large advantage over pump and bottle sampling (to be discussed later) because it allows the researcher to observe the behavior of turbulent processes acting on the sediment. Pump and bottle sampling average over these processes, providing no information on short duration events (Thorne et al., 1994).

Previous researchers who have urged further development of the method (Van Rijn and Schaafsma, 1986; Van Rijn, 1993) have recognized the potential of acoustic suspended-sediment measurement. Other researchers (Osborne et al., 1994) have also recognized these advantages of the acoustic method over optical methods.

Disadvantages

Translation of acoustic backscatter data into sediment concentration and size is a difficult problem (Hanes et al., 1988). Laboratory calibration has been used to determine the relationship between backscattered signal strength and sediment parameters. However, another problem is the difficulty of creating a calibration apparatus that can maintain a uniform sediment concentration suitable for use in calibrating instruments. Considerable effort has been expended by several investigators on this problem alone (Wylie et al., 1994; Derrow & Kuhnle, 1996).

At high particle concentration, attenuation becomes a significant problem. In order to compute the conversion from backscattered signal to sediment parameters, the attenuation must be accounted for. This requires knowledge of the sediment concentration, the unknown value being sought. To overcome this problem, either a concentration at the range bin nearest the transducer (zero concentration at the surface, for example) must be assumed, or an independent measurement of concentration at some range bin must be made. Using the assumption method leads to errors that increase in magnitude as distance from the sensor increases (Thorne et al., 1995).

Bottle Sampling

Operating Principle

In its simplest form, bottle sampling involves extracting a water sample by dipping with a jar. However, if the velocity at the mouth of the jar differs from the local stream velocity, then the amount of sand-sized suspended sediment entering the jar may not be representative of that in the stream that is the subject of measurement. Performing isokinetic sampling in which the velocity in the jar is equal to the local velocity in the stream can rectify this error. In order to achieve isokinetic sampling, several types of apparatus have been joined with the simple bottle. These include point and depth integrating samplers described in Interagency Committee (1963). These samplers are in use by such agencies as the United States Geological Survey (Edwards and Glysson, 1999). Sediment concentration and size distribution are determined from the samples by laboratory analysis using standard techniques such as those described in Guy (1965).

Depth integrating samplers are used to sample the water column in a vertical section by lowering the apparatus to the desired level, usually as close to the bed as possible, then raising the sampler back to the surface at the same rate. This technique is dependent on the speed of the sampler as it moves through the water column. Point integrating samplers can sample sections of water depth by electronically opening a valve at the appropriate time. Point integrating samplers may also be used in the same manner as depth integrating samplers when necessary (Interagency Committee, 1963).

Advantages

Bottle sampling is a reliable, well documented, and widely used technique. Depth and point integrating samplers allow nearly the entire depth of the stream to be sampled. Bottle samplers are generally considered the standard against which other types of samplers are calibrated.

Disadvantages

As compared to techniques using instrumentation, bottle sampling has poor temporal resolution. Unlike automated methods such as pump sampling, personnel must be on hand to take samples. This often involves working late at night in storm conditions, which adds to the expense of taking the samples. Because their shape places the inlet nozzle of most bottle samplers above the lowest point on the sampler, most bottle samplers cannot sample the lowest 4-6 inches of the water column. Bottle samplers require an intrusion in the flow, although using streamlined samplers minimizes this effect.

Pump Sampling

Operating Principle

In pump sampling, a vacuum is applied to a line submerged in the channel, and a fluid/sediment sample is taken and stored until retrieved for laboratory analysis. The line's intake nozzle is usually pointed upstream. To avoid sample biasing, the intake velocity must be matched to the local stream velocity. The sediment concentration and size distribution are determined at a lab using standard techniques.

Advantages

Pump sampling provides a reliable method for collecting samples that works well for fine sediments (<0.062 mm). Automatic pump samplers can be programmed to take samples at predetermined intervals, or when coupled with appropriate sensors, at predetermined flows or depths. Pump samplers are often automated, which eliminates the need for personnel to be present in order to take samples.

Disadvantages

When compared to instrumented sampling techniques, pump sampling has poor temporal resolution. In the time necessary for a pump sampler to obtain a fluid/sediment sample, an instrumented technique would be able to take many readings, measuring changes in concentration over much smaller time scales. Personnel and laboratory analysis add expense to the sampling. The amount and size of sediment sampled are dependent on the pump's speed as well as the nozzle's orientation with respect to the flow direction. However, it has been shown that intake velocity will not cause errors greater than 20% as long as the intake velocity is not less than 80% or greater than 200% of the local flow velocity (Nelson & Benedict, 1950). Pump sampling is flow intrusive, a disadvantage when compared to techniques that require no flow intrusion.

Focused Beam Reflectance

Operating Principle

In focused beam reflectance measurement, a laser beam focused to a very small spot (<2 μm^2) in the sample volume is rotated very quickly (many times per second). As it rotates, the beam encounters particles that reflect a portion of the beam (Figure 2.5).

The time of this reflection event is used to determine the chord length of the particle(s) in the path of the laser. This information is used to calculate the volume of a sphere representing the particle (Phillips and Walling, 1995b; Law et al., 1997).

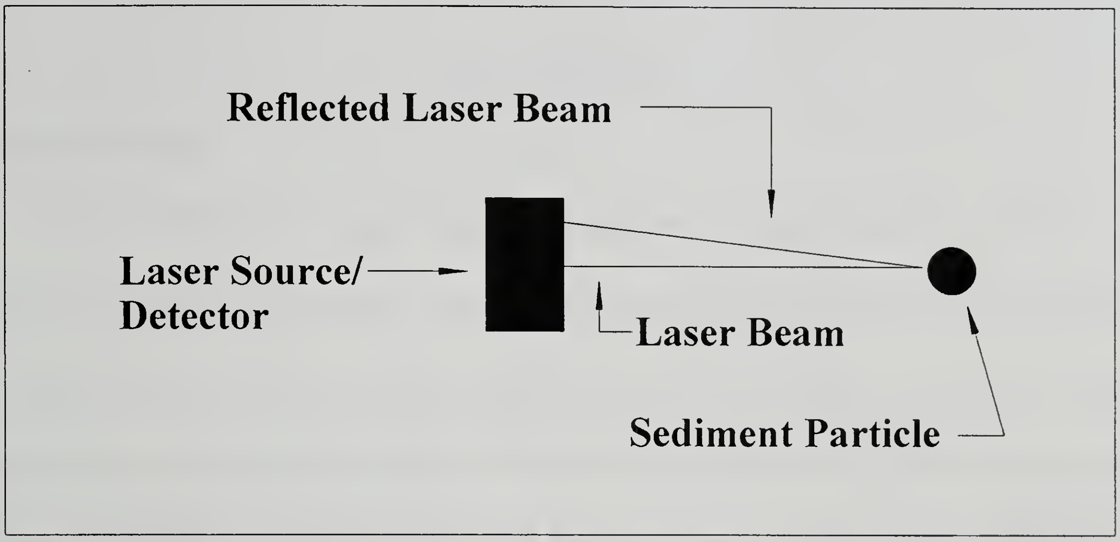

Figure 2.5. Focused beam reflectance.

Advantages

There is no particle size dependency since concentration measurements from focused beam reflectance are based on particle size. The instrument has a wide particle measuring range of roughly 1-1000 μm with measurements of over 1000 μm possible as well as a wide concentration range of 10 mg/l to 50 g/l. The instrument is easily portable. Good results from field studies were reported (Phillips and Walling, 1995b; Law et al, 1997).

Disadvantages

If particles have little or no reflectance, such as particles high in organic matter, the instrument will work poorly or not at all. At low particle concentrations (<1 mg/l), long counting times are required. Since particle sizes are based on chord lengths, the

assumption of sphericity is required. In a situation involving particle shapes that vary drastically from spheres, poor readings may result (Law et al., 1997). The nature of this instrument requires that it be flow intrusive. The instrument is relatively expensive.

Laser Diffraction

Operating Principle

In laser diffraction, a laser beam is directed into the sample volume where particles in suspension will scatter, absorb, and reflect the beam (Figure 2.6). Scattered laser light is received by a multi-element photo detector consisting of a series of ring shaped detectors of progressive diameters that allow measurement of the scattering angle of the beam. Particle size can be calculated from knowledge of this angle, using the Fraunhofer approximation or the exact Lorenz-Mie solution. By basing concentration measurements on these measured particle sizes, particle size dependency is eliminated (Agrawal and Pottsmith, 1994; Riley and Agrawal, 1991; Knight et al., 1991; Swithenbank et al., 1976). However, in the absence of additional information, particle density must be assumed.

Advantages

Particle size dependency is not a factor since sediment concentration is calculated from size measurements, thus calculating the concentration based on the volume of the particles. Calculated sediment parameters can be output at a rate of about 1Hz. Particle composition does not affect readings. This technique is widely used in other areas such as measuring particle sizes in cements, chocolates, or microbes (Agrawal and Pottsmith, 1996; Cao et al. 1991). Agrawal and Pottsmith, 1996, show the results of a test using a

commercially available laser backscatter instrument in suspensions with 2 polystyrene powders of differing sizes. They show that although the two suspensions produce nearly identical total scattered energy, the instrument accurately determines the particle size and the concentration by volume. Laser diffraction instrument readings are not affected by the refractive index of the particles (Agrawal and Pottsmith, 1996).

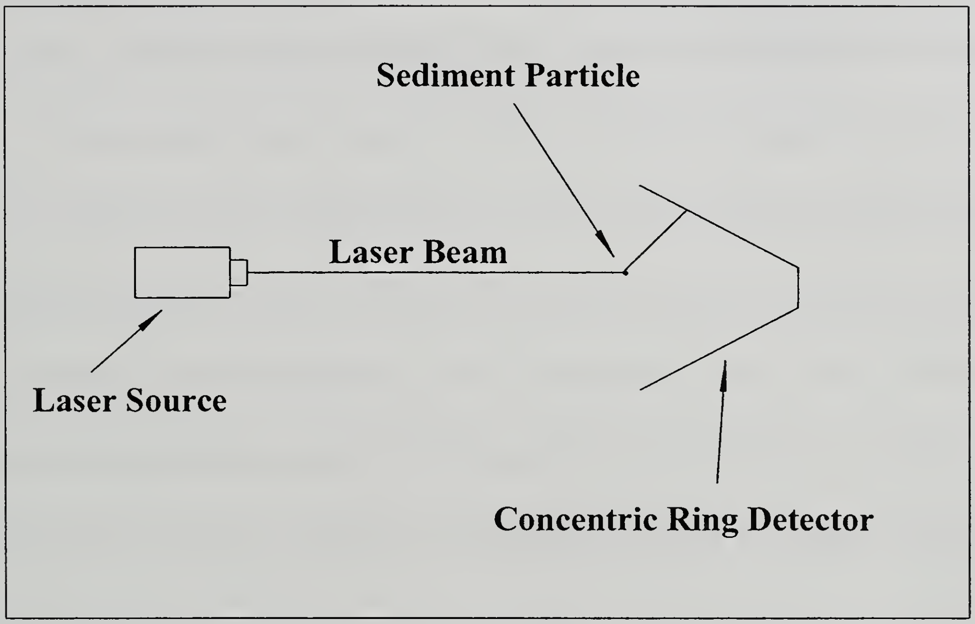

Figure 2.6. Laser diffraction.

<u>Disadvantages</u>

Laser diffraction devices are expensive. The principle of operation of the instrument limits the particle size measurement to 250 µm and the concentration range to 5000 mg/l (Pottsmith, 1997). This means that longer focal distances are necessary for measurement of larger particles (Witt and Rothele, 1996). Since the measuring volume of laser diffraction devices are very close to the instrument, they are flow intrusive. They are quite complicated devices that may require specialized training for operation and data

interpretation. The statistical algorithms that translate the data do not arrive at a unique concentration measurement. This process works better when the sediment has a smooth distribution (Friedricks, 1997).

Nuclear Measurement

Operating Principle

In general, nuclear sediment measurement utilizes the attenuation or backscatter of radiation. There are three basic types of nuclear sediment gauges: those that measure backscattered radiation from an artificial source, those that measure transmission of radiation from an artificial source, and those that measure radiation emitted naturally by sediments (Tazioli, 1981; McHenry et al., 1967; Welch and Allen, 1973). The first two have the broadest applicability and will be described in the following paragraph.

In backscatter gauges, radiation is directed into the measurement volume with the radioactive source isolated from the detector by lead. A sensor in the same plane as the emitter measures radiation backscattered from the sediment. In transmission gauges, the detector is opposed to the emitter and the attenuation of the radiation caused by the sediment is measured and compared to the attenuation of the rays caused by passage through distilled water. The ratio between these measurements allows calculation of sediment concentration. Ratio-type transmission instruments eliminate errors associated with radioactive decay of the source, drift in electronic components, and changes in water density due to temperature (McHenry et al., 1967 & 1970; Berke and Rakoczi, 1981; Rakoczi, 1973).

Advantages

Some advantages of using nuclear instruments in general are: they are well suited to installations where continuous monitoring is necessary due to the inherently low power consumption of the instruments, they can be used over a wide range of sediment concentrations (500-12,000 mg/l), and they are not affected by the color of water or by suspended organic matter (Papadopoulos and Ziegler, 1966; Tazioli, 1981; Berke and Rakoczi, 1981).

Disadvantages

Radioisotopes are, by nature, subject to decay, and the source must eventually be replaced (Welch and Allen, 1973). Changing chemical composition of sediments can affect readings. Licensing and training are requirements for the use of nuclear devices. The geometry of the gamma backscatter instruments prevents their use in streams less than 1.5 m deep (Berke and Rakoczi, 1981). Low sensitivity is an important limitation; nuclear instruments are best suited to sediment concentrations above 1000 mg/L (Crickmore et al., 1990). Field calibration is difficult and laboratory calibration cannot be substituted for field calibration due to the different chemical characteristics exhibited by river water and tap or distilled water. This problem is multiplied because periodic re-calibration of nuclear instruments is required. Most instruments require 3-5 minutes of observation time per measurement, thus averaging over any processes occurring during that time (Crickmore et al. 1990; Rakoczi, 1973; Skinner et al., 1969).

Optical Backscatter

Operating Principle

In optical backscatter (OBS) sensing, infrared or visible light is directed into the sample volume. A portion of the light will be backscattered if particles are in suspension. A series of photodiodes positioned around the emitter detect the backscattered signal. The strength of this backscattered signal is used to determine the sediment concentration. Readings from known sediment concentrations are used to calibrate the instrument.

Advantages

OBS response to varying concentrations of homogeneous sediments is nearly linear (Black & Rosenberg, 1994; Green & Boone, 1993; and others). This linearity extends over a wider range than optical transmission instruments (D & A Instruments, 1991). OBS sensors allow very good spatial and temporal resolution. OBS units are readily available from several manufacturers, and they provide real-time output as well as the option of remote deployment and data recording.

Disadvantages

Particle size dependency is the main problem with using OBS (Black & Rosenberg, 1994; Ludwig & Hanes, 1990; Green and Boon 1993; Xu 1997; Kineke and Sternberg 1992; Conner & Devisser 1992). The concentration as measured with an OBS sensor may increase by as much as 10 times when compared to readings for the same concentration but with a different particle size (Ludwig and Hanes, 1990). In particular, OBS sensors are more sensitive to smaller particle sizes. A 20 to 50 μm change in particle size can change the OBS gain (V/(g/l)) by 70%, while a change from 200-300 μ

m results in a 30% change in gain. In environments with particle sizes of less that 100 μm, OBS gain is greatly affected. OBS performs well for measuring concentrations where particle size is constant or remains in the 200-400 μm range (Conner and De Visser, 1992). There has been extensive work on quantifying and offsetting this effect (Kineke and Sternberg, 1992; Green & Boon 1993; Conner and DeVisser 1992; Black and Rosenberg, 1994; Xu, 1997). OBS instruments do intrude into the flow; however, the sampling volume is offset from the instrument by an amount dependent on the degree of turbidity.

At high particle concentrations, OBS instruments can reach a saturation concentration. Black and Rosenberg, 1994, found that their OBS instrument reached saturation at about 100 kg/m^3. In the presence of relatively homogenous sediments, the saturation problem can be overcome by careful adjustment of the instrument's gain (Kineke and Sternberg, 1992). These problems are compounded when the OBS is used in a heterogeneous sediment mixture. Ludwig and Hanes, 1990, do not recommend the use of OBS devices in sand/mud mixtures. Green and Boon, 1993, describe a procedure whereby a pair of instruments may be used to surmount this problem. They suggest the co-deployment of the OBS device with another type of sensor, such as acoustic backscatter. Conner and De Visser, 1992, recommend the use of an in-situ particle sizing sensor along with an OBS device. When used to record field data over long periods of time, fouling of the sensor face is a problem.

Optical Transmission

Operating Principle

In optical transmission sensing, light is directed into the sample volume. Sediment present in the sample volume will absorb and/or scatter a portion of the light. A sensor located opposite the light source allows determination of the degree of attenuation of the light beam. Using information from known sediment concentrations, the sediment concentration can be calculated from instrument readings.

Advantages

Optical transmission instruments have most of the same advantages as optical backscatter instruments. Optical transmission sensors allow very good spatial and temporal resolution and are generally more sensitive to low particle concentrations than OBS instruments. They are readily available from several manufacturers.

Disadvantages

Optical transmission devices exhibit weaknesses similar to OBS devices, although the particle size dependency is somewhat less severe than with OBS (Clifford et al. 1995). The refractive index of the particles also affect transmission devices (Baker and Lavelle, 1984). Optical transmission instruments show a non-linear response to increasing particle concentrations with disproportionately small changes in output being produced by large changes in sediment concentration in the upper range of the instrument. This can be corrected by using a shorter optical path length; however, this solution induces more flow obstruction. Large variations in sediment concentration will

require multiple transmission instruments or a multiple path instrument (D & A Instruments, 1991). These instruments are flow intrusive.

Spectral Reflectance

Operating Principle

Spectral reflectance measurement of suspended-sediment concentration is based on the relationship between the amount of radiation, generally in the visible or infrared range, reflected from a body of water and the properties of that water (Figure 2.7). The radiation is measured by a hand held, airborne, or satellite based spectrometer. The correlation between concentration of suspended sediment and the reflected radiation has been observed and validated by several researchers (Blanchard & Leamer, 1973; Ritchie & Schiebe, 1986; Novo et al., 1989a, 1989b; Bhargava & Mariam, 1991; Choubey, 1994). This relationship is dependent on many parameters such as the optical properties of the sediment type, sensor observation angle, solar zenith angle, and the spatial resolution of the measurements. (Choubey, 1994; Gao and O'Leary, 1997; Novo et al., 1989a, 1989b).

Advantages

The ability to measure sediment concentrations over broad areas is an important advantage. In addition, the ability to "see" changes in time over these broad areas is important. In particular, conservation agencies can use this type of data to identify water bodies with high-suspended-sediment concentrations. This allows conservation efforts to be concentrated on areas with significant erosion problems (Ritchie and Schiebe, 1986).

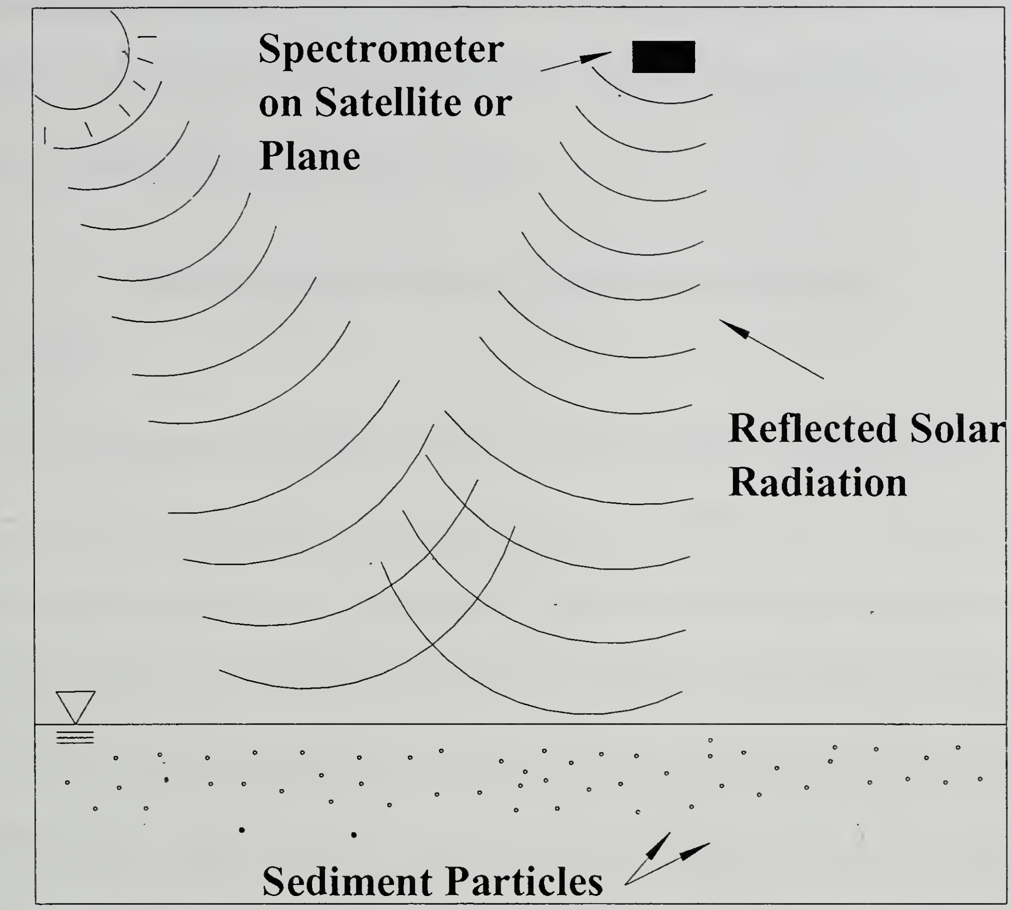

Figure 2.7. Remote spectral reflectance.

Disadvantages

There is a large range of suspended-sediment concentration related to a small range of reflectance values. Water will rarely reflect more than 10% of its incident radiation, yet a 50 mg/l increase in suspended-sediment concentration is likely to cause only a 1% increase in reflected radiation. Furthermore, a 1% change in reflected radiation is less than the variability associated with the sensor, incoming irradiance, water surface, or atmosphere (Chen et al., 1992). In higher sediment concentrations, the measuring range is limited to the top few feet of the water column. Due to a strong correlation between spectral readings and the mineral composition of the sediment, larger

errors in measured suspended-sediment concentration readings may be introduced when the sediment type is unknown (Choubey, 1994). Particle size dependence is also a problem with the method (Novo et al., 1989b).

Other Suspended-sediment Measurement Techniques

Vibrating Tube

In this measurement scheme, water is routed through a vibrating tube in a stationary housing located either on the stream bank or in the stream. The tube vibrates continuously and is electronically monitored. Use of the vibrating tube is based on two relationships: between the sediment concentration and the density of the sediment-water mixture, and between the density of the sediment water mixture and the vibrational period of the tube. There are several sources of error. Shifts in dissolved solids concentration, water temperature, water pressure, flow rate, and debris on the tube's walls all contribute to error. The first four errors can be eliminated by the use of sensors to quantify the changes in the parameters. However, the changes in vibration caused by debris or algae has not been successfully solved in a fluvial environment (Skinner, 1989).

Differential Pressure

Lewis and Rasmussen (1996) describe a method for using two pressure transducers to determine differences in the specific weight of sediment bearing water. They propose a method for field application, but field experiments had not been performed.

Impact Sampler

Van Rijn and Schaafsma (1986) describe an impact sampler developed at the Institute of Oceanographic Sciences in Taunton, England. The sampler works on the principle of momentum transfer. The impact rate of sediment particles hitting a sensor is measured. The detected impact rate is dependent on the mass, velocity, and angle of particle impact.

Video Microscopy

In video microscopy, a video camera films the water-sediment mixture in-situ. This film can be used to visually confirm the nature of the sediment. The film can also be examined by a computer-controlled automated analysis system for determining the size, shape, and number of sediment particles. Some factors in this measuring scheme are the type of lighting used, the sensitivity of the video system, and the method of image processing used to analyze the samples (Baier and Bechteler, 1996). This process does not appear feasible for the study of sediment flux; however, it has the potential to provide excellent information on the specific nature of sediment particles.

Conclusions

Many options exist for the measurement of suspended sediment in fluvial environments. Each researcher must decide what technique to use based on budget constraints, manpower, desired quality of data, etc. At present, it appears that multi-frequency acoustic backscatter shows merit for use in measuring suspended-sediment concentration. Its ability to measure sediment concentration in a vertical section, while estimating the particle size distribution, would make it a good choice for many

applications. However, further refinement and research are necessary before widespread use of this instrumentation is possible. In many situations, simultaneous deployment of different instrument types may be the best option (Green and Boone, 1993; Clifford et al., 1995; Osborne et al., 1994; Conner and De Visser, 1992). Simultaneous use of different sensor types for measuring suspended sediment is a sound practice that has been endorsed by several researchers in the field.

CHAPTER III

VARIABILITY IN SUSPENDED-SEDIMENT CONCENTRATION OVER MOBILE, SAND BEDS

Introduction

Accurate measurements of suspended-sediment concentration are essential in many areas of watershed management. Human impact on fluvial systems, sediment transport to oceans, measurement of soil losses, and reservoir sedimentation can all be assessed with the help of suspended-sediment data (Vanoni, 1975; Edwards and Glysson, 1999). The identification of Total Maximum Daily Loads (TMDL) for clean sediment (sediment that is not contaminated by chemical substances (USEPA, 1999)) as a means for determining areas that are impaired requires accurate concentration measurements to characterize sediment load in a stream or river. Much work has focused on the use of concentration measurements with various sampling schemes to calculate suspended-sediment load (Walling, 1977; Thomas, 1985; Ashmore and Day, 1988; Ingram et al., 1991; Thomas and Lewis, 1993; Kawanisi and Yokosi, 1993; and many others).

The collection and analysis of suspended-sediment samples is expensive and can be a large source of error in sediment load determination (Nelson and Benedict, 1950; Burkham, 1985; Edwards and Glysson, 1999). Another factor in obtaining accurate sediment load data is the selection of the best technique from the large number of methods employed to measure suspended-sediment concentration (Van Rijn and Schaafsma, 1986; Wren et al., 2000). Suspended-sediment load is highly variable in both time and space, further compounding the difficulty in obtaining accurate measurements (Lapointe, 1992, 1993, and 1996; Kostaschuk and Church, 1993; Hay and Bowen, 1994;

Kostachuk and Villard, 1996; Thorne et al., 1996). In the field, this variability is related to turbulence, bed conditions, sediment characteristics, proximity to tributaries, bank conditions, local weather conditions, hydraulic geometry, unsteady flow, non-uniform flow, and others. In a laboratory flume, the causes of variability can be reduced to turbulence, bed condition, and sediment characteristics. Given all of the sources of error in measurement of suspended-sediment load, the interpretation and application of concentration data should be carried out carefully while considering all of the controlling factors listed above. The purpose of this work is to aid in this understanding by examining the variability in suspended-sediment concentration using a discrete sampling strategy in a laboratory flume.

The causes for variability in suspended-sediment concentration may be reduced to three situations that are based on the viewpoint of the observer (in this case, the sampler). These situations can be used to examine the variability in suspended-sediment concentration: (1) a stationary observation point, (2) a moving observation point, and (3) laterally separated simultaneous samples. For the stationary observation point, the sampling position relative to the bed, along with the suspended-sediment concentration, changes constantly as turbulence intensity varies and as bedforms migrate past a fixed position. A moving observer follows one bedform as it migrates downstream in a steady, uniform flow and sees suspended-sediment concentration at the same position relative to that bed form. Here, the observed variation is a result of variations in turbulence, the changing shape of the bedform, and upstream conditions. In the third situation, two samples equidistant from a horizontal datum and the channel centerline are collected

simultaneously. Since bedform geometries are highly variable, bed conditions and sediment concentration can fluctuate greatly over channel width, resulting in large concentration differences for the paired samples. Lateral variability is of particular concern since samples must be taken from a limited number of cross-sections (Horowitz et al., 1990)

Most sediment sampling that is performed by federal agencies relies on isokinetic bottle (usually depth integrated) or pump sampling to measure sediment concentration (Interagency Committee, 1963; Edwards and Glysson, 1999). These are discrete sampling strategies as opposed to the continuous techniques such as optical backscatter, acoustic, and laser that are used by many researchers. This study simulates discrete sampling techniques that are often used in the field to study the variation in concentration for discrete suspended-sediment samples.

The objectives of the experiment were as follows: (1) to provide insight into the variability in suspended-sediment concentration in dune and upper-stage plane bed conditions in the context of discrete samples, (2) to determine the feasibility of using a side-by-side arrangement to test different types of suspended-sediment measurement equipment, and (3) to provide guidance on necessary sampling period to obtain accurate measurements of the mean concentration. Two bed configurations were chosen: upper-stage plane bed (USPB) and dune. The upper-stage plane bed has a minor amount of bed topography while still suspending significant amounts of sediment, while a dune-covered bed has much greater bed relief: These conditions represent the two end-member cases for flow field complexity and concentration variability.

Methods and Equipment

Experiments were carried out at the USDA-ARS National Sedimentation Laboratory in Oxford, MS. A 15 m x 1 m x 0.3 m sediment recirculating flume with adjustable slope and a frequency-controlled motor was used. Fluctuations in flow velocity were measured using a two-component (cross-stream and downstream) acoustic Doppler velocimeter that sampled velocities at 25 Hz and an electromagnetic current meter that sampled at 10 Hz. Fluctuations in bed height were monitored using an ultrasonic bed height probe that sampled at 1 Hz. An ultrasonic water-surface probe that sampled at 6 Hz monitored water surface fluctuations. Instrument positions are shown in Figure 3.1.

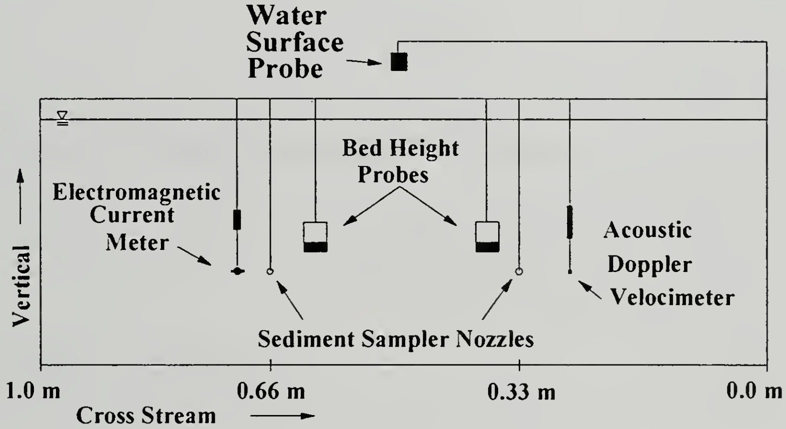

Figure 3.1. Instrument positions for paired samples.

Suspended-sediment samples were collected using a vacuum system in which the intake velocity was calibrated to approximately match the average flow velocity. For the dune experiment, intake velocity was approximately 0.5 m/s and for the USPB it was 1.7 m/s. The inadvertent selection of the high intake velocity for the USPB experiment is estimated from Nelson and Benedict, 1950, to cause a 13% undersampling of sediment particles, but does not effect the results discussed here since the main topic is

concentration variation rather than absolute concentration. All reported sampling positions are based on average bed heights as measured by the ultrasonic probe during vacuum sampling periods.

Table 1 summarizes the flow conditions in the experiments. Water surface slope, S, was calculated by linear regression of water surface elevations about a horizontal datum. Mean boundary shear stress, τ_0, was determined from

$$\tau_0 = \rho g d S \tag{3.1}$$

where ρ= fluid density, g=acceleration of gravity, and d=water depth. Shear velocity, u_*, was calculated from

$$u_* = \sqrt{\tau_0 / \rho}\ . \tag{3.2}$$

Depth-integrated flow velocity, U, was determined from

$$U = \frac{1}{d}\int_0^d \bar{u}\,dy \tag{3.3}$$

where y=distance above the bed and

$$\bar{u} = \frac{1}{n}\sum_{i=1}^{n} u_i\ , \tag{3.4}$$

where n=total number of observations and u_i= instantaneous downstream velocity. Froude number, Fr, was determined from

$$Fr = U / \sqrt{gd}\ . \tag{3.5}$$

It was necessary to employ different water depths and sediment sizes to obtain dune and upper-stage plane bed conditions in the flume used in this study. Several unsuccessful attempts were made to obtain an upper-stage plane bed with 0.5 mm sediment.

Table 3.1. Flow conditions from dune and upper-stage plane bed experiments.

Parameter	Dunes	USPB
Slope, S	0.00497	0.00270
Shear Velocity, u_* (m/s)	0.0858	0.0557
Froude, Fr	0.528	0.704
Depth, d (m)	0.149	0.117
Bed Shear Stress, τ_0 (Pa)	7.3	3.1
Velocity, U (m/s)	0.640	0.755
Discharge, Q (m^3/s)	0.095	0.088
Grain Size, D (mm)	0.50	0.23

Suspended-sediment samples were collected in simultaneous pairs at five different fixed depths relative to the flume bottom for both the upper-stage plane bed and dune bed. Suspended-sediment samples were collected over approximately 1.5 hour time periods in sets of 45 pairs of samples. Each sampling run was performed on a separate day. Sampling runs with like bed conditions had the same water depth, pump setting, and flume slope. The floor of the flume was used as the horizontal datum for sample nozzle placement.

Sediment concentrations were determined by weighing each fluid-sediment sample, decanting the sample, and washing the sediment into pre-tared pans that were oven dried. The pans were weighed to obtain the dry weight of sediment in each sample. The water used to fill the flume was filtered water from an on site well, so it was assumed that no total dissolved solids correction was necessary. There were 368 suspended-sediment samples analyzed for the dune experiment and 458 suspended-sediment samples were analyzed for the upper-stage plane bed. See Appendix B for a full listing of sample concentrations and locations. Example bed height and sample concentration time series

collected at z=0.33 m (Probe 1 position) are displayed in Figure 3.2. Suspended-sediment samples were collected at an average rate of 27 samples/hour.

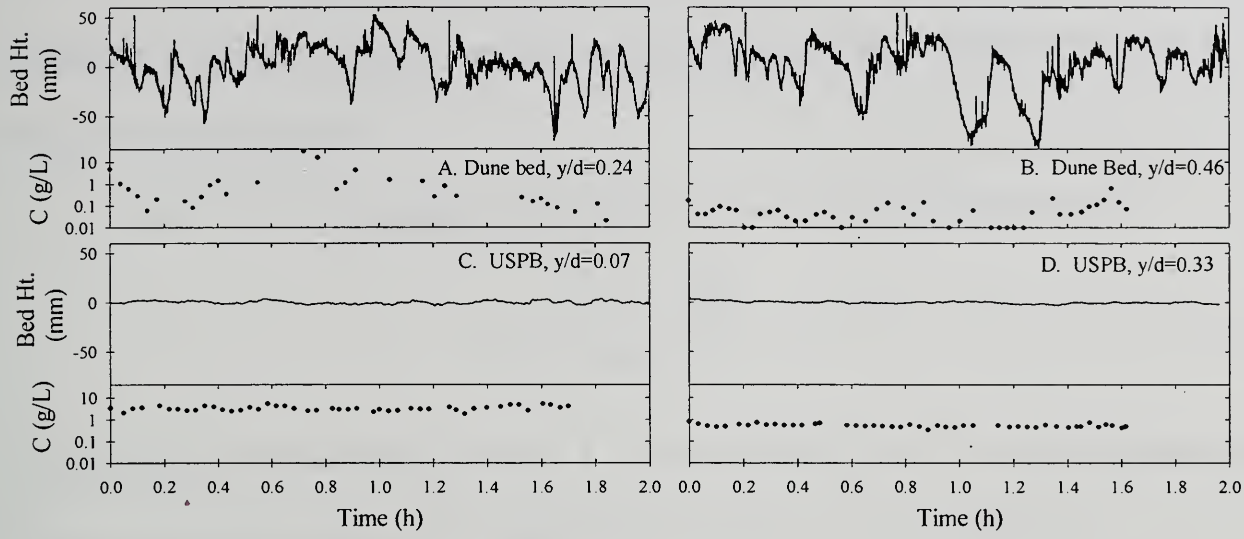

Figure 3.2. Examples of bed height (upper) and concentration (lower) time series for dune bed at *y/d* of (A) 0.24 and (B) 0.46, and for an upper-stage plane bed at *y/d* of (C) 0.07 and (D) 0.33. Bed height is shown as variation about the mean. The data was collected at z=0.33 m (Probe 1 position).

Running the flume for a period of approximately 10 hours, after which average dune periods and heights were found to be stable, ensured equilibrium dune populations. The equilibrium bed was not altered between experiments, and the flume was run for 2 hours prior to sampling for each experiment. The USPB reached equilibrium conditions quickly. The flume was run for approximately 1 hour before sampling over upper-stage plane beds.

Experimental Results

In the sections below, results are presented for three different observational viewpoints. The amount and type of variability observed in each situation are discussed.

Stationary Observation Point

Most suspended-sediment sampling takes place from a stationary observation point with constantly changing bed conditions beneath the sampler. Observed suspended-sediment concentrations at a stationary point relative to the bed will change along with bed topography.

A key measure of variability in a data set is the standard deviation where

$$s_x = \sqrt{\frac{\left(X - \overline{X}\right)^2}{\left(n-1\right)}}\,, \tag{3.6}$$

X represents individual measurements, $\overline{X}$ represents the mean of the measurements, and n is the number of samples. The coefficient of variation, or CV, is defined as

$$CV = s_x / \overline{X}\,. \tag{3.7}$$

The CV for suspended-sediment samples is several times larger for the dune bed than for the plane bed (Figure 3.3). For different vertical positions over a dune bed, the CV shows no definite pattern with height while in the upper-stage plane bed, it generally decreases with height. These results illustrate the highly variable nature of suspended-sediment concentration over a dune bed, where samples may vary up to 245% about the mean concentration. In upper-stage plane beds, samples are clustered much more tightly around the mean, but samples may vary up to 43% about the mean.

The sampling period required to match the average concentration obtained at a point was determined graphically as shown in Figure 3.4. Implicit in this discussion is the assumption that the 1.5-2 hour time series were long enough to yield a true approximation of the mean suspended-sediment concentration.

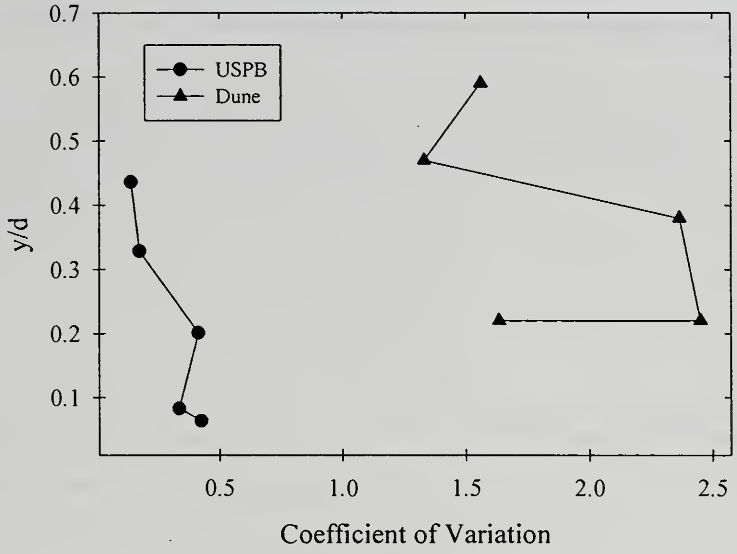

Figure 3.3. Coefficient of variation for suspended-sediment concentration measurements in dune and upper-stage plane bed conditions, where y is height above the bed and d is flow depth

For a given point, i, in a time series, the cumulative average up to that point will be:

$$\frac{1}{n}\sum_{j=1}^{n} X_j \,. \tag{3.8}$$

The time when the cumulative average entered and stayed within 20% of the mean was found for each concentration time series. For example, in Figure 3.4A, 1.6 hours would be the necessary sampling period to obtain the average concentration. Using this method, the average time for the cumulative mean to match the average concentration in dune bed conditions was found to be 1.2 hours. In the conditions reported here, if samples were collected in one position it would be necessary, on average, to sample for over an hour to obtain a reasonable estimate of mean suspended-sediment concentration. This time generally decreases with increasing height above the bed. The same procedure was used for an upper-stage plane bed resulting in a time of 0.06 hour to approximate the average

concentration. Since nearly all samples were within 20% of the mean, there was no clear trend relating vertical sample position to time of average concentration. Table 2 gives

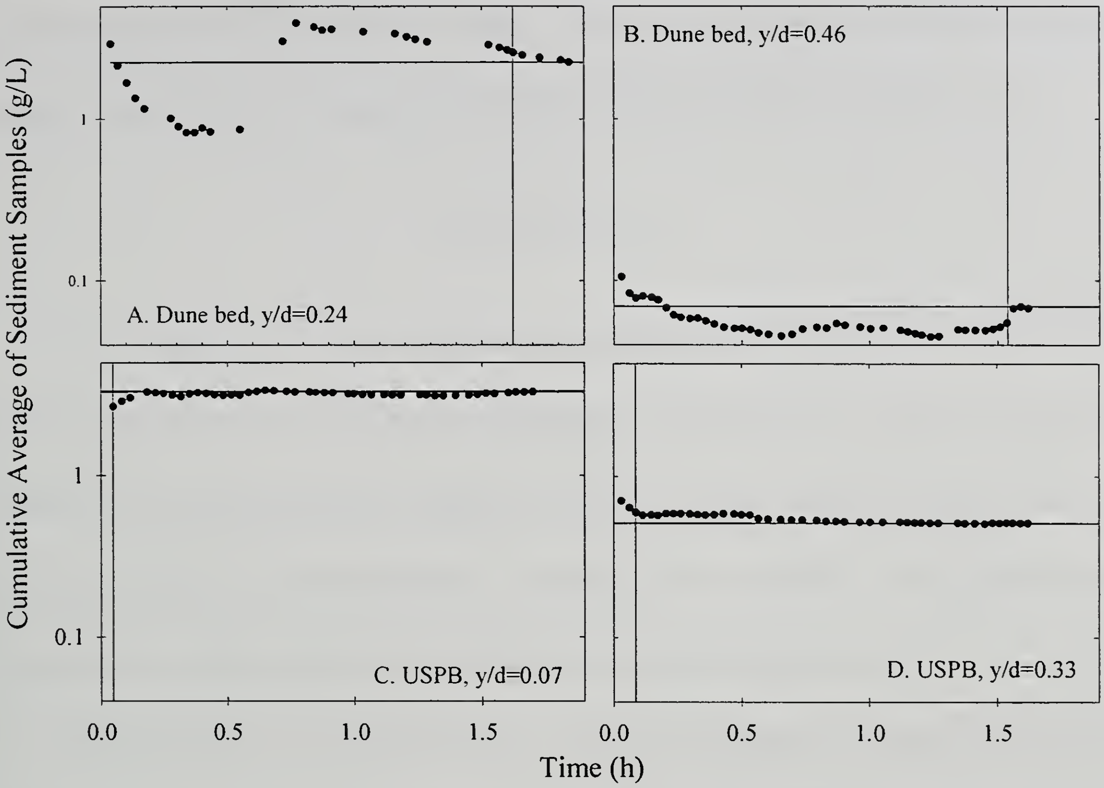

Figure 3.4. Cumulative average of suspended-sediment concentration related to average concentration for single sampler at *y/d* of (A) 0.24 and (B) 0.46 for the dune bed and (C) 0.07 and (D) 0.33 for the USPB. Samples were collected at an average rate of 27 samples/hour.

detailed experimental results for dune and upper-stage plane beds. For the upper-stage plane beds, it was not necessary to sample over multiple low-relief bedwaves for the cumulative mean to reach and stay within ±20% of the mean, but for the dune covered bed, the passage of several bedforms was required.

The previous discussion was based on cumulative averages of sample time series. The probability that individual sample concentrations would fall within 620% of the mean was also investigated. It was found that for dune beds, there was a 5% chance that

any one sample would fall within the 20% bounds while for the upper-stage plane beds there was a 63% chance. In both cases, the chances of falling within the error bounds were generally greater further from the bed. This is a significant result and again points the highly variable nature of suspended-sediment concentration over dune beds.

Moving Observer

The viewpoint of an observer moving with a specific bedform is valuable because it provides insight into the mechanics of sediment suspension. For a dune-covered bed, such data aids in determining the segment of the dune from which the most sediment is entrained and transported downstream. In addition, the variability of suspended-sediment concentration for different parts of a bedform may also be examined.

The viewpoint of a moving observer can be simulated by dividing each bedform into equal parts and comparing sediment concentrations from the same section on each bedform. Figure 3.5 shows the average, maximum, and minimum suspended-sediment concentration as well as the average y/d values for suspended-sediment samples from different positions relative to bedform length for all experiments. Only 5E shows the highest suspended-sediment concentration over the crest region. In 5A-5D, the highest concentration is over some part of the stoss region. Despite being sampled farthest from the bed, the highest concentration is over the first 25% of the dune in 5A and 5B. This is likely due to flow reattachment from upstream dunes; although it is unknown how far upstream the suspension occurs (Bennett and Best, 1995; and Kostaschuk and Church, 1993). There is evidence that the flow reattachment point on a dune can result in high magnitude suspension events (see Nezu and Nakagawa 1993, Fig 9.6; Kostaschuk and

Church, 1993). The present data confirm that concentration is higher over the dune's stoss region. In addition, in Figure 3.2A and 3.2B, the highest peaks in concentration occur away from the highest bed elevations.

Table 3.2. Results from sediment sampling time analysis.

Bed	Probe 1				Probe 2			
	y/*d*	Mean Conc. (g/L)	Time to mean ±20% (h)	Number of Bedforms to mean ±20%	*y*/*d*	Mean Conc. (g/L)	Time to mean ±20% (h)	Number of Bedforms to mean ±20%
Dune	0.24	3.55	1.15	5	0.20	3.22	1.36	9
Dune	0.24	2.25	1.60	5	0.20	3.23	1.57	7
Dune	0.41	0.40	0.83	6	0.34	1.19	1.09	3
Dune	0.46	0.07	1.56	7	0.48	0.12	0.49	6
Dune	0.62	0.06	0.93	7	0.56	0.08	1.07	8
USPB	0.07	3.30	0.006	0.03	0.06	14.09	0.180	1.0
USPB	0.09	1.66	0.006	0.03	0.08	3.60	0.200	0.8
USPB	0.20	0.77	0.006	0.02	0.20	0.86	0.006	0.02
USPB	0.33	0.52	0.090	0.24	0.33	0.63	0.006	0.01
USPB	0.44	0.40	0.130	0.57	0.44	0.45	0.006	0.01

In Figure 3.5F-3.5J, low-relief bedforms on the order of 2 to 4 mm result in no clear pattern of suspended-sediment concentration with bedform position. It is unlikely that there is flow separation over these small bedforms. Bennett et al. (1998) observed little variation in flow and suspended-sediment concentration over upper-stage plane beds.

Lateral Separation

The similarity of laterally separate, simultaneous sediment samples is directly related to the testing of suspended-sediment measurement equipment. A laterally

homogenous concentration field could be used to perform side-by-side verification of sediment concentration measurement techniques, provided that the samples are from the same vertical position. This section of work was carried out to determine the feasibility of using simultaneous samples to test measurement equipment. Once again, both the dune and upper-stage plane beds were used. The simultaneous time series of concentration data were also used to examine similarities in mean concentration at laterally separate locations. The similarity of simultaneous sample time series were determined by using a variety of statistical procedures as applied by a commercially-available statistical software package. All data sets failed the Kolmogorov-Smirnov normality test and were subjected to the Spearman correlation procedure, a non-parametric procedure that does not require the assumption of normality or equal variance.

The Spearman rank order correlation coefficient is computed by ranking all values of each variable, then computing the Pearson Product Moment Correlation coefficient, *r*, defined below, of the ranks.

$$R = \frac{\left(X - \bar{X}\right)\left(Y - \bar{Y}\right)}{\sqrt{\left(X - \bar{X}\right)^2 \quad \left(Y - \bar{Y}\right)^2}} \tag{3.9}$$

where $\bar{X}$ and $\bar{Y}$ are the means of X and Y, and R is the sample correlation coefficient. If r is close to +1 or −1, there is a strong positive or negative correlation between X and Y. A near-zero value for R indicates a lack of correlation between the variables (Jandel, 1995). Table 3.3 summarizes the results of the statistical tests on the simultaneous sample data sets. No paired data sets show significant correlation, which would be defined by $P<0.05$, where P is the probability of being wrong in concluding that there is a true

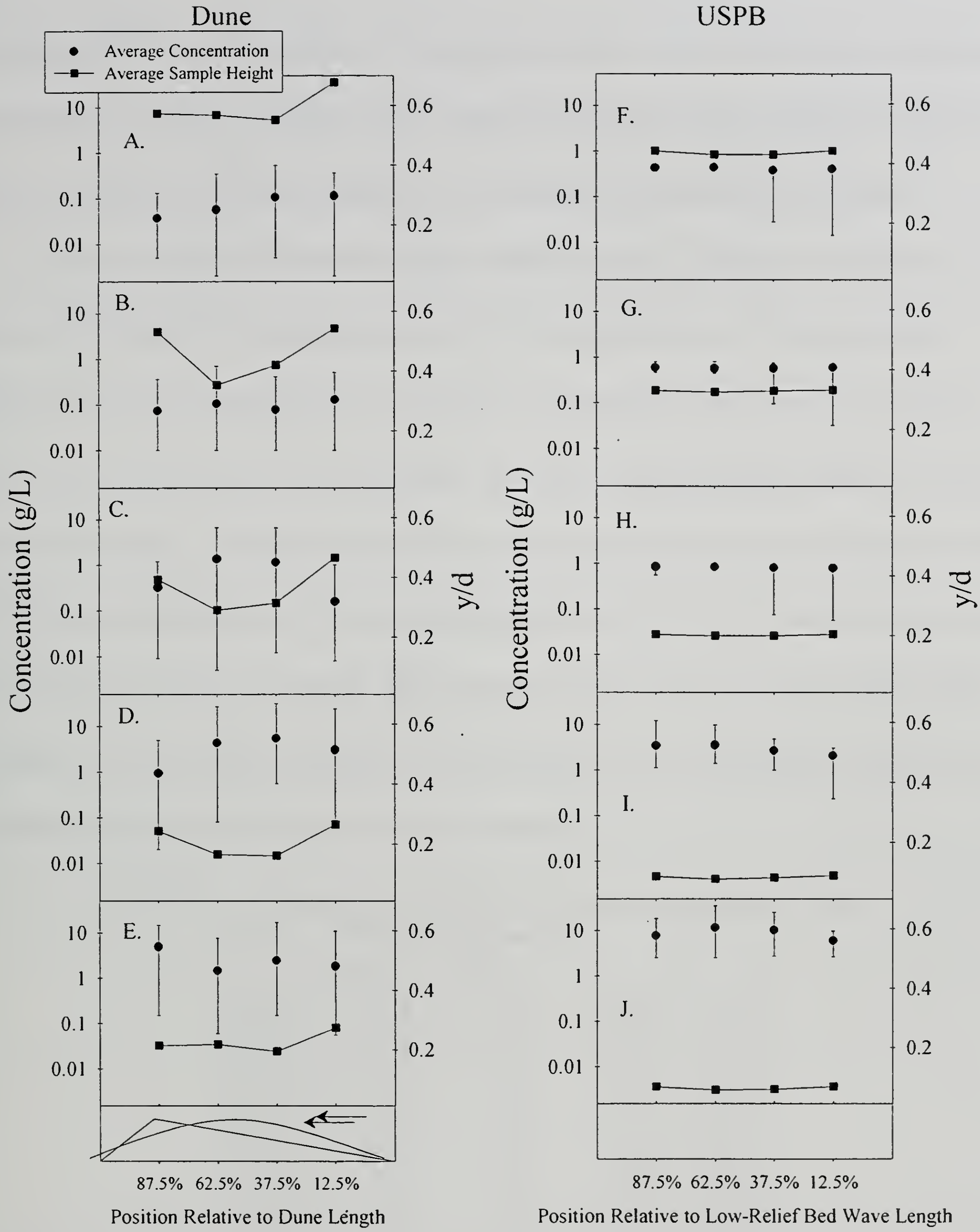

Figure 3.5. Concentration variation with bedform position for dunes at *y/d* of (A) 0.59, (B) 0.47, (C) 0.38, (D) 0.22, and (E) 0.22 and for upper-stage plane bed at *y/d* of (F) 0.44, (G) 0.33, (H) 0.20, (I) 0.08, and (J) 0.06. Boxes (right hand axes) represent average sampling height for all samples taken in that particular section of bedform length, circles (left hand axes) are average suspended-sediment concentration for each section, and error bars represent the maximum and minimum concentration collected for each section. The center of each section is labeled in percent of average bedform length beginning at the upstream end.

association between the variables. From these results, it is reasonable to conclude that simultaneous sampling in either dune or upper-stage plane bed conditions would not be reliable for testing suspended-sediment concentration measurement techniques.

However, this conclusion should be further qualified. Figure 3.6 shows the results of dividing the concentration data into 2-mm depth bins. All concentration samples falling into a depth bin are averaged. The results indicate that if a constant distance from the bed could be maintained, the upper-stage plane bed could be used for side-by-side testing. For a given depth bin, the average difference in concentrations for laterally separate samples in the upper stage plane bed was 24%. This was not the case for the dune bed where the average difference was 91%, due to the 3-dimensional bed topography and associated turbulence. This further illustrates the highly variable nature of suspended-sediment concentration over a dune bed.

Table 3.3. Summary of statistics on simultaneous data sets.

Bed	Probe 1 (y/d)	Probe 2 (y/d)	r	P
Dune	0.24	0.20	0.38	0.13
Dune	0.24	0.20	0.07	0.71
Dune	0.41	0.34	-0.18	0.24
Dune	0.46	0.48	0.27	0.07
Dune	0.62	0.56	-0.21	0.16
USPB	0.07	0.06	0.03	0.84
USPB	0.09	0.08	-0.16	0.29
USPB	0.20	0.20	0.28	0.06
USPB	0.33	0.33	0.20	0.18
USPB	0.44	0.44	0.17	0.26

Discussion

The results presented here have many implications for suspended-sediment sampling programs, particularly those that rely on discrete sampling. The various types

of sampling equipment will be affected in different ways by variability in concentration. All types of measurement equipment are affected by the amount of time necessary to approximate mean suspended-sediment concentration. Sampling over the passage of 4 to 8 dunes is not feasible for most discrete sampling strategies. However, the present study shows the critical need for continuous electronic monitoring, such as the acoustic or optical backscatter techniques, of suspended-sediment concentration.

The variable nature of concentration as a function of dune position also strongly affects discrete sampling strategies. If the dune passage time is several times the length of sampling period, larger errors can result. Great care should be taken in these situations to sample over multiple bedform lengths. Using a boat to follow a moving dune in the field would shed more light on this variability and also help to model the origin of macroturbulent flow structures. Pump, depth-integrating, and point-integrating samplers are affected by bedform position, particularly if the sampling is taking place near the bed and for a short time period. Near the bed, concentration variability is highest and concentration measurements will be strongly affected by sampling period.

Conclusions

The variability in suspended-sediment concentration was examined in a series of experiments over a dune covered bed and an upper-stage plane bed in steady, uniform conditions. The coefficient of variation was found to be much smaller for the upper-stage plane bed than for the dune bed. Time to obtain average concentration was significantly smaller for the upper-stage plane bed, reflecting the relatively small changes in bed height as compared to the dune bed. The stoss region of a dune was found to have the

highest suspended-sediment concentration, likely due to the suspension of sediment at reattachment. Laterally separate, simultaneous sediment concentrations were poorly correlated, with no statistically significant correlation between any paired time series. However, after correcting for height above the bed, the upper-stage plane bed showed similar concentrations for laterally separate samples in the same depth bin.

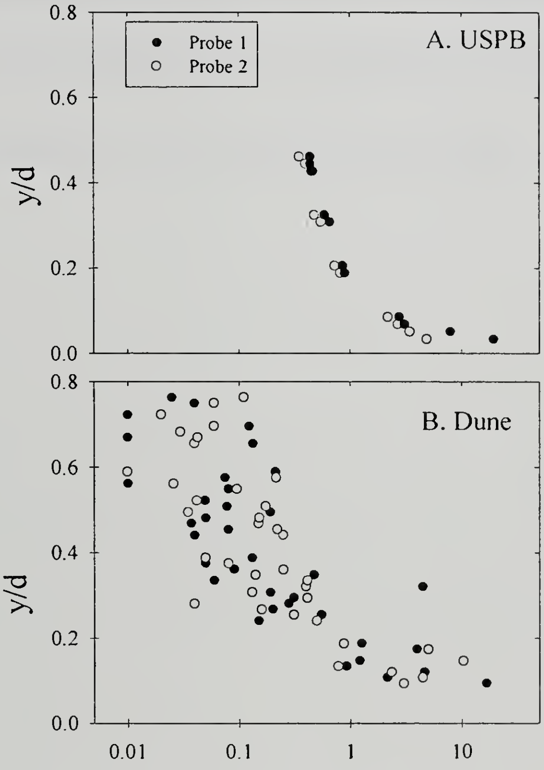

Figure 3.6. Suspended-sediment concentration data for (A) upper-stage plane bed and (B) dune bed, binned into 2-mm increments above the bed. Paired samples are shown at the same *y/d*.

The experimental results presented here have several implications for sediment sampling plans. The long time period needed to match average concentration over dunes highlights the difficulty of obtaining accurate and unbiased data. The variable nature of suspended-sediment concentration over different dune sections illustrates the sensitivity

of dune position on suspended-sediment concentration measurements. On large-scale dunes, where an entire sample can be taken over only one section of a dune, this could cause a large bias in measured concentrations. Based on the results of simultaneous sampling, it is not recommended that side-by-side instrument testing be performed using a live sand bed, unless some method for maintaining equal distances from the bed is available. This lack of correlation has not been shown for streams or rivers, however. Examination of average concentration for the simultaneous, laterally separate, time series showed that 1.5 hours of sampling was sometimes not enough to get within 20% of the mean concentration.

CHAPTER IV

THE CALCULATION OF TRANSVERSE EDDY DIFFUSIVITY USING TURBULENCE DATA

Introduction

The calculation of the transverse spreading rate of contaminants is important in several areas of water resources engineering such as mixing at river confluences, the spread of entrained contaminants, and in modeling overbank sediment mixing during flood events (Sayre and Chang, 1968; James, 1985; Pizzuto, 1987). In a straight channel with a flat bed, the lateral spread of a contaminant is caused by turbulent diffusion and secondary circulation (Fischer et al., 1979). A diffusion coefficient, ε_z, is used to relate the flow properties of the channel to a rate of dispersion and lumps together the effects of turbulent diffusion and secondary circulation. The coefficient is usually determined by measuring the spreading rate of a tracer material such as a dye or salt solution using the following equation:

$$\varepsilon_z = (u/2)(d\sigma_z^2/dz), \tag{4.1}$$

where ε_z=transverse diffusion coefficient, u is downstream velocity, σ_z^2=lateral variance of concentration, and x=longitudinal distance (Holley and Abraham, 1973; Miller and Richardson, 1974). The variance of the concentration is found by measuring several cross-stream concentration profiles downstream of a steady-state dye release point. ε_z is usually presented as the non-dimensionalized dispersion coefficient

$$k=\varepsilon_z/(u_* d), \tag{4.2}$$

where

$$u_* = \sqrt{\tau_0 / \rho}\,, \tag{4.3}$$

τ_0 is the mean bed shear stress, ρ is the fluid density, and d is the water depth. Values for k are generally in the range 0.1-0.3 (Rutherford, 1994; Lau and Krishnappan, 1977).

Experimentally determining the diffusion coefficient can be difficult and time consuming. Many measurements at multiple channel cross-sections are necessary for determining the diffusion coefficient. Efforts have been focused on determining the dependence of the transverse diffusion coefficient on physical parameters such as the Darcy-Weisbach friction factor,

$$f = 8\tau_0 / \left(\rho \bar{u}^2\right), \tag{4.4}$$

where $\bar{u}$ is the average downstream velocity, the width-to-depth ratio, b/d, where b is the channel width and d is the channel depth, the Froude number,

$$Fr = \bar{u} / \sqrt{gd} \tag{4.5}$$

where g is gravitational acceleration, and the Reynolds number,

$$\mathrm{Re} = \left(\rho \bar{u} l\right) / \mu \tag{4.6}$$

where l is a characteristic length scale and μ is the dynamic viscosity. There has been considerable debate over the relative importance of these factors and their effect on the turbulent diffusion coefficient (Webel and Shatzmann, 1984).

The purpose of this work is to describe an alternate method for calculating the transverse diffusion coefficient that utilizes multiple velocity profiles from a single cross-section to define transverse velocity gradients and Reynolds stresses which are then used to calculate the transverse diffusion coefficient. Experiments were performed in a laboratory flume over a mobile, flat bed with a high sediment transport rate. This

allowed estimation of the transverse diffusion coefficient in the presence of suspended sediment and in the absence of significant bed topography.

Methods and Equipment

Experiments were carried out at the USDA-ARS-National Sedimentation Laboratory in Oxford, MS. A 15-m x 1-m x 0.3-m sediment recirculating flume with adjustable slope and a frequency-controlled motor was used. Three personal computers were dedicated to log data from a two-component (cross-stream and downstream) Acoustic Doppler Velocimeter (ADV) that sampled velocities at 25 Hz, an ultrasonic bed height probe that sampled bed elevation at 10 Hz, and an optical backscatter probe that sampled turbidity at 10 Hz. Bed height records were filtered to remove aberrant points caused by the high suspended-sediment concentrations near the bed. Sampled positions are shown Figure 4.1. Suspended-sediment samples were collected using a vacuum system in which the intake velocity was calibrated to approximately match the average flow velocity. All reported instrument positions are based on average bed heights as

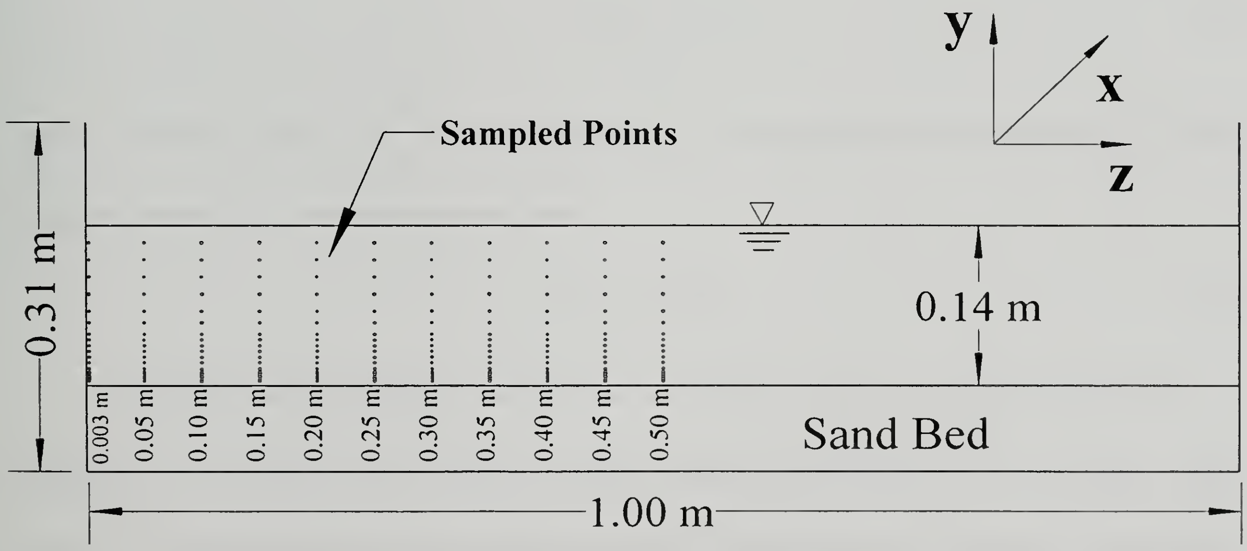

Figure 4.1. Sampled positions for supercritical flat-bed flow.

measured by the ultrasonic probe over periods of about 30 seconds. Eleven profiles of suspended-sediment concentration and fluid velocity were taken during the course of the experiment. The profiles were taken on different days, but the water depth, flume slope, and pump speed were nearly identical.

Table 4.1 summarizes the flow conditions in the experiment. Water surface slope, *S*, was calculated by linear regression of water surface elevations about a horizontal datum. Mean boundary shear stress, τ_0, was determined from

$$\tau_0 = \rho g d S \,. \tag{4.7}$$

Shear velocity was calculated from

$$u_* = \sqrt{\tau_0 / \rho} \,. \tag{4.8}$$

Mean flow velocity, $\bar{u}$, was determined from

$$\bar{u} = \frac{1}{n} \sum_{i=1}^{n} u_i \,, \tag{4.9}$$

where n=total number of observations and u_i= instantaneous downstream velocity. Froude number, *Fr*, was determined from

$$Fr = \bar{u} / \sqrt{gd} \,. \tag{4.10}$$

An upper-stage plane bed was the intended bed configuration because of its relative lack of bedforms and high suspended-sediment concentrations. The upper-stage plane bed is characterized by low relief bed forms on the order of 2 to 4 mm with little or no flow separation. As can be seen in Table 1, $Fr>1$, indicating a slightly supercritical flow. This was necessary in order to obtain flat bed conditions in the particular flume used in this study. Despite this, the array of bed form heights and periods (Figure 4.2)

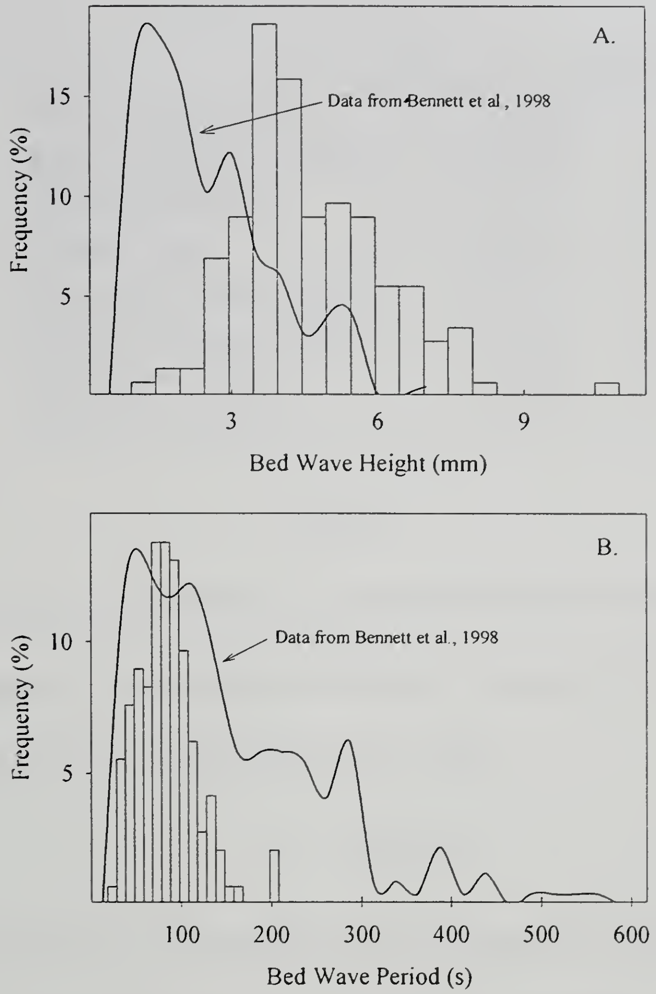

Figure 4.2. Low-relief bed wave (A) heights and (B) periods with data from Bennett et al., 1998.

shows some agreement with expected values for upper-stage plane beds from the literature (Bennett et al., 1998). However, elsewhere in the literature, it is claimed that bed features must be antidunes if supercritical conditions exist (Southard, 1971; Southard and Boguchwal, 1990). For this reason, the bed phase will be referred to as low-relief antidunes.

Table 4.1. Flow conditions for supercritical flat-bed flow.

Water surface slope, S	0.0051
Shear velocity, u_* (m/s)	0.084
Froude number, Fr	1.13
Depth, d (m)	0.14
Bed shear stress, τ_0 (Pa)	6.99
Mean velocity, $\bar{u}$ (m/s)	1.33
Discharge, Q (m^3/s)	0.186
Grain size, D_{50} (mm)	0.55

Theory

The vertical mixing coefficient can be theoretically determined using Prandtl's mixing length hypothesis, where vertical diffusivity is related to the vertical velocity gradient as in the following equation (Henderson, 1966):

$$\varepsilon_y = L_m^2 \left| d\bar{u}/dy \right| \tag{4.11}$$

where y is vertical distance, ε_y is vertical diffusivity, and L_m is Prandtl's mixing length. Using this approach for the transverse diffusivity was criticized by Rutherford, 1994, because the mean velocity does not vary across a channel in plane shear flow. Rutherford also argued that if the gradient, $d\bar{u}/dy$, were replaced with $d\bar{u}/dz$, the resulting equation would only predict the diffusivity near the sidewalls and not in the central portion of the flow. In the following paragraphs, justification is given for using $d\bar{w}/dz$, (where $\bar{w}$ is the mean cross-stream velocity) rather than $d\bar{u}/dz$, along with the transverse Reynolds stress to predict the transverse diffusivity.

In the downstream direction, fluid flow is resisted by shear stresses caused by fluid viscosity and by the movement of slower moving fluid near the wall into areas with

higher average velocities. If both of these retarding effects are termed fluid shear, the total resistance to fluid flow due to shear can be written

$$\tau = (\mu + \eta)(d\bar{u}/dy), \tag{4.12}$$

where τ is shear stress, μ is dynamic viscosity, and η is eddy viscosity. In a turbulent environment, the dynamic viscosity can be considered small, so that

$$\tau_t = \rho \varepsilon_y (d\bar{u}/dy) \tag{4.13}$$

and

$$\eta = \rho \varepsilon_y, \tag{4.14}$$

where ε_y is kinematic eddy viscosity, and τ_t is turbulent shear stress. Turbulent shear may also be represented by

$$\tau_t = -\rho \overline{u'v'} \tag{4.15}$$

where u' and v' are the turbulent velocity fluctuations in the x and y directions. If the two expressions for turbulent shear are equated, an expression for the kinematic eddy viscosity can be found:

$$\varepsilon_y = -\overline{u'v'}/(d\bar{u}/dy) \tag{4.16}$$

(Nezu and Nakagawa, 1993). If it is assumed that fluid and its entrained particles move at the same velocity, the kinematic eddy viscosity is equal to the turbulent diffusion coefficient.

Downstream fluid flow is resisted by fluid moving away from both the bottom and sidewalls of a channel. In natural channels and most flumes, the shear due to the bottom is much larger since the width is generally much larger than the depth. Sidewall

effects are not important over a significant portion of the channel width. For this reason, flow resistance or mixing caused by fluid movement in the y-z plane requires a different treatment from fluid movement in the x-y plane. It is arguable that little flow resistance will be caused by fluid moving in the y-z plane, except near the sidewalls. However, fluid moving in the y-z plane will certainly affect transverse mixing. In order to predict transverse mixing with a single coefficient, the effect of secondary currents and turbulent diffusion must be combined. If the same reasoning from the previous paragraph is applied in the transverse direction, the resulting equation for the transverse diffusion coefficient would be

$$\varepsilon_z = -\overline{u'w'}/\left(d\overline{u}/dz\right), \tag{4.17}$$

where w' is the turbulent velocity fluctuation in the z direction. As previously stated, the gradient, $d\overline{u}/dz$, will only be present near the wall and will not adequately predict mixing due to secondary circulation cells. It is proposed that $d\overline{w}/dz$ would be the more appropriate quantity to use in calculating the transverse eddy diffusivity because it addresses the changes in transverse velocity across the channel. Using this, the expression for the transverse diffusion coefficient is

$$\varepsilon_z = -\overline{u'w'}/\left(d\overline{w}/dz\right). \tag{4.18}$$

It is important to note here that both $-\overline{u'w'}$ and $d\overline{w}/dz$ are small quantities.

Calculation Method

Several steps were necessary for calculating the transverse diffusion coefficient over the entire sampled flow field. Because of the moving bed, velocity samples from

different profiles were not at the same average height over the bed. The mean cross-stream velocity values were entered into a commercial software package that uses Kriging to create a regularly spaced grid. Figure 4.3 is a contour map of $\overline{w}$ over a 50x50 grid.

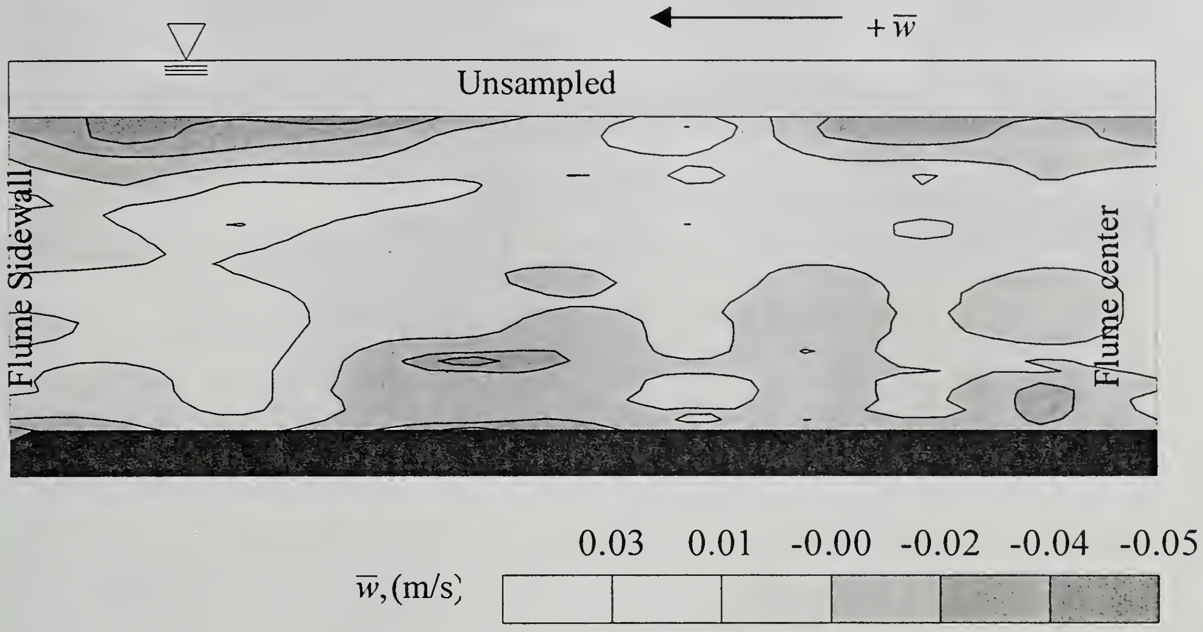

Figure 4.3. $\overline{w}$ over ½ the flume width.

To calculate gradients, horizontal rows of gridded $\overline{w}$ data were fitted by a high-order polynomial. The derivative of the polynomial was then taken so that the gradient, $d\overline{w}/dz$, was known for all points in the grid (Figure 4.4). Figure 4.5 shows an example curve fit for one horizontal row of $\overline{w}$ and the resulting values of $d\overline{w}/dz$. The transverse Reynolds stress (Figure 4.6) was calculated using the following:

$$-\overline{u'w'} = -\frac{1}{n}\sum_{i=1}^{n}(u_i - \overline{u})(w_i - \overline{w}). \tag{3.17}$$

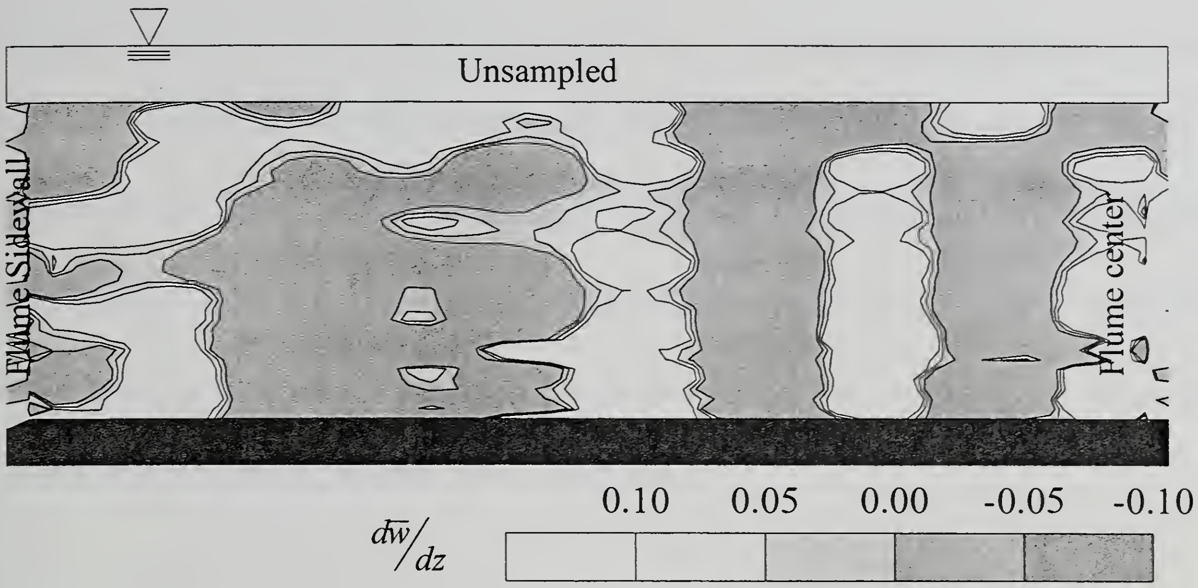

Figure 4.4. $d\overline{w}/dz$ over ½ the flume width.

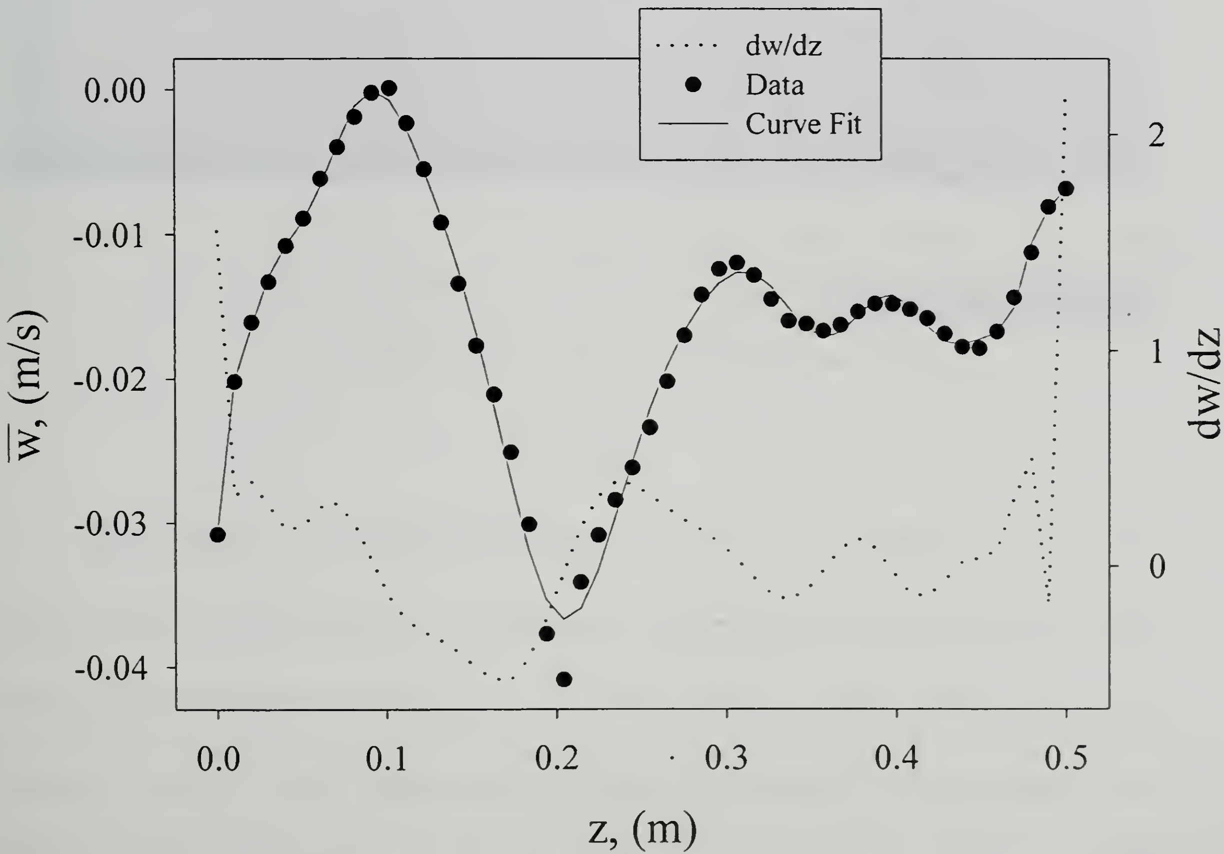

Figure 4.5. Curve fit and $d\overline{w}/dz$ for one horizontal row of data.

The fluid density canceled out in the calculation of the transverse diffusion coefficient and was not included. The final step in calculating ε_z is to divide each point in the grid of $-\overline{u'w'}$ by each value of $d\overline{w}/dz$, resulting in Figure 4.7, a map of ε_z over the sampled half of the flume width. Since the transverse diffusion coefficient is not used to determine a direction for mixing, results are presented as absolute values. In Figure 4.7 ε_z has been non-dimensionalized by dividing it by u_* and depth.

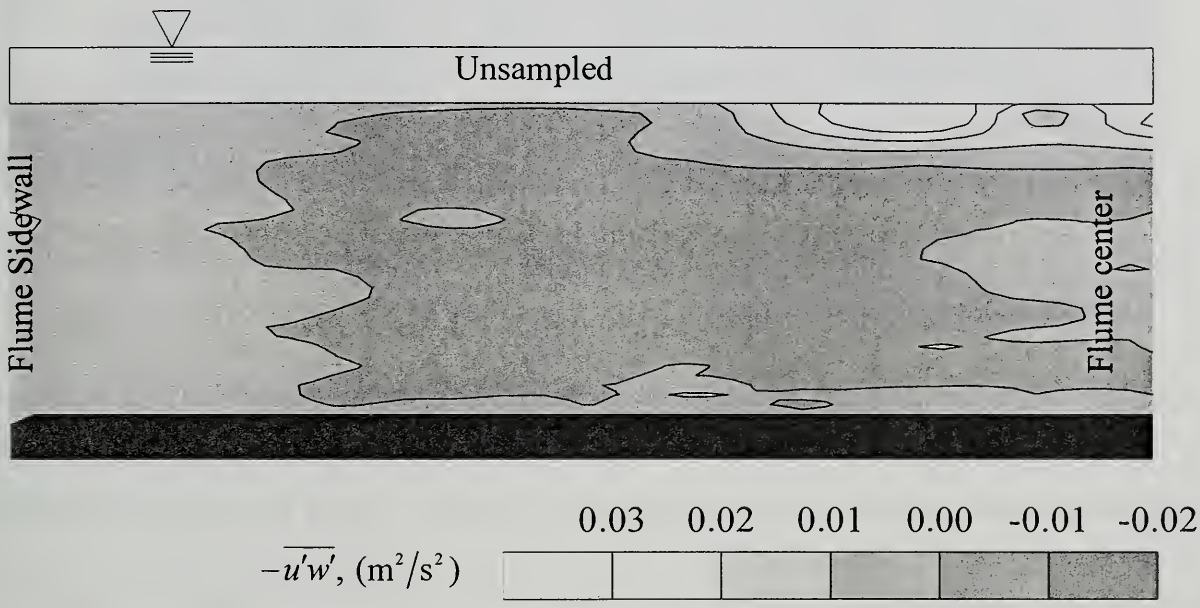

Figure 4.6. $-\overline{u'w'}$ over ½ the flume width.

Results

The majority of the calculated values of the dispersion coefficient across the sampled flume are less than 0.2. If the results directly from the map in Figure 4.7 are averaged, and the highest 20% of the data is removed, the average value is 0.21. It is necessary to remove these higher values because at extrema of the polynomial fit of $\overline{w}$, $d\overline{w}/dz$ can be small, causing some very high values of the diffusion coefficient. Examples of this are seen in Figure 4.4 where the plot for $d\overline{w}/dz$ crosses 0 each time the

plot of fitted data for $\overline{w}$ reaches a peak or valley. As seen in Figure 4.7, there is no clearly discernable pattern for ε_z. However, it can be seen that two areas in particular exhibit higher values for the transverse diffusion coefficient. Near the sidewall,

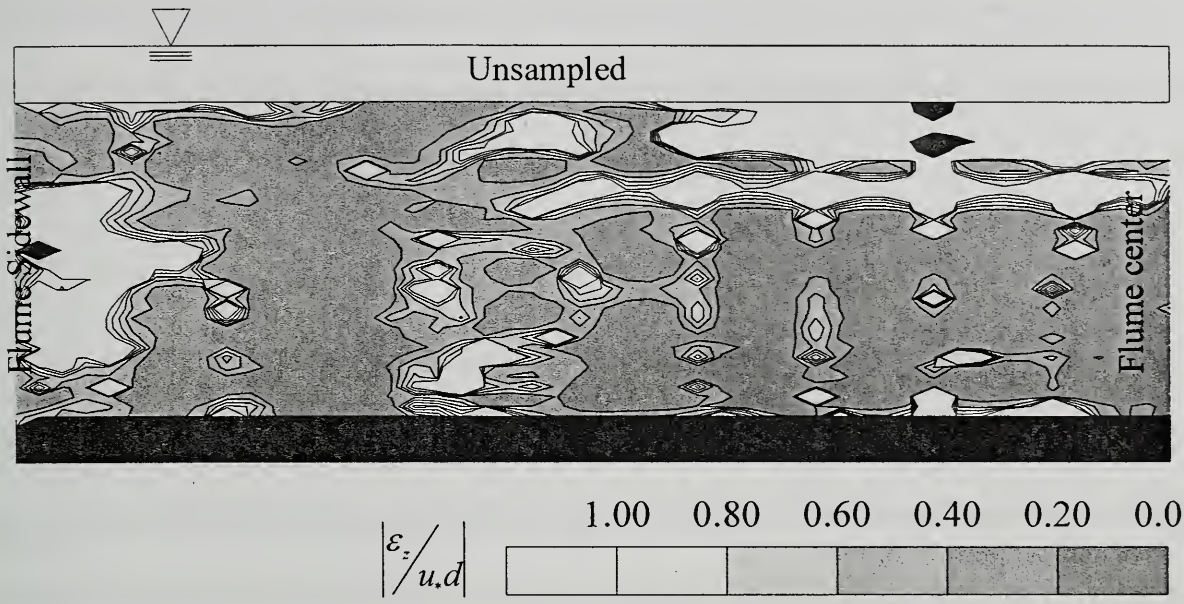

Figure 4.7. Transverse diffusion coefficient non-dimensionalized with shear velocity and flow depth.

turbulence intensity is higher, resulting in higher u' and w' values; hence the diffusion coefficient is higher. The top right corner of Figure 4.7 corresponds to the flume centerline near the surface, and the higher values there are likely due to secondary circulation. The presence of secondary circulation cells is confirmed by the depression of maximum downstream velocity below the water surface (not shown).

The value for the non-dimensionalized diffusion coefficient agrees well with previous studies. Webel and Schatzmann , 1982, report values in the range 0.130-0.177 for their experiments. Lau and Krishnappan, 1978, compiled data from earlier

experiments that were in the range 0.08-0.24 and note that published values for natural streams are as high as 10. Beltaos (1980) reported values of 0.4-2.5.

The effectiveness of the procedure described here for calculating the diffusion coefficient could be validated by performing laboratory and field tests using the new method and the dye injection method and making direct comparisons of the results. For the best results, the tests should be carried out simultaneously.

Conclusions

A new method for calculating the transverse dispersion coefficient from velocity and turbulence data was investigated. It is based on measurements of fluid velocity and turbulence collected with an acoustic Doppler velocimeter in a laboratory flume. The method reports values that are comparable with those measured by previous researchers. However, the method does produce locally high values of ε_z that must be filtered out before a meaningful result can be obtained.

CHAPTER V

DISTRIBUTIONS OF VELOCITY, TURBULENCE, AND SUSPENDED-SEDIMENT OVER LOW-RELIEF ANTIDUNES

Introduction

The study of suspended-sediment transport is important for those involved in many areas of fluvial hydraulics. The modeling of sediment transport is key in forecasting the effectiveness of hydraulic structures such as dams and grade control structures. The associated study of turbulence as the mechanism for the transport of suspended sediment is equally important. While sub-critical flows have been studied extensively, much less information is available on the application of standard velocity, turbulence intensity and concentration profile equations in a supercritical flow. Although much less common than subcritical flow, supercritical flows occur in limited reaches of high-gradient streams and in isolated areas of lower-gradient streams (Trieste, 1992; Simon and Hardison, 1994; and Jarrett, R. D, 1984). Experimental objectives were to examine distributions of velocity, turbulence intensity, and suspended-sediment concentration over a flat, equilibrium sand bed in supercritical flow conditions and to assess theories and empirical functions commonly used in subcritical flows.

Many areas of hydraulics and sediment transport require the modeling of the vertical velocity profile. Although only strictly applicable to the first 20% of flow depth, the Kármán-Prandtl law of the wall,

$$u/u_* = (1/\kappa)\ln(y/y_0), \tag{5.1}$$

where u=downstream velocity, κ is the Von Karman coefficient,

$$u_* = \sqrt{\tau_0/\rho} \tag{5.2}$$

where τ_0 is bed shear stress, ρ is the fluid density, and y_0 is the zero velocity roughness height, is often applied to the entire flow depth and may be used to examine the effects of suspended sediment on the velocity profile. The law of the wall is a key equation that is widely used in hydraulic modeling. Of particular interest is the effect of suspended sediment on the velocity profile. (Itakura and Kishi, 1980; Lyn, 1992; Coleman, 1981 and 1986; Hino, 1963; and others). In this work, the applicability of law of the wall in a sediment-laden, supercritical flow is assessed.

The distribution of turbulence intensity in a channel is an indicator of a flow's ability to maintain sediment in suspension. A semi-theoretical approach to predicting the vertical variation of turbulence intensity was taken by Nezu and Nakagawa, 1993. Data from numerous studies was used to calibrate a theoretical model for turbulence intensity resulting in the following equations:

$$\mathrm{rms}\, u'/u_* = 2.30\exp(-y/d), \tag{5.3}$$

$$\mathrm{rms}\, v'/u_* = 1.27\exp(-y/d), \tag{5.4}$$

$$\mathrm{rms}\, w'/u_* = 1.63\exp(-y/d), \tag{5.5}$$

where

$$\mathrm{rms}\, u' = \left[\frac{1}{n}\sum_{i=1}^{n}(u_i - \bar{u})^2\right]^{0.5}, \tag{5.6}$$

$$\mathrm{rms}\, v' = \left[\frac{1}{n}\sum_{i=1}^{n}(v_i - \bar{v})^2\right]^{0.5}, \tag{5.7}$$

and

$$\text{rms}\, w' = \left[\frac{1}{n} \sum_{i=1}^{n} \left(w_i - \overline{w} \right)^2 \right]^{0.5}, \tag{5.8}$$

where n is the number of measurements, u_i, v_i, and w_i are instantaneous velocities in the downstream, vertical and lateral directions, respectively. The data on which these equations are based was taken for clear water flows over smooth beds. One goal of the present experiment was to compare these equation's to results obtained on a reasonably flat, equilibrium sand bed with large suspended-sediment concentrations.

Predicting the variation of suspended-sediment concentration with depth is one of the most important areas in sediment research. This information is used to calculate suspended-sediment flux from limited sample information and to model the vertical concentration gradient. Probably the most well known equation for predicting the vertical variation of suspended-sediment concentration was derived by Hunter Rouse in 1936. The Rouse equation is:

$$\frac{C}{C_a} = \left[\frac{d-y}{y} \frac{a}{d-a} \right]^{r} \tag{5.9}$$

where C is suspended-sediment concentration at a given depth, d, C_a is the reference concentration at the reference depth a, d is the total depth, y is the vertical position,

$$r = {}^{w_s}\!\!\diagup_{\beta \kappa u_*} \tag{5.10}$$

where w_s is sediment particle fall velocity, β is a numerical constant relating momentum transfer to mass transfer, and u_* is the shear velocity (Vanoni, 1975). Some of the main assumptions on which the Rouse equation was based follow. For a stream in equilibrium,

the rate of upward sediment transfer by turbulence will be equaled by the downward movement due to settling:

$$Cw_s + \varepsilon_s \, dC/dy = 0\,, \tag{5.11}$$

where ε_s is the sediment transfer coefficient. The turbulent transport of momentum is related to the transport of particles:

$$\varepsilon_s = \beta \varepsilon_m\,, \tag{5.12}$$

where

$$\varepsilon_m = \kappa y u_* (1 - y/d)\,. \tag{5.13}$$

The distribution of shear stress is linear with depth:

$$\tau = \tau_0 ((d - y)/d), \tag{5.14}$$

where τ is fluid shear stress and τ_0 is the shear stress at the bed. Distributions of mixing length, l, and eddy viscosity, ε_m, are parabolic:

$$l = \kappa y \sqrt{1 - y/d} \tag{4.15}$$

and ε_m is defined above. Other early work on modeling the vertical concentration profile came from Lane and Kalinske (1941) and Vanoni (1941). Since then, many authors have either modified the Rouse equation or formulated new approaches (Willis, 1979; Jobson and Sayre, 1970; Itakura and Kishi, 1980; Antsyferov and Kos'yan 1980; McTigue 1981; Samaga et al. 1985; Van Rijn, 1984; Karim and Kennedy, 1987; Nielson, 1995). Here, the applicability of the Rouse equation in a supercritical flow over low-relief anti-dunes is examined.

The goals of the present experiment can be summarized as follows: (1) assess the applicability of the law of the wall in a sediment-laden, supercritical flow, (2) compare measured turbulence intensities with semi-theoretical equations, and (3) to assess the effectiveness of the Rouse equation in predicting concentration profiles in a supercritical flow.

Experimental Equipment and Procedure

Experiments were carried out at the USDA-ARS-National Sedimentation Laboratory in Oxford, MS. A 15 m x 1 m x 0.3 m sediment recirculating flume with adjustable slope and a frequency-controlled motor was used. Three personal computers were dedicated to log data from a two-component (cross-stream and downstream) acoustic Doppler velocimeter (ADV) that sampled velocities at 25 Hz, an ultrasonic bed height probe that sampled bed elevation at 10 Hz, and an optical backscatter probe that sampled turbidity at 10 Hz. Instrument positions are shown Figure 1. ADV data were subjected to a Gaussian filter. Suspended-sediment samples were collected using a vacuum system in which the intake velocity was calibrated to approximately match the average flow velocity. All reported instrument positions are based on average bed heights as measured by the ultrasonic probe over periods of about 30 seconds. Eleven profiles of suspended-sediment concentration and fluid velocity were taken with an ADV during the course of the experiment. See Appendix A for detailed ADV profile data and Appendix C for maps of various flow parameters created from gridded ADV data. Four profiles of fluid velocity were taken with a Laser Doppler Anemometer (LDA) which recorded vertical and downstream flow velocity at a variable data rate. Only four LDA

profiles were possible because the high suspended-sediment concentrations in the flow prevented the laser from penetrating more than 20 cm into the flume. See Appendix A for velocity profile data.

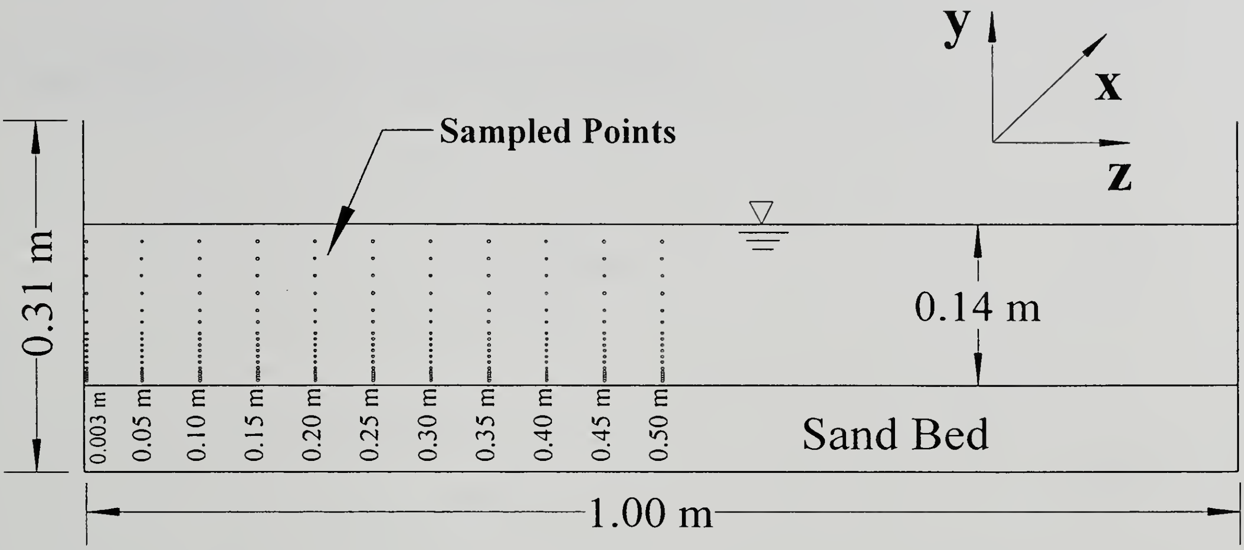

Figure 5.1. Sampled positions for supercritical flow parameter study.

Table 5.1. Flow conditions for ADV and LDA data collection.

	ADV	LDA
Water surface slope, S	0.0051	0.0046
Shear velocity, u_* (m/s)	0.084	0.079
Froude number, Fr	1.13	1.09
Depth, d (m)	0.14	0.14
Bed shear stress, τ_0 (Pa)	6.99	6.32
Mean velocity, $\bar{u}$ (m/s)	1.33	1.28
Discharge, Q (m^3/s)	0.186	0.179
Grain size, D_{50} (mm)	0.55	0.55

Table 5.1 summarizes the flow conditions in the experiment. Water surface slope, S, was calculated by linear regression of water surface elevations about a horizontal datum. Mean boundary shear stress, τ_0, was determined from

$$\tau_0 = \rho g d S \tag{5.16}$$

where ρ= fluid density, g=acceleration of gravity. Shear velocity, u_*, was calculated from

$$u_* = \sqrt{\tau_0/\rho}\,. \tag{5.17}$$

Depth-integrated flow velocity, U, was determined from

$$U = \frac{1}{d}\,{}^{d}_{0}\,\bar{u}\,dy \tag{5.18}$$

where

$$\bar{u} = \frac{1}{n}\,{}^{n}_{i=1}\,u_i\,, \tag{5.19}$$

where n is the total number of observations and u_i is a single measurement of downstream velocity. Froude number, Fr, was determined from

$$Fr = U/\sqrt{gd}\,. \tag{5.20}$$

The discrepancies in bulk hydraulic parameters between ADV and LDA runs are due to a slowly degrading pump impeller, which had the effect of lowering discharge while having the same indicator setting for the motor controller. This problem was not revealed until after the experiment when the data was analyzed. For the purposes of the comparisons used here, the similarity of the conditions was considered acceptable.

Bed Phase

The goals of the experiment were not related to a specific bed phase, but they did require an equilibrium sediment bed without separated flow created by large-scale bedforms. The available flume and sediment were not able to produce a subcritical flow

with low-relief bed features, but a supercritical flow with suitably low-scale features was attainable. With this in mind, it was necessary to determine a suitable designation for the bed phase. The following discussion addresses this issue.

The minimal relief of low antidunes and upper-stage plane beds makes it difficult to distinguish between the two bed phases. Visual observation of the bed is not reliable, because of the small scale of the features and because of the subtle influence of these features on the water surface (Cheel, 1990). If detailed measurements of the water surface elevation are available, the distinction can be made based on whether water surface waves are in-phase with bed waves (antidunes) or out of phase (upper-stage plane bed) (Simons and Richardson, 1961; Task Force, 1966). Sediment size, water depth, velocity and Froude number may also be used as indicators (Southard, 1971; Southard and Boguchwal, 1990). $Fr>1$ is generally accepted as a criterion for antidunes; however, experiments show that upper-stage plane beds occur in some supercritical flows (Guy et al., 1966). In the present case, detailed measurements of the water surface were not available, and only a single acoustic probe was available for measuring bed-height fluctuation. This arrangement allowed only period and amplitude of bed-waves to be measured. In a direct comparison of frequency distributions of bed-wave height and period with the data of Bennett et al., 1998 (Figure 5.2), the distributions from the present work show that bed waves were higher and bed wave periods were shorter and had a smaller range of frequencies. Comparisons to various bed-phase diagrams of Southard and Boguchwal, 1990, and Allen, 1985 place the current conditions in the antidune region.

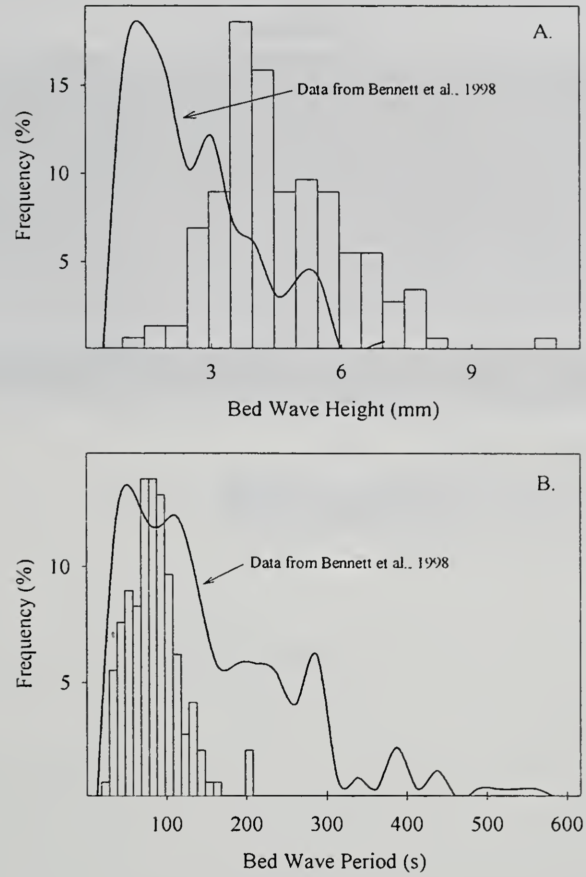

Figure 5.2. Low-relief bed wave (A) heights and (B) periods with data from Bennett et al., 1998.

The bed condition in this experiment was likely a transition phase between low-relief bed waves of the upper-stage plane bed and anti-dunes. It was decided to call the bed phase low-relief antidunes.

Velocity Profiles

A contour map (Figure 5.3A) of the downstream velocity illustrates the presence of a velocity defect in the flow. Where, necessary, velocity points in the defect region were eliminated and δ, the defect height, was used in place of d. Vertical velocity

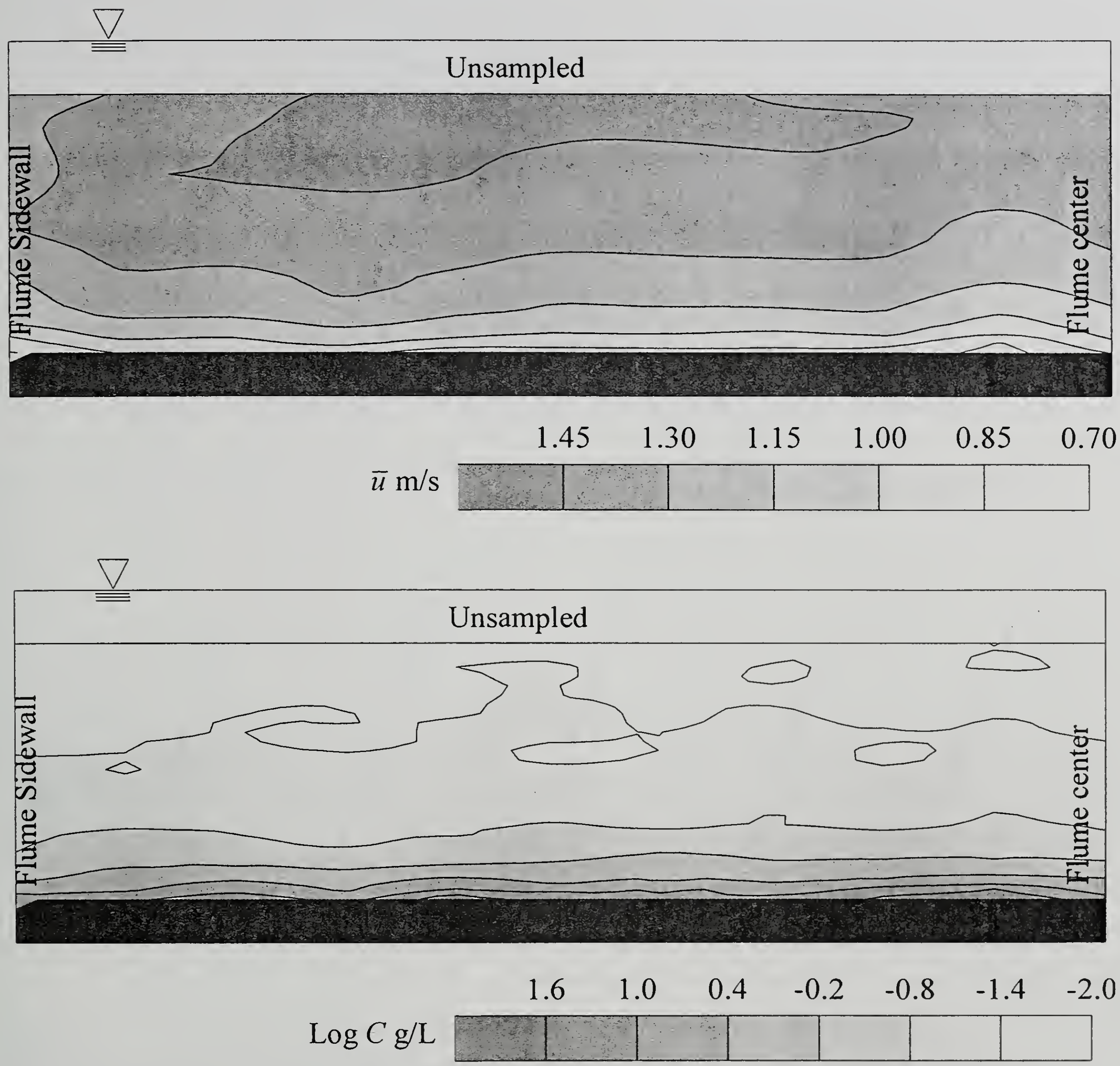

Figure 5.3. Contour maps of (A) downstream velocity and (B) suspended sediment concentration.

profiles were compared with the Kármán-Prandtl law of the wall by regressing time averaged downstream velocity, $\bar{u}$, against $\ln y$ so that

$$\kappa = u_*/m \tag{5.21}$$

where m is the slope of the regression line and

$$y_0 = e^{-b/m} \tag{5.22}$$

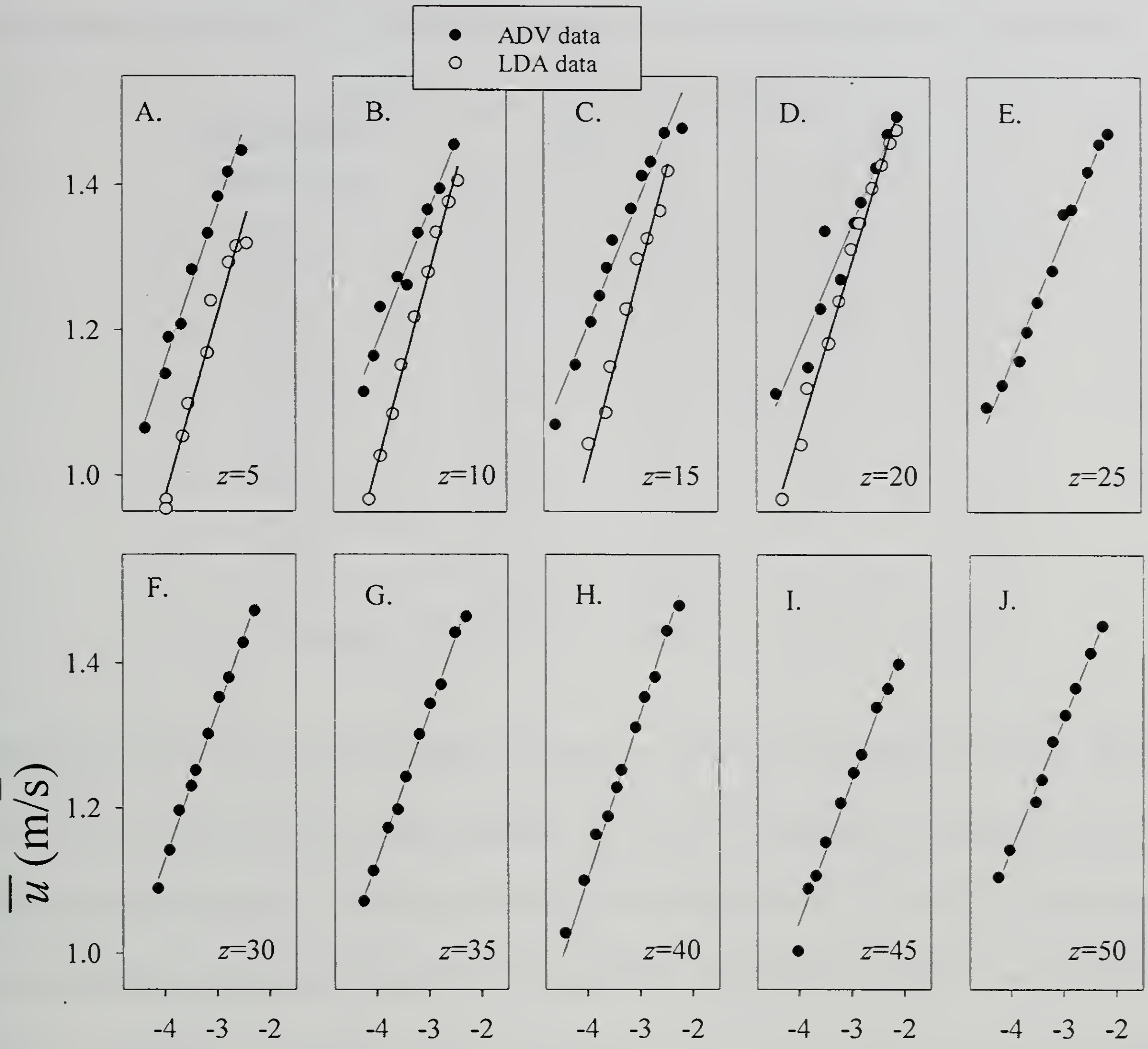

Figure 5.4. Velocity profiles regressed against $\ln y$ for (A) 5, (B) 10, (C) 15, and (D) 20 cm from the sidewall measured with both an ADV and an LDA and for (E) 25, (F) 30, (G) 35, (H) 40, (I) 45, and (J) 50 cm from the sidewall measured with an ADV only.

where b is the y intercept of the regression line (Figure 5.4). Velocity profiles included points where $10\,\text{mm} < y < \delta$. 10 mm was chosen as the cutoff point because it is just above the highest bed waves measured in the experiment. Using u_* as defined above, $\kappa \approx 0.42$ and $y_0 \approx 0.07\,\text{mm}$. The average equivalent sand roughness,

$$k_s = 30.2 y_0, \tag{5.23}$$

was approximately 2 mm. The detailed results in Table 5.2 show that κ, in profiles

Table 5.2. Law of the wall results.

Distance From Sidewall (m)	ADV		LDA	
	k_s (mm)	κ	k_s (mm)	κ
0.05	2.5	0.39	11.4	0.32
0.10	0.9	0.46	12.6	0.30
0.15	0.7	0.47	14.1	0.29
0.20	0.6	0.48	6.5	0.34
0.25	0.8	0.47	----	----
0.30	2.2	0.41	----	----
0.35	2.2	0.41	----	----
0.40	4.2	0.37	----	----
0.45	2.6	0.43	----	----
0.50	0.9	0.47	----	----
Averages:	1.77	0.44	11.2	0.31

measured by the ADV, varies slightly but averages near the accepted clear-water value of 0.41. The κ values from profiles measured with the LDA are lower, averaging 0.31. The difference in measured κ values may be due to several factors. The LDA probe has a much smaller measurement volume and higher data collection rate when compared to the ADV. The LDA was unable to measure points below y/d=0.12 due to the convergence angle of the beams; measurements below this point could have altered the value of κ. Lastly, even though the conditions were deemed acceptably close, the differences in bulk flow may have played a role in the differences in κ. The differences in bulk flow properties are a possible cause of the difference in equivalent sand roughness.

Turbulence Intensities

The ADV has been used to examine turbulence intensities and/or turbulence spectra in a number of studies (Nikora and Goring, 2000, Vendetti and Bennett, 2000, Lane et al. 1998). The ADV is reported to measure Reynolds stresses, and therefore

turbulence intensities, with equal accuracy to a laser instrument (Lohrmann, et al., 1994). The interpretation of ADV measurements has also received attention (Nikora and Goring, 1998).

Velocity profile data was used to examine the vertical distribution of turbulence intensities. Figure 5.5 shows the turbulence intensity as measured with the ADV and the LDA. In 5.5A and 5.5B, the LDA data shows good agreement with the semi-theoretical curves. This result appears to show that, over low-relief antidunes, the turbulence intensity is independent of both roughness and suspended sediment. In figures 5.5C and 5.5D, the ADV data shows a noticeable shift to lower intensities than either the semi-theoretical curves or the LDA data. Reasons for this may include the larger sampling volume and lower frequency of data collection as compared to the LDA.

Suspended-Sediment Concentration Profile

A map of the suspended-sediment concentration data obtained in this experiment is seen in Figure 5.3B. The suitability of the Rouse equation for predicting concentration profiles in this supercritical flow is verified by the successful application of the law of the wall velocity distribution in the previous section, by the linear fit of measured values of $-\overline{u'v'}$ seen in Figure 5.6, and, in Figure 5.7, the parabolic shape of the distribution of eddy viscosities. In Figure 5.7, the measured eddy viscosities fit reasonably well up to $y/\delta=0.3$. Except for z=0.15 m, agreement of measured eddy viscosities with the Karman eddy viscosity model exhibit correlation coefficients above 0.9, further demonstrating agreement.

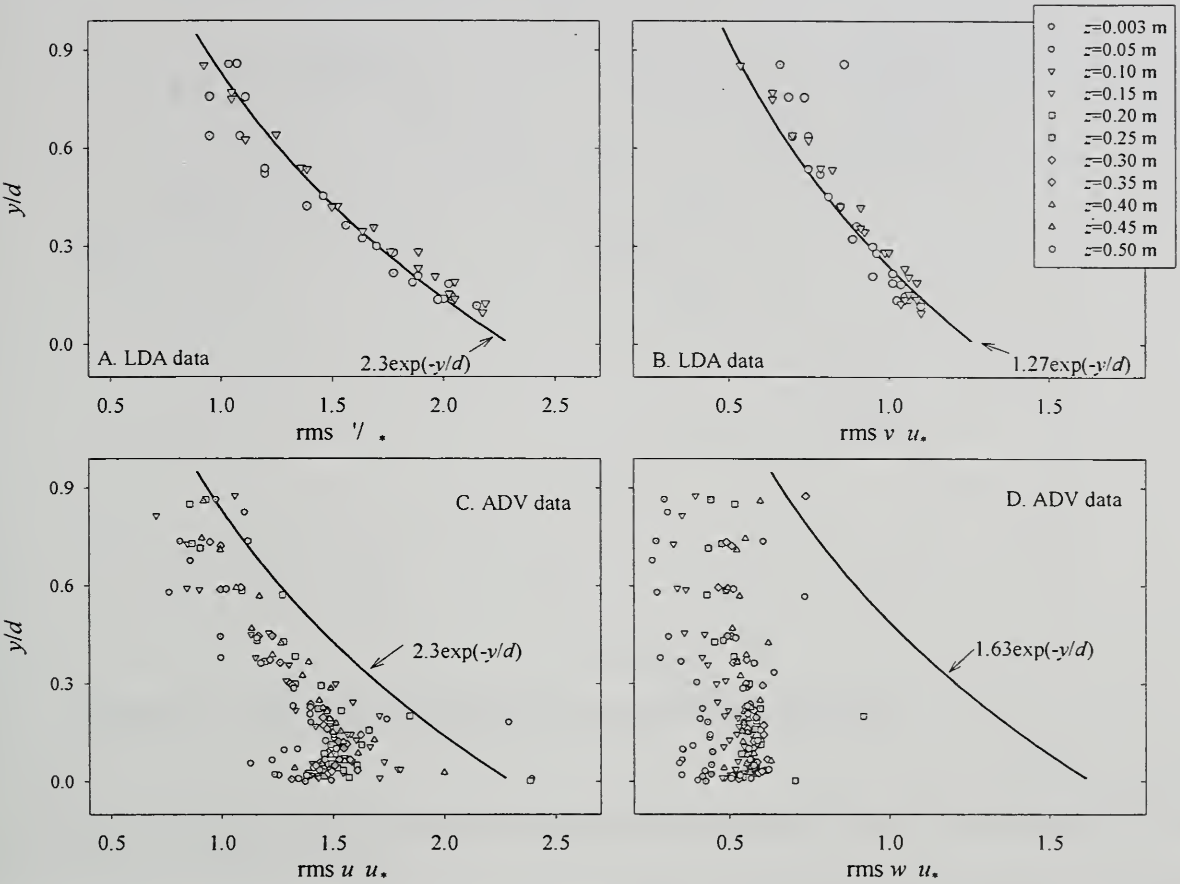

Figure 5.5. Non-dimensionalized turbulence intensities collected with (A) and (B) an LDA and (C) and (D) an ADV compared to semi-theoretical curves from Nezu and Nakagawa, 1993.

The Rouse equation was found to deviate from the measured concentration data around y/d=0.2 (Figure 5.8). Bennett et al., 1998, show a similar result, with the deviation occurring near y/d=0.4 (Figure 5.9B). Wren (2000) (from an unpublished data set: D_{50}=0.23 mm, Fr=0.70, u_*=0.056 m/s, U=0.76 m/s, w_s=0.025 m/s (fall velocity from Dietrich, 1982)), also shows a similar result, with the deviation around y/d=0.3. Since this deviation occurs in the upper section of flow, its effect on sediment flux as modeled by the Rouse equation will be small.

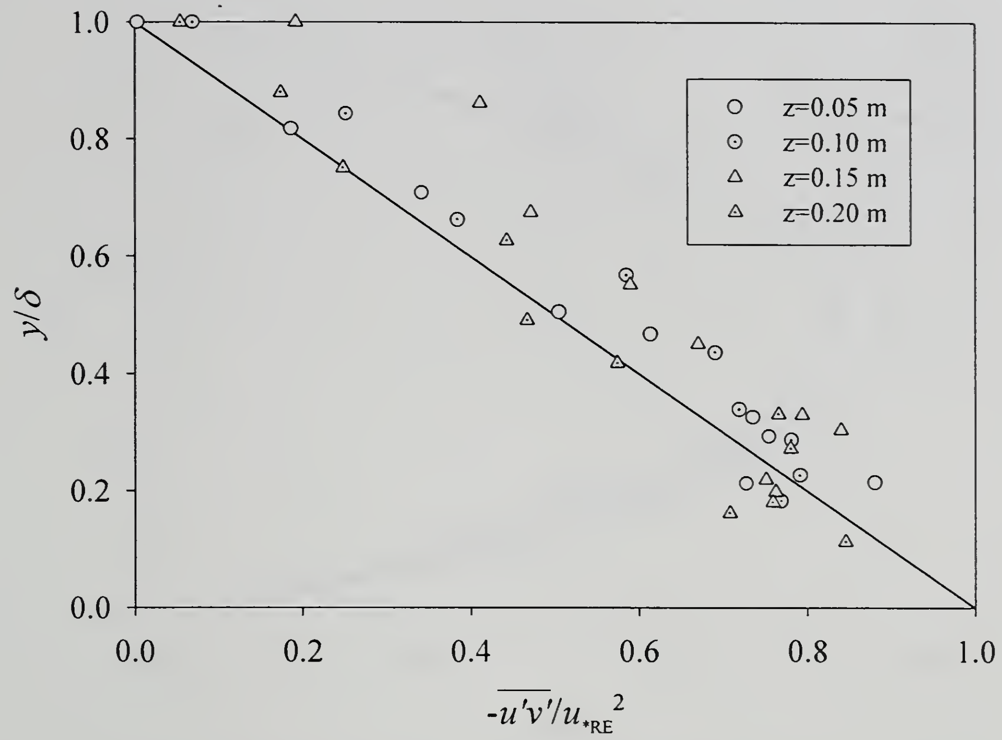

Figure 5.6. Profiles of spatially averaged Reynolds stress

In Table 3, measured and calculated suspended-sediment fluxes are compared. In each concentration profile, a, and its corresponding C_a was chosen as close to 2.5 mm as possible based on the results of calculating the saltation height of sand grains (Bridge and Dominic, 1984; Bagnold, 1973; Einstein, 1950). w_s was estimated to be 0.078 m/s from Dietrich (1982) and was measured by timing the fall of particles to be 0.061 m/s, which was the value used for fall velocity for 0.55-mm sand in this work. In three of the ten profiles, the modified equation yields worse results, but in the others, it yielded a marginally better approximation. These results show that the deviation in the upper section of the profile is relatively unimportant in flux calculations. However, as a method for examining the physics of the flow, a better fit for Rouse equation was sought by allowing the β function vary from 1 to 2 with depth. This approach is described below.

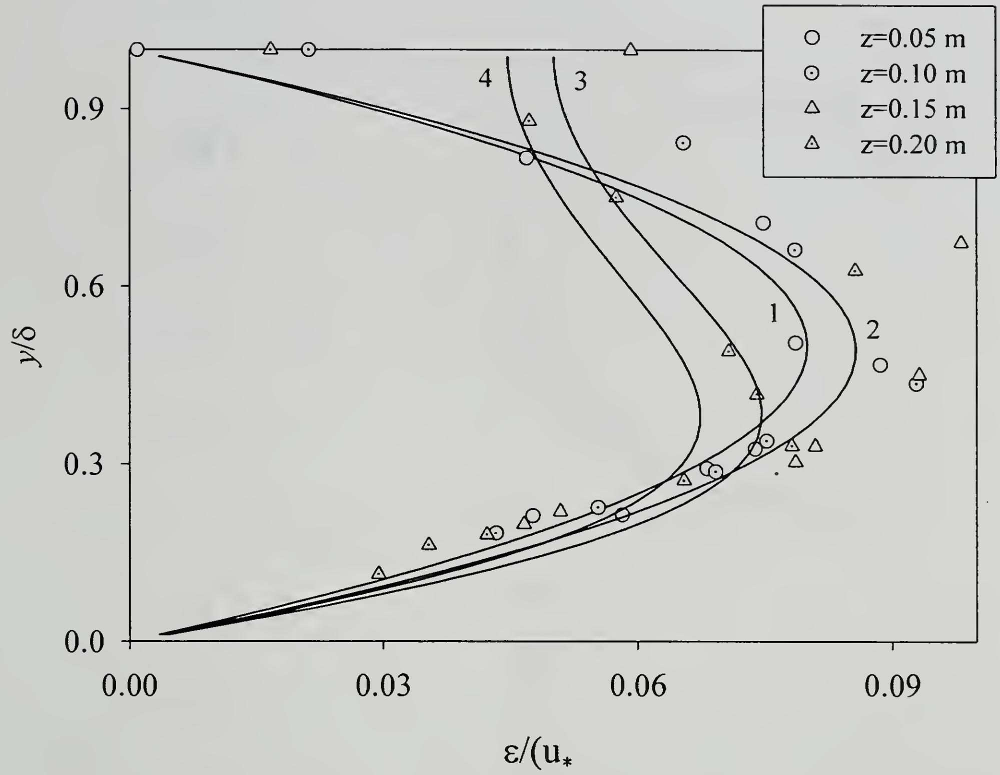

Figure 5.7. Eddy viscosities from LDA data (points) with several models for eddy viscosity. Curve 1 is from the Karman model given in the text, curve 2 is from Itakura and Kishi (1980), curve 3 from Gelfenbaum and Smith, (1980), and curve 4 is from Smith and McLean (1977).`

Coleman (1970) used the diffusion settling balance equation to directly calculate the sediment transfer coefficient from point sampled suspended-sediment concentration data. Figure 5.10 shows the result of applying this approach to the current data set. As in Coleman's work, ε_s follows a different trend from ε_m, showing no tendency to decrease near the water surface. This suggests that β may vary for different flows or even within a vertical concentration profile, a conclusion that has previously been reached (Cellino and Graf, 2000; Bennett et al. 1998, van Rijn, 1984). The empirical fit function in Figure 5.11 was arrived at after much trial and error. Using any higher than second power for

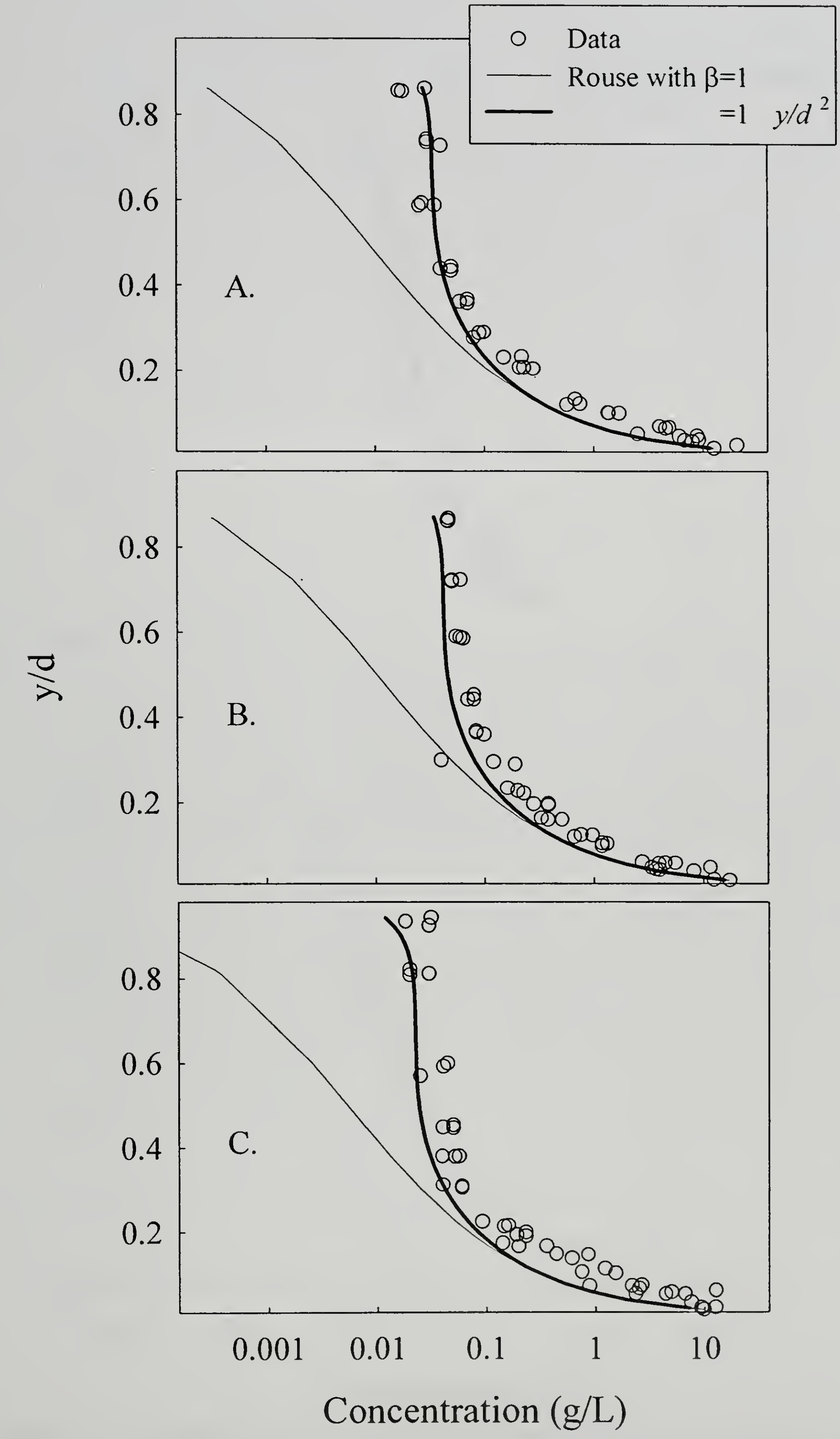

Figure 5.8. Rouse equation fits of suspended-sediment concentration data with $\beta=1$ and $\beta=1+(y/d)^2$ for three distances from the flume sidewall: (A) 0.5, (B) 0.35 m, and (C) 0.15 m.

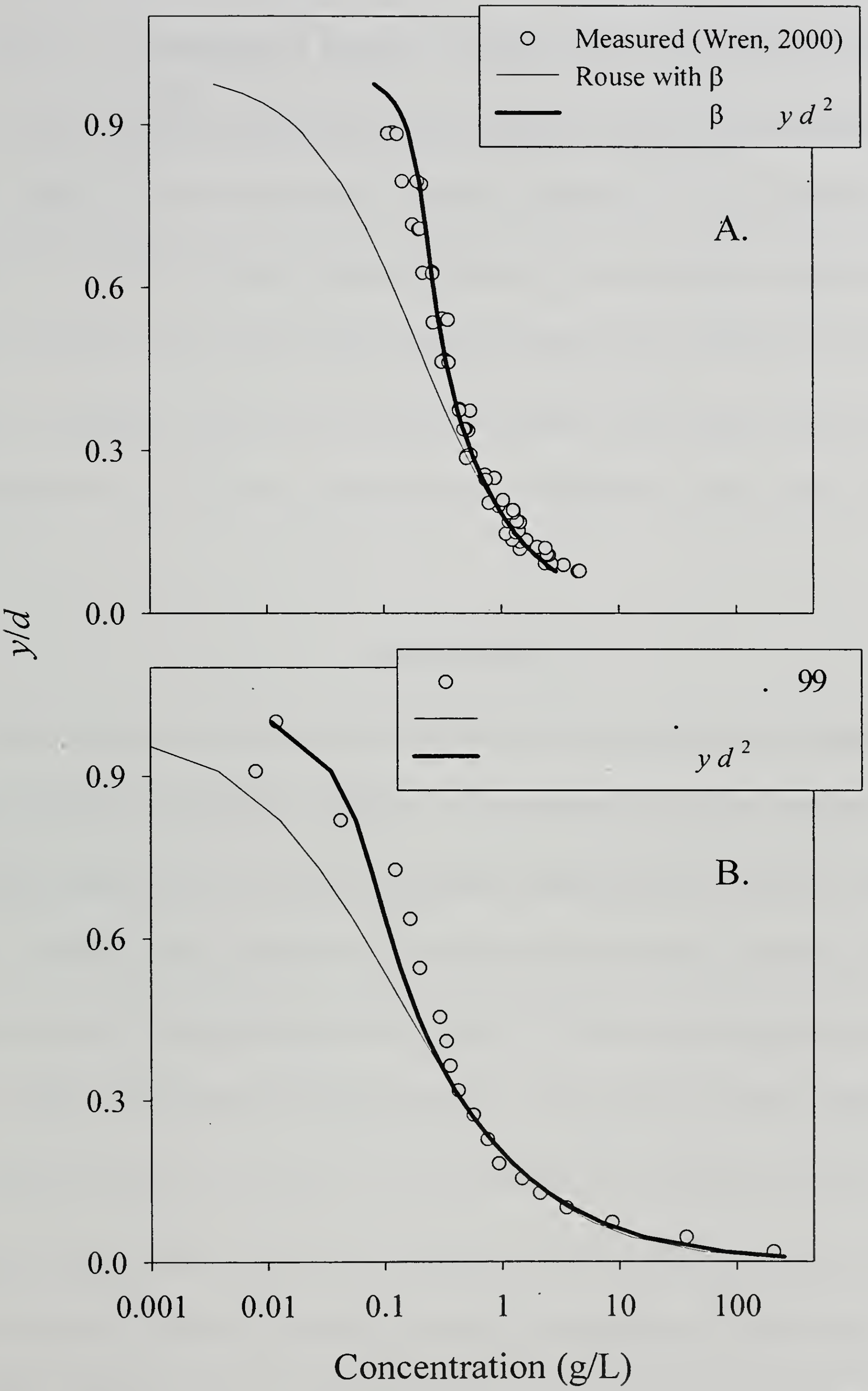

Figure 5.9. Comparison of concentration data from (A) Bennett et al., 1998, and (B)Wren, 2000 with the Rouse equation and a modified version of the Rouse equation that varies *β* from 1-2 with depth.

y/d resulted in poor fits when the β function was introduced into the Rouse equation. Above y/d=0.7, the empirical β function diverges from the calculated points, but, as shown in Figure 5.8, the empirical function results in a better fit in the upper portion of the flow depth for the concentration profiles obtained in this experiment. w_s was estimated to be 0.078 m/s from Dietrich, 1982 and was measured by timing the fall of particles to be 0.061 m/s, which was the value used for fall velocity for 0.55 mm sand in this work. In Figure 5.9, the same approach is applied to the upper-stage plane bed data from Bennett et al., 1998, and to the data set collected by Wren, 2000, with similar results.

Discussion

The extension of relationships developed for subcritical flows to supercritical conditions should be undertaken carefully. In the current experiment, several such relationships were shown to be valid in a slightly supercritical flow over low-relief antidunes. Velocity profiles agreed well with the law of the wall, indicating that it is an appropriate model for this particular flow. Figure 5.4 illustrates the log linearity of velocity profiles, demonstrating the applicability of the log law in these conditions.

The deviation of u'/u_* and w'/u_*, collected by the ADV, from the semi-theoretical curves of Nezu and Nakagawa, indicate that for similar flows the ADV may not be well suited for collecting turbulence data in such highly energetic flows. The ADV is likely better suited for less energetic flows. Reasons for the differences in measured turbulence intensity may be due to the larger measurement volume and lower rate of data collection than the LDA. The agreement of LDA measured turbulence

intensities with the semi-theoretical curves suggest that, at this flow stage, the turbulence intensities are not greatly altered from those in a clear-water flow

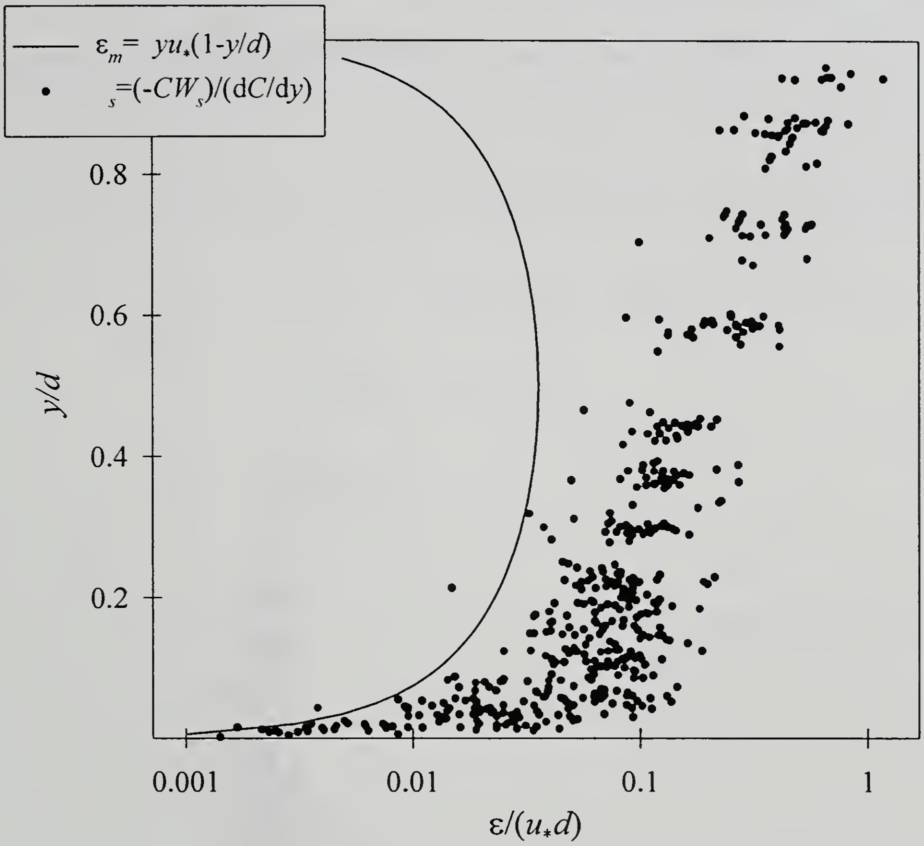

Figure 5.10. ε_m calculated from the Von Karman model and from the diffusion settling balance equation.

The deviation of the Rouse predicted concentration from the sampled concentration creates a trivial difference in calculated suspended-sediment flux. It does, however, create an opportunity to examine why there would be such a sharp departure from the theoretical curve. Using $\beta=1+(y/d)^2$ to modify the Rouse equation implies that the relationship between ε_s and ε_m may vary with depth. This may be due in part to slip velocity between the fluid and sediment and the decoupling between fluid and sediment in turbulent eddies. Allowing β to vary with depth implies that the relationship between sediment particles and the entraining fluid changes with depth. Near the bed, where

sediment is entrained, the scales of turbulent eddies are generally smaller than they are farther from the bed. It is speculated here that the increase in eddy scale further from the bed will cause a decoupling of the fluid and sediment motions.

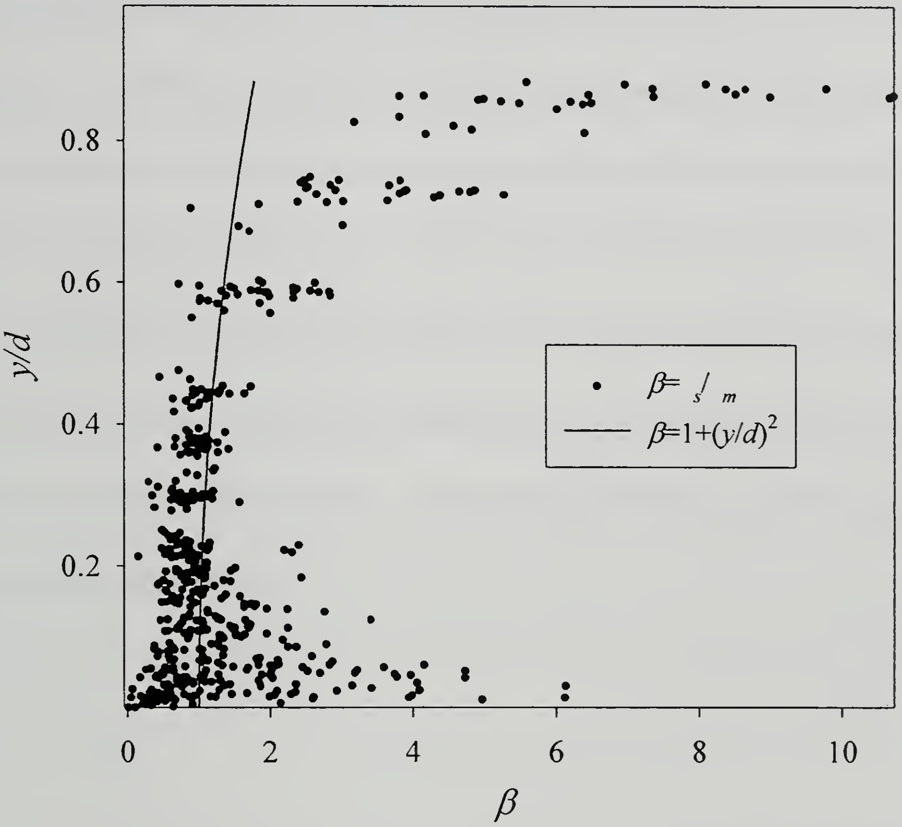

Figure 5.11. Calculated β coefficient and empirical fit function.

This decoupling is thought to be larger than that caused by the greater acceleration of fluid in eddies nearer to the bed. The modification of the Rouse equation discussed here is not intended to be universal, but instead it used to aid in the study of a particular set of conditions. The steeper concentration profiles in the experiments reported on here could be due to relatively high turbulence intensities that are able to maintain more sediment in suspension higher in the flow.

Conclusions

Velocity, turbulence intensity, and suspended-sediment profiles were collected in supercritical conditions over low-relief antidunes. Velocity profiles were found to agree well with the law of the wall, resulting in κ=0.42 for profiles collected with an ADV. Eddy viscosity was shown to have a similar distribution to relationships developed in subcritical flows. Turbulence intensities measured with an ADV did not agree with previous experimental results, but those measured with an LDA agree well in both downstream and vertical components. Concentration profiles diverged from that predicted by the Rouse equation above y/d=0.2.. This was modified by allowing β to vary as a function of $(y/d)^2$, resulting in better fit for most profiles, but only small differences in calculated sediment flux. The same modification of β was applied to two other data sets with good results.

CHAPTER VI

CONCLUSIONS

This chapter summarizes very briefly the most important conclusions arrived at from the body of work reported in this document.

1. The technique of acoustic measurement of profiles of suspended-sediment concentration, if further developed, represents the best option for advancing the study of fluvial sediment transport.
2. Simultaneous, laterally separated, suspended-sediment samples in dune and upper-stage plane beds show very poor correlation. The main implication of this is that the lateral position of a sediment sample has an impact on the measured concentration.
3. For suspended-sediment samples collected in series at a single point, approximately 1.2 hours of sampling was required to make a good estimate of the mean suspended-sediment concentration. For the upper-stage plane bed, only 0.06 hour was required.
4. The area above the stoss region of a dune was found to have more sediment higher in the flow than other areas relative to a dune's length.
5. The upper-stage plane bed was determined to be unsuitable for side-by-side instrument testing.
6. The transverse dispersion coefficient can be estimated using transverse Reynolds stresses calculated from multiple vertical profiles of fluid velocity.
7. Velocity profiles in a supercritical flow with high suspended-sediment

concentrations agreed well with the law of the wall.

8. The measured von Karman constant differed when measured by Laser Doppler Anemometer and Acoustic Doppler Velocimeter.
9. Turbulence intensities measured with a Laser Doppler Anemometer are greater than those measured with an Acoustic Doppler Velocimeter.
10. The fit of the Rouse equation for suspended-sediment profiles over flat, mobile, sand beds can be improved by varying β with depth.

CHAPTER VII

FUTURE WORK

This chapter describes some research that could be performed to further the understanding of topics covered in this work.

1. The correlation of simultaneous samples could be more fully explored by varying the spacing and the number of simultaneous samples collected.
2. The time required to obtain the mean suspended-sediment concentration from discrete samples could be assessed in the field, yielding more valuable information for those making decisions based on suspended-sediment concentration measurements.
3. Video records collected during dune experiments could be used to visually correlate periods of high suspended-sediment concentration with sampling position relative to dune length. This would provide more insight into the mechanics of sediment suspension over dunes.
4. The calculation of transverse eddy diffusivity from turbulence measurements could be further validated by performing a conventional dye tracer test in parallel with the method described here and comparing the results.
5. The comparison between hydraulic parameters as measured by Acoustic Doppler Velocimetry and Laser Doppler Anemometry could be furthered by measuring the same sampling volume with both instruments simultaneously. This experiment could be repeated for smooth wall, rough wall, sediment-laden flow, and flow

downstream of a negative step to fully evaluate the differences in instrumentation and to explore the topic of turbulence modulation by suspended sediments.

6. The modification of the Rouse equation could be more fully explored by examining the effect of grain size on the empirical β function.

REFERENCES

REFERENCES

Agrawal, Y.C. and Pottsmith, H.C. (1994). "Laser Diffraction Particle Sizing in STRESS." Continental Shelf Research. 14(10/11):1101-1121.

Agrawal, Y.C. and Pottsmith, H.C. (1996) "Laser Instruments for Particle Sizing and Settling Velocity Measurements in the Coastal Zone." Oceans-Coference-1996; Vol. I. Sept. 23-26 , Ft. Lauderdale Fl. pp. 1135-1142.

Antsyferov, S. M. and Kos'yan, R. D. (1980). "Sediments Suspended in Stream Flow." Journal of Hydraulic Engineering. 106(HY2): 313-330.

Ashmore, P. E. and Day, T. J. (1988). "Effective Discharge for Suspended Sediment Transport in Streams of the Saskatchewan River Basin." Water Resources Research. 24(6),864-870.

Ashworth, P.J., Bennett, S.J., Best, J.L., and McLelland, S.J. (1996). Coherent Flow Structures in Open Channels. John Wiley and Sons, New York. 733 p.

Bagnold, R. A., (1973). "The Nature of Saltation and of 'Bedload' Transport in Water." Proc. Royal Soc. Of London, 332a, 473-504.

Baier, V. and Bechteler, W. (1996). "An Underwater Videomicroscope to Determine the Size and Shape of Suspended Particles by Means of Digital Image Processing." Proc. of the Sixth Int. Offshore and Polar Eng. Con.

Baker, Edward T. and Lavelle, J. William. (1984). "The Effect of Particle Size on the Light Attenuation Coefficient of Natural Suspensions." Journal of Geophysical Research. 89(C5):8197-8203

Beltaos, S. (1980). "Transverse Mixing Tests in Natural Streams." Journal of the Hydraulics Division, ASCE. 106(HY10):1607-1625.

Bennett, S. J. and Best, J. L. (1995). "Mean Flow and Turbulence Structure Over Fixed, Two-Dimensional Dunes: Implications for Sediment Transport and Bedform Stability." Sedimentology, 42, 491-513.

Bennett, S. J., Bridge, J. S., and Best, J. L. (1998). "Fluid and Sediment Dynamics of Upper Stage Plane Beds." Journal of Geophysical Research. 103(C1):1239-1274.

Berke, B. and Rakoczi, L. (1981). "Latest Achievements in the Development of Nuclear Suspended Sediment Gauges." Erosion & Sediment Transport Measurement (Symposium). Florence Italy. IAHS pub. no. 133 pp. 83-90.

Bhargava, D. S. and Mariam, D. W. (1991). "Light Penetration Depth, Turbidity and Reflectance Related Relationships and Models." ISPRS Journal of Photogrammetry and Remote Sensing. 46:217-230.

Black, K. P. and Rosenberg, M. A. (1994). "Suspended Sand Measurements in a Turbulent Environment: Field Comparison of Optical and Pump Sampling Techniques." Coastal Engineering. 24:137-150.

Blanchard, B. J., and Leamer, R. W. (1973). "Spectral Reflectance of Water Containing Suspended Sediment." Remote Sensing and Water Resources Management. 17:339-347.

Bridge, J. S. and Dominic, D. F. (1984). "Bed Load Grain Velocities and Sediment Transport Rates." Water Resources Research. 20:476-490.

Burkham, D. E. (1985). "An Approach for Appraising the Accuracy of Suspended Sediment Data." Professional Paper No. 1333, U. S. Government Printing Office. Washington, D.C.

Cao, J., Brown, D.J. and Rennie, A. G. (1991). "Laser-Diffraction Particle Sizing in Dense Suspensions and Sprays, with Correction for Multiple Scattering." Journal of the Institute of Energy. 64(458):26-30.

Cellino, M., and Graf, W. H. (2000). "Experiments on Suspension Flow in Open Channels with Bed Forms." Journal of Hydraulic Research. 38(4):289-298.

Cheel, R. J. (1990). From a discussion on "Flow, Sediment Transport and Bedform Dynamics Over the Transition from Dunes to Upper-stage Plane Beds: Implications for the Formation of Planar Laminae." Sedimentology. 37:549-553.

Chen, Z., Curran, P. J., and Hansom, J. D. (1992). "Derivative Reflectance Spectroscopy to Estimate Suspended Sediment Concentration." Remote Sensing of the Environment. 40:67-77.

Choubey, V. K. (1994). "The Effect of Properties of Sediment Type on the Relationship Between Suspended Sediment Concentration and Radiance." Hydrological Sciences. 39(5):459-471.

Clifford, N. J., French, J. R., and Hardisty, J. (1993). Turbulence, Perspectives on Flow and Sediment Transport. John Wiley and Sons, New York. 360 p.

Clifford, N. J., Richards, K. S., Brown, R. A. and Lane, S. N. (1995). "Laboratory and Field Assessment of an Infrared Turbidity Probe and its Response to Particle Size and Variation in Suspended Sediment Concentration." Hydrological Sciences. 40(6):771-791.

Coleman, N. L. (1970). "Flume Studies of the Sediment Transfer Coefficient." Water Resources Research. Vol. 6, No. 3. 801-809.

Coleman, N. L. (1986). "Effects of Suspended Sediment on the Open-Channel Velocity Distribution." Water Resources Research. 22(10): 1377-1384.

Coleman, N. L. (1981). "Velocity Profiles with Suspended Sediment." Journal of Hydraulic Research. 19(3): 211-229.

Conner, C. S. and DeVisser, A. M. (1992). "A Laboratory Investigation of Particle Size Effects on an Optical Backscatterance Sensor." Marine Geology. 10:151-159.

Crawford, A. M. and Hay, A. E. (1993). "Determining Suspended Sand Size and Concentration from Multifrequency Acoustic Backscatter." Journal of Acoustic Society of America. 94(6):3312-3324.

Crickmore, M. J., Tazioli, G. S., Appleby, P.G., Oldfield, F. (1990). The Use of Nuclear Techniques in Sediment Transport and Sedimentation Problems. Unesco, Paris.

D & A Instrument Company. (1991). Instruction Manual for OBS-1 & 3. D & A Instrument Company, 40-A Seton Road, Port Townsend, WA, 98368.

Derrow, R. W. and Kuhnle, R. A. (1996). "Preliminary Analysis of the NCPA-NSL Suspended Sediment Calibration System." Proceedings of the Sixth Federal Interagency Sedimentation Conference 1996. Vol. 2:58-65.

Downing, A., Thorne, P. D. and Vincent, C. E. (1995). "Backscattering from a Suspensions in the Near Field of a Piston Transducer." Journal of Acoustic Society of America. 97(3):1614-1619.

Droppo, I. G., and Ongley, E. D. (1992) "The State of Suspended Sediment in the Freshwater Fluvial Environment: A Method of Analysis." Water Research. 26(1):65-72.

Droppo, I. G., and Ongley, E. D. (1994). "Flocculation of Suspended Sediment in Rivers of Southeastern Canada." Water Research. 28(8):1799-1809.

Edwards, T. K. and Glysson, D. (1999). Field Methods for Measurement of Fluvial Sediment. U.S. Geological Survey Techniques of Water-Resources Investigations Book 3, Chapter C2, 89 pp.

Einstein, H. A., (1950). "The Bed-Load Function for Sediment Transport in Open Channel Flows." Soil Conserv. Ser. Tech. Bull. No. 1026, U.S. Dept. Agric., Washington, D. D.

Fischer, H. B., List, J. E., Koh, C. Y. R., Imberger, J., and Brooks, N. H. (1979). Mixing in Inland and Coastal Waters. Academic Press, Inc. Boston.

Friedricks, C. Assistant Professor of Marine Science, School of Marine Science, College of William and Mary. Personal communication on 9/4/97.

Gao, Jay and O'Leary, Stephen. (1997). "The Role of Spatial Resolution in Quantifying Suspended Sediment Concentration from Airborne Remotely Sensed Data." Photogrammetric Engineering & Remote Sensing. 63(3):267-271.

Gelfenbaum, G., and Smith, J. D.. "Experimental Evaluation of a Generalized Suspended-Sediment Transport Theory." In Shelf Sands and Sandstones, edited by R. J. Knight and J. R. Mclean, Mem. Can. Soc. Petrol. Geol., II, 133-144, 1986.

Green, M. O. and Boon, J. D. III. (1993). "The Measurement of Constituent Concentrations in Nonhomogeneous Sediment Suspensions Using Optical Backscatter Sensors." Marine Geology. 110:73-81.

Guy, H. P. (1965). Techniques of Water -Resources Investigations of the United States Geological Survey-Laboratory Theory and Methods for Sediment Analysis. United States Department of the Interior, United States Geological Survey.

Guy, H. P., Simons, D. B., and Richardson, E. V. (1966). "Summary of Alluvial Channel Data from Flume Experiments, 1956-61." Geological Survey Profession Paper 462-I. U. S. Government Printing Office, Washington.

Hanes, D. M., Vincent, C. E., Huntley, D. A., and Clarke, T. L. (1988). "Acoustic Measurements of Suspended Sand Concentration in the C2-S2 Experiment at Stanhope Lane, Prince Edward Island." Marine Geology. 81:185-196.

Hay, A. E. and Bowen, A. J. (1994). "Coherence Scales of Wave-Induced Suspended Sand Concentration Fluctuations." Journal of Geophysical Research, 99(C6), 12,749-12,765.

Henderson, F. M. (1966). Open Channel Flow. Prentice Hall, New Jersey.

Hino, M. (1963). "Turbulent Flow with Suspended Particles." *Journal of Hydraulic Research*. 89(HY4):1963.

Holeman, John M. (1968). "The Sediment Yield of Major Rivers of the World." *Water Res. Res.* 4(4): 737-747.

Holley, E. R. and Abraham, G. (1973). "Field Tests on Transverse Mixing in Rivers." *Journal of Hydraulic Engineering*. 99(HY12):2313-2331.

Horowitz, A. J., Rinella, F. A., Lamothe, P., Miller, T., L., Edwards, T. K., Roche, R. L., and Rickert, D. A. (1990). "Variations in Suspended Sediment and Associated Trace Element Concentrations in Selected Riverine Cross Sections." Environ. Sci. Technol. 24,1313-1320

Ingram, J. J., Abt, S. R., Richardson, E. V. (1991). "Sediment Discharge Computation Using Point-Sampled Suspended-Sediment Data." Journal of Hydraulic Research. 117(6):758-773.

Inter-agency Committee on Water Resources, Subcommittee on Sedimentation. (1963). A Study of Methods Used in Measurement and Analysis of Sediment Loads in Streams-Report No. 14 Field Practice and Equipment Used in Sampling Suspended Sediment Report #14. St. Anthony Falls Hydraulic Laboratory.

Itakura, T. and Kishi, T. (1980). "Open Channel Flow with Suspended Sediments." *Journal of Hydraulic Engineering*. 106(HY8): 1325-1343.

James, C. S. (1985) "Sediment Transfer to Overbank Sections." *Journal of Hydraulic Research*. 23(5): 435-452.

Jandel Corporation (1995). SigmaStat Statistical Software version 2.0.

Jarrett, R. D. (1984). "Hydraulics of High-Gradient Streams." *Journal of Hydraulic Engineering*. 110(11):1519-1539.

Jobson H. E., and Sayre, W. W. (1970). "Predicting Concentration Profiles in Open Channels." *Journal of Hydraulic Engineering*. 96(HY10): 1983-1996.

Karim, M. F. and Kennedy, J. F. (1987). “Velocity and Sediment-Concentration Profiles in River Flows.” *Journal of Hydraulic Engineering.* 113(2):159-178.

Kawanisi, K. and Yokosi, S. (1993). “Measurements of Turbulence and Suspended Sediment in a Tidal River.” Journal of Hydraulic Engineering. 119(6):704-724.

Kineke, G. C., Sternberg, R. W. (1992). “Measurements of High Concentration Suspended Sediments Using the Optical Backscatterance Sensor.” *Marine Geology.* 108:253-258.

Knight, J. C., Ball, D., and Robertson, G. N. (1991). "Analytical Inversion for Laser Diffraction Spectrometry Giving Improved Resolution and Accuracy in Size Distribution." *Applied Optics.* 30(33):4795-4799.

Kostaschuk, R. A., and Church, M. A. (1993). “Macroturbulence Generated by Dunes: Fraser River, Canada.” Sedimentary Geology, 85, 25-37.

Kostaschuk, R. and Villard, P. (1996). “Flow and Sediment Transport Over Large Subaqueous Dunes: Fraser River, Canada.” Sedimentology, 43, 849-863.

Kuhnle, R. A., and Willis, J. C. (1998). “Statistics of sediment transport in Goodwin Creek.” *Journal of Hydraulic Engineering*, 124(11), 1109-1114.

Lane, E. W. and Kalinske, A. A. (1941). “Engineering Calculations of Suspended Sediment.” Trans. AGU 4/3-5/3, Washington D.C. pp. 603-607.

Lane, S. N., Biron, P. M., Bradbrook, K. F., Butler, J. B., Chandler, J. H., Crowell, M. D., McLelland, S. J., Richards, K. S., and Roy, A. G. (1998) “Three-Dimensional Measurements of River Channel Flow Processes Using Acoustic Doppler Velocimetry.” Earth Surface Processes and Landforms. 23:1247-1267.

Lapointe, M. F. (1992). “Burst-like Sediment Suspension Events in a Sand Bed River.” Earth Surface Processes and Landforms, 17, 253-270.

Lapointe, M. F. (1993). “Monitoring Alluvial Sand Suspension by Eddy Correlation.” Earth Surface Processes and Landforms, 18, 157-175.

Lapointe, M. F. (1996). “Frequency Spectra and Intermittency of the Turbulent Suspension Process in a Sand-bed River.” Sedimentology, 43:439-449.

Lau, Y. L., and Krishnappan, B. G. (1977). “Transverse Dispersion in Rectangular Channels.” *Journal of the Hydraulics Division, ASCE.* 103(HY10):1173-1189.

Law, D. J., Bale, A. J., and Jones, S. E. (1997). "Adaptation of Focused Beam Reflectance Measurement to In-Situ Particle Sizing in Estuaries and Coastal Waters." *Marine Geology.* 140(1-2):47-59.

Lewis, A. J., and Rasmussen, T. C. (1996). “A New, Passive Technique for the In Situ Measurement of Total Suspended Solids Concentrations in Surface Water.” Technical Completion Report for Project # 14-08-001-G-2013 (07), U.S. Department of the Interior, Geological Survey. August 1996.

Lohrmann, A., Cabrera, R., and Kraus, N. C. (1994). “Acoustic-Doppler Velocimeter (ADV) for Laboratory Use.” Fundamentals and Advancements in Hydraulic Measurements and Experimentation Proceedings, sponsored by the Hydraulics Division/ASCE, August 1-5, 1994, Buffalo, New York.

Ludwig, K. A. and Hanes, D. M. (1990). “A Laboratory Evaluation of Optical Backscatterance Suspended Solids Sensors Exposed to Sand-Mud Mixtures.” *Marine Geology.* 94:173-179.

Lyn, D. A. (1992). “Turbulence Characteristics of Sediment-Laden Flows in Open Channels.” *Journal of Hydraulic Research.* 118(7):971-988.

McHenry, J. R., Coleman, N. L., Willis, A. C., Sansom, O. W., and Carrol, B. R. (1967). "Effect of Concentration Gradients on the Performance of a Nuclear Sediment Concentration Gage." *Water Res. Res.* 6(2)538-548.

Mctigue, D. F. (1981). “Mixture Theory of Suspended Sediment Transport.” *Journal of Hydraulic Engineering.* 107(HY6): 659-673.

Miller, A. C. and Richardson, E. V. (1974). “Diffusion and Dispersion in Open Channel Flow.” *Journal of Hydraulic Engineering.* 100(HY1):159-171.

Nelson, M. E. and Benedict, P. C. (1950). “Measurement and Analysis of Suspended Loads in Streams.” Transactions of the American Society of Civil Engineers. Paper No. 2450:891-918.

Nezu, I. and Nakagawa, H. (1993). Turbulence in Open Channel Flows. IAHR Monograph. A.S. Balkema, Brookfield.

Nikora, V. and Goring, D. (1998). “ADV Measurements of Turbulence: Can We Improve Their Interpretation?” *Journal of Hydraulic Engineering.* 124(6):630-634.

Nikora, V. and Goring, D. (2000). “Flow Turbulence Over Fixed and Weakly Mobile Gravel Beds.” *Journal of Hydraulic Engineering.* 126(9):679-690.

Novo, E. M. M., Hansom, J. D., and Curran, P. J. (1989a). "The Effect of Viewing Geometry and Wavelength on the Relationship between Reflectance Data and Suspended Sediment Concentration." *International Journal of Remote Sensing.* 10(8):1357-1372.

Novo, E. M. M., Hansom, J. D., and Curran, P.G. (1989b). “The Effect of Sediment Type on the Relationship between Reflectance and Suspended Sediment Concentration.” *International Journal of Remote Sensing.* 10(7):1283-1289.

Osborne, P. D., Vincent, C. E. and Greenwood, B. (1994). “Measurement of Suspended Sand Concentrations in the Nearshore: Field Intercomparison of Optical and Acoustic Backscatter Sensors.” *Continental Shelf Research.* 14(2/3):159-174.

Papadopoulos, J. and Ziegler, C. A. (1966). “Radioisotope Technique for Monitoring Sediment Concentration in Rivers and Streams.” From: Proc. on Radioisotope Instruments in Industry and Geophysics. IAEA, Vienna, Austria. SM-68/26:pp. 381-394.

Phillips, J. M., and Walling, D. E. (1995a). “An Assessment of the Effects of Sample Collection, Storage and Resuspension on the Representativeness of Measurements of the Effective Particle Size Distribution of Fluvial Suspended Sediment.” *Water Resources.* 29(11):2498-2508.

Phillips, J. M., and Walling, D. E. (1995b). "Measurement in situ of the Effective Particle-size Characteristics of Fluvial Suspended Sediment by means of a Field-Portable Laser Backscatter Probe: Some Preliminary Results." *Mar. Freshwater Res.* 46:349-357.

Pizzuto, J. E. (1987). “Sediment Diffusion During Overbank Flows.” *Sedimentology.* 34: 301-317.

Pottsmith, H. C. (1997). Sequoia Scientific, Inc. PO Box 592, Mercer Is. WA 98040. Personal Communication on 7/28/97.

Rakoczi, L. (1973). “Critical Review of Current Nuclear Suspended Sediment Gauges.” Technical Reports Series No. 145, Tracer Techniques in Sediment Transport. Panel Meeting held June 1971 sponsored by the International Atomic Energy Agency.

Riley, J. B., and Agrawal, Y. C. (1991). "Sampling and Inversion of Data in Diffraction Particle Sizing." *Applied Optics.* 30(33):4800-4817.

Ritchie, J. C. and Schiebe, F. R. (1986). "Monitoring Suspended Sediments with Remote Sensing Techniques." Proceedings of workshop: "Hydrologic Applications of Space Technology." IAHS publication no. 160.

Rouse, H. (1936). "Modern Conceptions of the Mechanics of Fluid Turbulence." *ASCE Trans.* Vol. 102 463-543.

Rutherford, J. C. (1994). River Mixing. John Wiley and Sons, New York.

Samaga, B. R., Ranga Raju, K. G., and Garde, R. J. (1985). "Concentration Distribution of Sediment Mixtures in Open-Channel Flow." *Journal of Hydraulic Research.* 23(5):467-482.

Sayre, W. W., and Chang, F. M., (1968). "A Laboratory Investigation of the Open Channel Dispersion Process for Dissolved, Suspended and Floating Dispersants," U. S. Geological Survey Professional Paper 433-E. 71 p.

Schat, J. (1997). "Multifrequency Acoustic Measurement of Concentration and Grain Size of Suspended Sand in Water." *Journal of Acoustic Society of America.* 101(1):209-217.

Simon, A. and Hardison, J. H. III. (1994). "Critical and Supercritical Flows in Two Unstable Mountain Rivers, Toutle River System, Washington." Hydraulic Engineering '94 Proceedings of the ASCE Hydraulics Division August 1-5, 1994, Buffalo, New York.

Skinner, J. V. (1969). Discussion of paper entitled "Field Test of an X-ray Sediment Concentration Gauge." *J. Hydraul. Div. Amer. Soc. Civil Eng.* 95(HY1)531-532.

Skinner, J. V. (1989). "Model-B Sediment-Concentration Gage: Factors Influencing its Readings and a Formula for Correcting its Errors." From "A Study of Methods Used in Measurement and Analysis of Sediment Loads in Streams." U.S. Army Engineer District St. Paul, Minnesota.

Smith, J. D., and McLean, S. R. (1977). "Spatially averaged Flow Over a Wavy Surface." *Journal of Geophysical Research.* 82:1735-1746.

Southard, J. B. (1971). "Representation of Bed Configurations in Depth-Velocity-Size Diagrams." *Journal of Sedimentary Petrology.* 41(4):903-915.

Southard, J. B. and Boguchwal, L. A. (1990). "Bed Configurations in Steady Unidirectional Water Flows. Part 2. Synthesis of Flume Data." *Journal of Sedimentary Petrology*. 60(5):658-679.

Swithenbank, J., Beer, J. M., Taylor, D. S., Abbot, D., McCreath, G. C. (1976). "A Laser Diagnostic Technique for the Measurement of Droplet and Particle Size Distribution." From: AIAA 14th Aerospace Sciences Meeting, January 1976.

Task Force on Bed Forms in Alluvial Channels of the Committee on Sedimentation. (1966). "Nomenclature for Bed Forms in Alluvial Channels." *Journal of Hydraulic Engineering*. 92(HY3):51-64.

Tazioli, G. S. (1981). "Nuclear Techniques for Measuring Sediment Transport in Natural Streams-Examples from Instrumented Basins." From: Erosion and Sediment Transport Measurement. IAHS pub 133. Florence, Italy.

Thomas, R. B. (1985). "Estimating Total Suspended-Sediment Yield with Probability Sampling." Water Resources Research. 21(9):1381-1388.

Thomas, R. B. and Lewis, J. (1993). "A Comparison of Selection at List Time and Time-Stratified Sampling for Estimating Suspended-Sediment Loads." Water Resources Research. 29(4):1247-1256.

Thorne, P. D., Vincent, C. E., Hardcastle, P. J., Rehman, S., and Pearson, N. (1991) "Measuring Suspended Sediment Concentrations Using Acoustic Backscatter Devices." *Marine Geology*. 98:7-16.

Thorne, P. D., and Campbell, S. C. (1992). "Backscattering by a Suspension of Spheres." Journal of Acoustic Society of America. 92(2):978-986.

Thorne, P. D., P. J. Hardcastle, and R. L. Soulsby. (1993). "Analysis of Acoustic Measurements of Suspended Sediments." Journal of Geophysical Research. 98(C1):899-910.

Thorne, P. D., Hardcastle, P. J., Flatt, D. and Humphery, J. D. (1994). "On the Use of Acoustics for Measuring Shallow Water Suspended Sediment Processes." IEEE Journal of Oceanic Engineering. 19(1):48-57.

Thorne, P. D., Waters, K. R., Brudner, T. J. (1995). "Acoustic Measurements of Scattering by Objects of Irregular Shape." Journal of Acoustic Society of America. 97(1):242-251.

Thorne, P. D., Hardcastle, P. J., and Hogg, A. (1996). "Observations of Near-bed Suspended Sediment Turbulence Structures using Multifrequency Acoustic Backscattering." From Coherent Flow Structures in Open Channels. Edited by Ashworth, P. J.; Bennett, S. J.; Best J. L., and McLelland, S. J.

Trieste, D. J. (1992). "Evaluation of Supercritical/Subcritical Flows in High-Gradient Channel." Journal of Hydraulic Engineering. 118(8):1107-1118.

U.S. Environmental Protection Agency. (1999). Protocol for Developing Sediment TMDLs. EPA 841-B-00-004. Office of Water (4503F), United States Environmental Protection Agency, Washington D.C. 132 pp.

Van Rijn, L. C. (1984). "Sediment Transport, Part II: Suspended Load Transport." Journal of Hydraulic Engineering, 110, 1613-1641.

Van Rijn, L. C. and Schaafsma, A. S. (1986). "Evaluation of Measuring Instruments for Suspended Sediment." International Conference on Measuring Techniques of Hydraulics Phenomena in Offshore, Coastal & Inland Waters. London, England: April 9-11:401-423.

Van Rijn, L. C. (1993). Principles of Sediment Transport in Rivers, Estuaries and Coastal Seas, Aqua Publications, Amsterdam.

Vanoni, V. A. (1941). "Some Experiments on the Transportation of Suspended Load." Trans. AGU 4/3-5/3, Washington D.C. pp. 608-621.

Vanoni, V. A. Ed. (1975) Sedimentation Engineering. 745 pp. Am. Soc. of Civ. Eng., New York.

Venditti, J. G. and S. J. Bennett. (2000). "Spectral Analysis of Turbulend Flow and Suspended Sediment Transport Over Fixed Dunes." *Journal of Geophysical Research.* 105(C9):22,035-22,048.

Walling, D. E. (1977). "Assessing the Accuracy of Suspended Sediment Rating Curves for a Small Basin." Water Resources Research, 13(3):531-538.

Walling, D. E. and Moorehead, D. W. (1989). "The Particle Size Characteristics of Fluvial Suspended Sediment." *Hydrobiologia.* 176/177:125-149.

Walling, D.E., and Woodward, J.C. (1993). "Use of a Field Based Water Elutriation System for Monitoring the *In-Situ* Particle Size Characteristics of Fluvial Suspended Sediment." *Water Research.* 27(9):1413-1421.

Webel, G. and Schatzmann, M. (1984). “Transverse Mixing in Open Channel Flow.” *Journal of Hydraulic Engineering.* 110(4):423-435.

Welch, N. H., and Allen, P. B. (1973). “Field Calibration and Evaluation of a Nuclear Sediment Gage.” *Water Resources Research.* 9(1):154-158.

Willis, J. C. (1979). “Suspended Load from Error-Function Models.” *Journal of Hydraulic Engineering.* 105(HY7): 801-816.

Willis, J. C., and Bolton, G. G., (1979). “Statistical analysis of concentration records.” Journal of the Hydraulics Division, ASCE, 105(HY1), 1-15.

Witt, W. and Rothele, S. (1996). "Laser Diffraction-Unlimited?" Part. Part. Syst. Charact. 13:280-286.

Woodward, J. C., and Walling D. E. (1992). “A Field Sampling Method for Obtaining Representative Samples of Composite Fluvial Suspended Sediment Particles for SEM Analysis.” Journal of Sedimentary Petrology. 62:742-744.

Wren, D.G., Barkdoll, B. D., Kuhnle, R. A., and Derrow, R. W. (2000). “Field Techniques for Suspended-Sediment Measurement.” Journal of Hydraulic Engineering. 126(2):97-104.

Wylie, T., Taylor, K, and Born, A. J. (1984). “Design and Calibration of the Sediment Tower.” Proudman Oceanographic Internal Document No. 69, Proudman Oceanographic Laboratory, Bidston, Merseyside, UK.

Xu, J. P. (1997). “Converting Near Bottom OBS Measurements into Suspended Sediment Concentrations.” *Geo-Marine Letters.* 17:154-161.

APPENDICES

Appendix A: Flat bed flow and concentration data

This appendix consists of the raw data used for chapters 2 and 3. Eleven profiles of suspended-sediment concentration and fluid velocity data taken with the ADV are included. Four profiles taken with the LDA are included.

z (m)	y (mm)	y/d	C (g/L)	$\overline{u}$	$\overline{w}$
0.003	0.5	0.004	26.742	0.646	-0.020
0.003	1.3	0.009	39.133	0.596	-0.035
0.003	2.8	0.020	6.253	0.701	-0.011
0.003	7.8	0.056	1.306	0.807	0.001
0.003	9.3	0.066	0.877	0.840	-0.003
0.003	13.6	0.097	0.470	0.922	0.007
0.003	13.9	0.099	0.300	0.959	0.009
0.003	15.3	0.109	0.297	1.021	0.014
0.003	25.4	0.181	0.103	1.103	0.011
0.003	26.7	0.191	0.145	1.077	0.014
0.003	46.7	0.333	0.067	1.145	0.003
0.003	53.0	0.378	0.060	1.279	0.021
0.003	79.3	0.566	0.031	1.175	-0.007
0.003	94.8	0.677	0.023	1.249	0.015
0.003	115.5	0.825	0.018	1.206	-0.006
0.05	2.2	0.016	35.703	0.793	-0.011
0.05	3.0	0.022	12.757	0.779	-0.011
0.05	4.6	0.033	10.990	0.853	-0.005
0.05	7.1	0.051	3.237	0.912	-0.004
0.05	12.7	0.091	1.260	1.059	-0.001
0.05	18.9	0.135	0.750	1.122	0.004
0.05	20.0	0.143	0.460	1.168	0.003
0.05	25.5	0.182	0.277	1.192	0.004
0.05	31.3	0.224	0.270	1.259	0.011
0.05	42.4	0.303	0.080	1.317	0.013
0.05	51.3	0.367	0.040	1.372	0.013
0.05	62.1	0.444	0.037	1.411	0.014
0.05	81.1	0.579	0.030	1.444	0.006
0.05	103.0	0.735	0.020	1.400	-0.007
0.05	121.0	0.864	0.019	1.291	-0.043
0.01	1.6	0.011	50.537	0.803	0.001
0.01	1.6	0.012	55.983	0.840	0.002
0.01	5.2	0.037	14.577	0.960	0.006
0.01	5.3	0.038	9.080	0.938	0.009
0.01	8.4	0.060	7.260	0.977	0.013
0.01	14.8	0.106	1.280	1.092	0.017

0.01	17.8	0.127	0.800	1.140	0.015
0.01	20.3	0.145	0.480	1.205	0.016
0.01	28.1	0.201	0.227	1.245	0.017
0.01	34.0	0.243	0.083	1.236	0.019
0.01	41.8	0.299	0.090	1.312	0.023
0.01	50.0	0.357	0.070	1.351	0.024
0.01	63.6	0.454	0.047	1.383	0.023
0.01	82.8	0.591	0.042	1.452	0.028
0.01	101.9	0.728	0.040	1.432	0.011
0.01	122.6	0.876	0.029	1.354	-0.028
0.15	2.8	0.020	10.633	0.827	-0.017
0.15	3.7	0.027	34.591	0.798	-0.018
0.15	7.7	0.055	3.913	1.004	-0.011
0.15	8.5	0.060	7.305	0.964	-0.007
0.15	10.3	0.073	1.900	1.068	-0.007
0.15	15.0	0.107	1.168	1.138	-0.007
0.15	20.2	0.144	0.637	1.190	-0.010
0.15	23.6	0.169	0.231	1.230	-0.008
0.15	27.2	0.195	0.217	1.268	-0.008
0.15	30.5	0.218	0.132	1.310	-0.008
0.15	43.2	0.309	0.053	1.357	-0.001
0.15	53.2	0.380	0.049	1.406	0.001
0.15	63.0	0.450	0.047	1.426	0.002
0.15	82.2	0.587	0.037	1.470	-0.005
0.15	114.0	0.814	0.023	1.478	-0.008
0.20	0.3	0.002	284.394	0.648	-0.045
0.20	1.7	0.012	165.317	0.782	-0.019
0.20	4.7	0.034	10.084	0.969	-0.010
0.20	6.0	0.043	18.060	0.929	-0.003
0.20	7.0	0.050	12.212	0.979	-0.014
0.20	11.9	0.085	2.243	1.106	-0.008
0.20	15.7	0.112	0.990	1.128	-0.014
0.20	22.0	0.157	0.470	1.206	-0.005
0.20	28.0	0.200	0.268	1.305	-0.055
0.20	30.4	0.217	0.137	1.250	-0.017
0.20	41.0	0.293	0.130	1.329	0.002
0.20	53.5	0.382	0.077	1.363	0.002
0.20	59.9	0.428	0.038	1.413	-0.002
0.20	80.0	0.571	0.043	1.463	0.003
0.20	100.1	0.715	0.037	1.491	0.013
0.20	119.0	0.850	0.030	1.488	0.003
0.25	2.3	0.017	30.073	0.793	-0.002
0.25	3.6	0.026	5.983	0.858	-0.001

0.25	4.9	0.035	4.640	0.964	-0.002
0.25	7.6	0.054	6.870	0.907	-0.002
0.25	11.9	0.085	1.113	1.083	-0.001
0.25	15.9	0.114	0.833	1.112	-0.002
0.25	22.4	0.160	0.317	1.145	-0.001
0.25	25.9	0.185	0.267	1.182	-0.002
0.25	31.2	0.223	0.183	1.225	-0.002
0.25	41.9	0.299	0.110	1.271	-0.001
0.25	51.5	0.368	0.063	1.354	0.000
0.25	60.4	0.432	0.040	1.362	-0.001
0.25	81.8	0.584	0.059	1.414	0.000
0.25	102.1	0.729	0.043	1.455	-0.001
0.25	120.9	0.864	0.032	1.468	0.001
0.30	3.6	0.026	50.047	0.820	-0.005
0.30	4.4	0.031	42.150	0.836	-0.008
0.30	4.9	0.035	8.413	0.909	0.002
0.30	9.4	0.067	4.433	1.026	-0.011
0.30	9.5	0.068	4.717	0.985	0.006
0.30	16.1	0.115	2.100	1.082	0.002
0.30	20.1	0.143	1.043	1.128	0.006
0.30	24.1	0.172	0.443	1.184	-0.010
0.30	30.6	0.218	0.233	1.216	-0.002
0.30	33.2	0.237	0.153	1.239	0.003
0.30	42.0	0.300	0.093	1.290	0.002
0.30	52.2	0.373	0.077	1.344	-0.001
0.30	62.4	0.446	0.047	1.373	0.012
0.30	83.2	0.595	0.029	1.424	0.011
0.30	102.7	0.734	0.020	1.470	0.015
0.30	122.5	0.875	0.025	1.472	0.028
0.35	1.1	0.008	20.614	0.818	-0.016
0.35	2.5	0.018	18.073	0.782	-0.020
0.35	6.0	0.043	7.927	0.886	-0.022
0.35	6.9	0.050	3.653	0.955	-0.010
0.35	8.2	0.059	4.257	0.921	-0.006
0.35	14.4	0.103	1.227	1.065	-0.020
0.35	17.2	0.123	0.797	1.105	-0.005
0.35	22.6	0.161	0.405	1.161	-0.018
0.35	27.4	0.196	0.347	1.185	-0.015
0.35	31.9	0.228	0.196	1.230	-0.023
0.35	41.3	0.295	0.117	1.290	-0.019
0.35	51.0	0.364	0.089	1.335	-0.015
0.35	62.5	0.446	0.077	1.362	-0.017
0.35	82.3	0.588	0.059	1.437	0.000

0.35	101.1	0.722	0.053	1.461	-0.006
0.35	121.1	0.865	0.046	1.420	-0.022
0.40	6.2	0.044	32.010	0.832	-0.010
0.40	8.8	0.063	22.850	0.920	0.010
0.40	11.4	0.081	6.205	0.967	0.005
0.40	12.0	0.085	3.300	1.038	0.000
0.40	17.0	0.122	1.647	1.092	-0.004
0.40	21.2	0.151	0.680	1.151	0.005
0.40	26.9	0.192	0.373	1.173	-0.007
0.40	31.6	0.226	0.283	1.215	0.005
0.40	34.6	0.247	0.146	1.237	0.011
0.40	45.3	0.323	0.077	1.301	0.000
0.40	54.3	0.388	0.070	1.346	0.000
0.40	65.6	0.469	0.030	1.374	0.006
0.40	83.1	0.594	0.023	1.441	0.015
0.40	104.3	0.745	0.020	1.477	0.014
0.40	123.4	0.882	0.017	1.316	-0.036
0.45	3.8	0.027	87.043	0.652	-0.023
0.45	5.9	0.042	12.343	0.757	-0.018
0.45	7.6	0.054	6.180	0.835	-0.029
0.45	17.8	0.127	0.887	0.995	-0.026
0.45	21.5	0.154	0.450	1.075	0.001
0.45	25.0	0.178	0.330	1.093	-0.011
0.45	30.0	0.214	0.150	1.138	0.001
0.45	40.0	0.285	0.133	1.197	-0.025
0.45	51.2	0.366	0.103	1.238	-0.017
0.45	59.4	0.424	0.070	1.267	-0.013
0.45	79.3	0.567	0.043	1.333	-0.004
0.45	99.3	0.709	0.040	1.363	-0.007
0.45	120.3	0.860	0.043	1.394	-0.011
0.50	1.4	0.010	51.367	0.823	-0.007
0.50	2.8	0.020	17.223	0.866	0.004
0.50	5.2	0.037	8.047	0.932	-0.007
0.50	6.9	0.049	5.833	0.984	-0.006
0.50	9.5	0.068	4.507	1.023	0.002
0.50	14.2	0.101	1.483	1.089	0.003
0.50	17.6	0.126	0.667	1.130	-0.008
0.50	29.0	0.207	0.240	1.195	0.002
0.50	32.5	0.232	0.185	1.226	0.002
0.50	40.1	0.286	0.090	1.281	0.007
0.50	50.8	0.363	0.067	1.321	0.002
0.50	61.6	0.440	0.047	1.360	0.001
0.50	82.6	0.590	0.029	1.411	0.006

0.50	103.1	0.736	0.033	1.446	0.004
0.50	120.2	0.859	0.021	1.364	-0.031

LDA data.			
y	y/d	$\bar{u}$	$\bar{v}$
19.1	0.137	0.966	0.0015
19.0	0.135	0.953	0.0047
26.1	0.187	1.053	0.0049
29.1	0.208	1.098	0.0067
41.8	0.298	1.168	0.0031
45.1	0.322	1.240	0.0067
63.2	0.451	1.293	0.0074
72.9	0.521	1.315	0.0077
89.2	0.637	1.319	0.0152
105.8	0.756	1.303	0.0068
120.0	0.857	1.274	0.0222
16.3	0.116	0.967	0.0030
20.2	0.145	1.027	0.0036
25.6	0.183	1.085	0.0070
30.3	0.216	1.152	0.0005
38.9	0.278	1.218	0.0039
50.7	0.362	1.280	0.0044
59.1	0.422	1.335	0.0034
75.1	0.537	1.377	0.0064
89.2	0.637	1.406	0.0108
106.0	0.757	1.376	0.0157
119.8	0.855	1.330	0.0120
17.4	0.124	0.946	0.0011
19.3	0.138	1.043	0.0066
26.6	0.190	1:086	0.0017
29.0	0.207	1.149	0.0086
39.5	0.282	1.229	0.0057
48.3	0.345	1.298	0.0041
59.1	0.422	1.326	0.0048
75.5	0.539	1.364	0.0092
87.6	0.625	1.419	0.0048
107.9	0.770	1.406	0.0124
13.5	0.097	0.967	0.0277
19.4	0.139	1.042	0.0072
21.6	0.154	1.120	0.0087

32.6	0.233	1.182	0.0131
39.6	0.283	1.240	0.0134
50.0	0.357	1.312	0.0119
58.7	0.419	1.348	0.0163
74.9	0.535	1.396	0.0155
89.6	0.640	1.428	0.0176
105.0	0.750	1.458	0.0294
119.4	0.853	1.476	0.0276

Appendix B: USPB and dune bed flow and concentration data

This appendix consists of the raw data collected for extended time series reported in chapter 2. The data are arranged into the five time series that were collected for each of the two bed phases. Each time series is labeled by the starting position of the sampler nozzles prior to the experiment. Data in the same row were taken simultaneously.

Data from paired samples over upper-stage plane beds. Velocity was measured only at probe 1. y is height over the bed, d is water depth, $\overline{u}$ is average downstream velocity, $\overline{w}$ average cross-stream velocity, z is distance from flume sidewall, and C is the suspended sediment concentration. Position measurements are average bed height plus some distance in mm. This was used to set probe height at the beginning of the experiment.

	Probe 1 (z=0.33 m)					Probe 2 (z=0.66 m)		
Position (mm)	y (mm)	y/d	C (g/L)	$\overline{u}$	$\overline{w}$	y (mm)	y/d	C (g/L)
Bed+5	8.5	0.078	3.309	0.577	0.018	6.8	0.062	6.000
Bed+5	8.1	0.074	2.050	0.547	0.017	7.3	0.066	4.240
Bed+5	6.9	0.063	3.279	0.559	0.022	5.9	0.054	8.996
Bed+5	6.2	0.057	3.512	0.548	0.015	4.4	0.040	23.072
Bed+5	6.1	0.056	4.284	0.561	0.023	5.6	0.051	26.128
Bed+5	6.5	0.059	3.030	0.552	0.020	5.2	0.048	16.213
Bed+5	7.3	0.067	3.050	0.548	0.022	5.3	0.049	13.442
Bed+5	7.5	0.068	2.572	0.543	0.022	6.5	0.059	18.493
Bed+5	6.1	0.056	2.677	0.532	0.021	5.3	0.049	11.372
Bed+5	6.2	0.057	4.199	0.544	0.024	5.3	0.048	10.306
Bed+5	7.4	0.068	3.757	0.574	0.017	7.6	0.069	6.454
Bed+5	9.2	0.084	2.835	0.606	0.012	7.8	0.071	5.091
Bed+5	9.2	0.084	2.440	0.611	0.017	5.4	0.049	12.703
Bed+5	8.4	0.077	2.665	0.614	0.015	5.1	0.046	18.121
Bed+5	7.9	0.072	3.633	0.596	0.020	5.6	0.051	22.730
Bed+5	7.5	0.069	2.941	0.574	0.029	4.5	0.041	26.957
Bed+5	4.6	0.042	5.348	0.515	0.030	4.7	0.043	23.924
Bed+5	5.9	0.054	4.201	0.552	0.017	6.2	0.057	11.470
Bed+5	6.9	0.063	4.224	0.582	0.014	4.5	0.041	25.673
Bed+5	7.9	0.072	3.079	0.578	0.014	5.7	0.052	32.537
Bed+5	10.4	0.095	2.500	0.606	0.010	5.1	0.047	19.641
Bed+5	9.7	0.089	2.583	0.601	0.012	5.0	0.045	23.512
Bed+5	8.7	0.079	3.153	0.608	0.020	5.6	0.051	9.040
Bed+5	9.9	0.091	2.909	0.610	0.010	6.9	0.063	8.918

Bed+5	9.5	0.086	2.951	0.610	0.012	6.5	0.059	6.403
Bed+5	9.2	0.084	3.224	0.622	0.005	5.6	0.051	15.435
Bed+5	9.4	0.086	2.218	0.623	0.012	4.6	0.042	36.867
Bed+5	8.5	0.077	2.858	0.623	0.017	4.1	0.038	33.827
Bed+5	10.2	0.093	2.377	0.621	0.014	5.6	0.051	14.767
Bed+5	10.1	0.093	2.531	0.637	0.018	6.5	0.059	9.374
Bed+5	8.2	0.075	3.269	0.592	0.020	6.7	0.061	7.904
Bed+5	7.2	0.066	2.929	0.572	0.023	7.4	0.067	7.775
Bed+5	8.3	0.076	2.856	0.599	0.015	6.0	0.055	10.870
Bed+5	8.6	0.079	3.772	0.622	0.017	7.3	0.067	11.131
Bed+5	8.6	0.078	2.680	0.597	0.008	7.0	0.064	12.827
Bed+5	9.8	0.089	1.845	0.625	0.021	7.6	0.070	6.328
Bed+5	9.2	0.084	3.173	0.612	0.013	7.9	0.072	5.290
Bed+5	6.2	0.056	3.473	0.552	0.024	6.8	0.062	6.032
Bed+5	7.1	0.065	3.848	0.592	0.023	7.6	0.070	6.122
Bed+5	8.5	0.078	4.798	0.624	0.014	6.3	0.058	6.480
Bed+5	8.5	0.078	4.710	0.614	0.015	6.7	0.061	7.530
Bed+5	9.0	0.082	2.575	0.616	0.015	6.8	0.062	5.187
Bed+5	5.8	0.053	5.211	0.566	0.021	6.6	0.061	20.245
Bed+5	5.0	0.046	4.795	0.523	0.023	5.2	0.048	12.928
Bed+5	8.3	0.076	3.468	0.621	0.020	6.1	0.055	10.605
Bed+5	6.6	0.060	4.128	0.594	0.024	7.4	0.067	9.029
Bed+8	11.4	0.097	1.796	0.629	-0.001	7.6	0.065	4.718
Bed+8	11.6	0.099	1.275	0.618	0.012	7.1	0.061	6.706
Bed+8	12.1	0.103	1.122	0.621	0.014	8.6	0.073	3.554
Bed+8	9.8	0.084	2.209	0.616	0.017	9.2	0.078	3.028
Bed+8	10.4	0.089	1.747	0.609	0.008	9.2	0.079	2.438
Bed+8	10.2	0.087	1.365	0.588	0.011	10.3	0.088	2.835
Bed+8	10.8	0.092	1.395	0.607	0.009	9.9	0.084	2.516
Bed+8	12.6	0.108	1.001	0.611	0.008	10.2	0.087	2.836
Bed+8	10.1	0.086	1.494	0.608	0.020	9.0	0.077	3.802
Bed+8	10.0	0.086	1.590	0.590	0.025	9.0	0.077	2.619
Bed+8	8.6	0.073	2.696	0.636	0.014	9.4	0.080	2.644
Bed+8	8.9	0.076	1.965	0.609	0.008	9.9	0.084	2.162
Bed+8	9.9	0.084	2.014	0.608	0.009	9.6	0.082	2.480
Bed+8	9.9	0.085	1.524	0.612	0.006	10.0	0.085	2.662
Bed+8	10.4	0.089	1.923	0.596	0.000	9.2	0.078	3.940
Bed+8	10.6	0.090	1.461	0.605	0.004	8.0	0.069	3.651
Bed+8	10.5	0.089	1.656	0.624	0.007	8.4	0.071	4.651

Bed+8	11.0	0.094	1.104	0.591	0.010	8.9	0.076	3.469
Bed+8	12.0	0.102	1.205	0.609	0.014	9.3	0.080	2.335
Bed+8	10.6	0.090	1.717	0.610	0.024	8.9	0.076	2.709
Bed+8	9.2	0.078	2.000	0.617	0.014	9.4	0.080	2.781
Bed+8	9.4	0.081	1.675	0.625	0.009	8.8	0.075	2.697
Bed+8	10.7	0.091	1.504	0.630	0.004	9.6	0.082	2.324
Bed+8	10.9	0.093	1.462	0.637	0.000	9.1	0.078	2.806
Bed+8	12.1	0.103	1.481	0.631	0.001	8.6	0.073	4.084
Bed+8	13.0	0.111	1.070	0.622	0.003	7.4	0.063	5.908
Bed+8	12.1	0.103	1.162	0.619	0.006	5.9	0.050	9.448
Bed+8	10.6	0.091	1.369	0.632	0.010	7.5	0.064	5.908
Bed+8	11.8	0.100	1.138	0.629	0.011	8.8	0.075	2.826
Bed+8	11.9	0.102	1.258	0.603	0.010	8.3	0.071	2.509
Bed+8	11.0	0.094	1.699	0.612	0.010	7.4	0.063	4.737
Bed+8	8.8	0.075	2.409	0.575	-0.001	6.3	0.054	5.749
Bed+8	9.1	0.078	2.332	0.625	0.022	8.1	0.069	4.543
Bed+8	9.3	0.079	2.475	0.619	0.019	8.7	0.074	3.654
Bed+8	10.5	0.090	1.698	0.623	0.017	9.7	0.083	3.295
Bed+8	11.1	0.095	1.460	0.610	0.011	10.2	0.087	3.004
Bed+8	10.7	0.091	1.989	0.619	0.008	11.2	0.095	3.059
Bed+8	10.5	0.089	1.850	0.588	0.007	11.6	0.099	3.159
Bed+8	11.1	0.095	1.274	0.595	0.002	10.7	0.091	2.770
Bed+8	9.3	0.079	2.349	0.790	0.048	11.3	0.096	1.810
Bed+8	8.7	0.074	2.391	0.592	0.005	9.9	0.084	2.493
Bed+8	8.9	0.076	2.125	0.612	0.002	8.7	0.075	4.316
Bed+8	10.6	0.090	1.569	0.606	0.003	7.9	0.067	2.792
Bed+8	11.5	0.098	1.417	0.633	0.001	8.6	0.073	3.022
Bed+8	11.1	0.095	1.353	0.613	0.008	7.2	0.061	6.511
Bed+23	25.2	0.207	0.833	0.685	0.002	23.9	0.197	1.055
Bed+23	25.6	0.211	0.581	0.726	0.002	23.8	0.196	0.844
Bed+23	25.4	0.209	0.595	0.716	0.001	23.7	0.195	0.997
Bed+23	25.7	0.212	0.523	0.730	0.004	23.3	0.192	0.777
Bed+23	24.4	0.201	0.589	0.687	0.007	22.9	0.189	0.790
Bed+23	24.5	0.202	0.828	0.731	0.011	26.0	0.214	0.777
Bed+23	24.2	0.199	0.719	0.698	0.010	24.7	0.203	0.976
Bed+23	23.9	0.197	0.679	0.717	0.003	25.4	0.209	0.913
Bed+23	23.8	0.196	0.692	0.688	-0.003	24.8	0.204	0.705
Bed+23	25.1	0.207	0.689	0.702	0.004	25.0	0.205	0.776
Bed+23	24.9	0.205	0.771	0.689	-0.002	24.7	0.204	0.856

Bed+23	24.2	0.199	0.763	0.667	-0.003	24.4	0.201	0.787
Bed+23	24.3	0.200	0.678	0.692	-0.001	23.8	0.196	1.030
Bed+23	23.9	0.197	0.595	0.698	0.007	23.8	0.196	0.984
Bed+23	24.4	0.201	0.532	0.675	0.005	24.0	0.198	0.802
Bed+23	25.2	0.208	0.727	0.686	0.009	26.1	0.215	0.765
Bed+23	25.9	0.214	0.748	0.699	-0.002	25.1	0.207	0.745
Bed+23	24.9	0.205	0.981	0.737	0.015	23.3	0.192	1.042
Bed+23	23.6	0.194	1.044	0.705	0.011	23.7	0.195	0.938
Bed+23	23.0	0.189	1.157	0.721	0.010	24.0	0.198	1.061
Bed+23	22.8	0.188	0.870	0.704	0.008	23.5	0.194	0.838
Bed+23	23.6	0.194	0.936	0.720	0.006	24.1	0.198	0.966
Bed+23	23.4	0.193	0.652	0.694	0.007	27.1	0.223	0.819
Bed+23	23.6	0.195	0.761	0.681	0.004	27.2	0.224	0.758
Bed+23	23.2	0.191	0.646	0.693	0.008	26.6	0.219	0.763
Bed+23	23.6	0.195	0.697	0.723	-0.002	25.3	0.208	0.856
Bed+23	24.6	0.202	0.721	0.702	-0.001	25.6	0.211	0.935
Bed+23	24.9	0.205	0.808	0.705	0.004	25.0	0.206	0.742
Bed+23	24.5	0.201	1.066	0.733	0.009	25.5	0.210	0.929
Bed+23	24.5	0.202	0.783	0.799	-0.010	25.9	0.213	0.867
Bed+23	23.6	0.194	0.932	0.694	-0.004	25.7	0.212	0.719
Bed+23	23.1	0.190	0.838	0.678	-0.003	24.7	0.204	0.921
Bed+23	24.0	0.197	0.850	0.693	-0.001	24.7	0.204	1.097
Bed+23	22.8	0.188	0.797	0.686	-0.009	23.9	0.196	0.983
Bed+23	25.1	0.207	0.923	0.703	0.002	22.7	0.187	0.954
Bed+23	25.2	0.207	0.621	0.689	0.008	25.6	0.210	0.793
Bed+23	26.1	0.215	0.683	0.675	0.006	26.9	0.221	0.683
Bed+23	25.7	0.212	0.678	0.686	0.007	26.5	0.218	0.825
Bed+23	24.4	0.201	0.704	0.706	-0.002	26.4	0.217	0.875
Bed+23	23.3	0.192	0.938	0.720	0.001	24.4	0.201	0.874
Bed+23	23.1	0.191	0.872	0.711	0.002	24.1	0.198	0.877
Bed+23	22.9	0.188	0.831	0.698	0.004	23.0	0.189	0.593
Bed+23	23.3	0.191	0.767	0.698	0.005	23.6	0.195	0.745
Bed+23	23.0	0.189	0.815	0.685	0.006	23.2	0.191	1.002
Bed+23	23.1	0.191	0.795	0.723	0.003	24.2	0.199	0.903
Bed+23	23.9	0.197	0.786	0.700	0.001	24.0	0.198	0.762
Bed+39	35.2	0.304	0.792	0.743	0.002	38.0	0.328	0.628
Bed+39	36.5	0.315	0.611	0.735	0.004	38.7	0.334	0.466
Bed+39	36.5	0.315	0.508	0.778	0.004	37.8	0.326	0.610
Bed+39	36.3	0.314	0.465	0.769	0.000	38.3	0.331	0.595

Bed+39	37.0	0.320	0.479	0.753	-0.003	38.1	0.329	0.514
Bed+39	38.4	0.331	0.589	0.743	0.004	37.9	0.327	0.682
Bed+39	37.1	0.320	0.554	0.757	0.000	36.4	0.314	0.677
Bed+39	37.2	0.321	0.698	0.777	-0.003	36.6	0.316	0.700
Bed+39	37.7	0.325	0.567	0.761	-0.001	36.5	0.315	0.742
Bed+39	37.5	0.323	0.594	0.767	0.001	36.5	0.315	0.707
Bed+39	38.4	0.332	0.538	0.755	0.005	37.7	0.326	0.618
Bed+39	37.8	0.327	0.541	0.758	0.004	37.1	0.320	0.604
Bed+39	38.6	0.334	0.545	0.734	0.002	37.8	0.327	0.684
Bed+39	38.1	0.329	0.615	0.716	-0.011	36.7	0.317	0.794
Bed+39	36.8	0.318	0.682	0.729	0.008	36.4	0.314	0.699
Bed+39	39.4	0.340	0.528	0.747	0.001	39.5	0.341	0.610
Bed+39	38.1	0.329	0.519	0.771	0.000	36.7	0.317	0.760
Bed+39	38.8	0.335	0.497	0.763	0.002	36.8	0.317	0.811
Bed+39	38.8	0.334	0.516	0.743	0.005	36.7	0.317	0.826
Bed+39	39.2	0.338	0.497	0.757	0.008	38.2	0.329	0.692
Bed+39	39.2	0.338	0.453	0.758	0.004	37.9	0.327	0.641
Bed+39	38.8	0.335	0.461	0.756	0.002	38.8	0.335	0.576
Bed+39	37.5	0.324	0.575	0.754	0.003	37.5	0.324	0.561
Bed+39	37.8	0.327	0.472	0.768	0.003	37.8	0.326	0.635
Bed+39	38.4	0.331	0.325	0.741	0.006	38.0	0.328	0.548
Bed+39	37.8	0.327	0.513	0.759	0.003	37.7	0.325	0.632
Bed+39	36.8	0.317	0.450	0.748	0.009	37.2	0.322	0.625
Bed+39	38.1	0.329	0.425	0.767	0.003	37.9	0.327	0.576
Bed+39	37.4	0.323	0.521	0.771	0.001	38.1	0.328	0.635
Bed+39	37.9	0.327	0.534	0.742	0.003	37.7	0.325	0.693
Bed+39	39.1	0.338	0.529	0.761	0.000	37.3	0.322	0.633
Bed+39	39.9	0.345	0.460	0.755	0.006	38.1	0.329	0.497
Bed+39	39.6	0.342	0.465	0.742	0.003	38.6	0.333	0.562
Bed+39	40.5	0.349	0.459	0.752	0.004	38.1	0.329	0.641
Bed+39	39.4	0.340	0.416	0.771	-0.001	39.0	0.337	0.738
Bed+39	40.5	0.350	0.552	0.764	0.000	38.9	0.336	0.670
Bed+39	40.0	0.345	0.484	0.781	0.004	37.2	0.321	0.673
Bed+39	38.1	0.329	0.436	0.790	0.008	37.4	0.323	0.628
Bed+39	38.6	0.334	0.476	0.787	0.007	37.6	0.325	0.516
Bed+39	39.3	0.339	0.473	0.786	0.008	37.7	0.325	0.531
Bed+39	39.0	0.337	0.724	0.774	0.005	38.1	0.329	0.520
Bed+39	39.2	0.338	0.456	0.788	0.000	38.3	0.330	0.613
Bed+39	37.6	0.325	0.598	0.773	0.001	37.8	0.327	0.625

Bed+39	38.1	0.329	0.517	0.786	-0.001	38.5	0.332	0.541
Bed+39	38.9	0.335	0.410	0.780	0.003	39.3	0.339	0.568
Bed+39	38.0	0.328	0.475	0.771	-0.001	39.0	0.337	0.621
Bed+57	51.2	0.423	0.672	0.782	-0.002	52.4	0.433	0.489
Bed+57	52.0	0.430	0.496	0.760	-0.003	52.7	0.435	0.467
Bed+57	52.5	0.434	0.423	0.769	0.000	52.6	0.435	0.394
Bed+57	53.5	0.441	0.361	0.790	0.003	52.6	0.434	0.408
Bed+57	53.4	0.441	0.406	0.778	0.007	52.8	0.436	0.372
Bed+57	53.7	0.444	0.393	0.789	0.004	52.3	0.432	0.442
Bed+57	53.4	0.441	0.440	0.753	0.033	53.2	0.439	0.461
Bed+57	53.1	0.438	0.356	0.780	0.005	54.7	0.451	0.416
Bed+57	52.1	0.430	0.413	0.772	0.002	55.0	0.455	0.459
Bed+57	50.5	0.417	0.422	0.778	-0.007	58.6	0.484	0.486
Bed+57	53.9	0.445	0.315	0.785	-0.012	51.3	0.424	0.503
Bed+57	54.9	0.454	0.343	0.764	-0.011	51.0	0.422	0.454
Bed+57	55.0	0.454	0.329	0.793	-0.009	50.4	0.416	0.404
Bed+57	54.1	0.447	0.363	0.760	0.002	50.7	0.419	0.557
Bed+57	54.7	0.452	0.311	0.790	0.006	49.8	0.411	0.570
Bed+57	53.8	0.444	0.445	0.777	0.007	50.6	0.418	0.450
Bed+57	53.5	0.442	0.425	0.782	0.009	50.7	0.419	0.529
Bed+57	53.5	0.441	0.326	0.768	0.006	51.8	0.428	0.490
Bed+57	53.0	0.438	0.352	0.679	0.022	51.7	0.427	0.300
Bed+57	53.4	0.441	0.336	0.776	-0.059	52.3	0.432	0.370
Bed+57	53.6	0.443	0.371	0.786	0.002	52.5	0.433	0.412
Bed+57	53.2	0.439	0.334	0.773	0.003	52.3	0.432	0.405
Bed+57	53.7	0.444	0.373	0.808	0.002	53.5	0.442	0.519
Bed+57	52.2	0.431	0.428	0.798	-0.006	53.4	0.441	0.527
Bed+57	52.0	0.430	0.432	0.788	0.002	52.1	0.430	0.443
Bed+57	50.5	0.417	0.497	0.810	0.003	52.6	0.434	0.511
Bed+57	50.6	0.418	0.416	0.806	-0.003	51.0	0.421	0.457
Bed+57	51.8	0.428	0.358	0.777	-0.002	51.5	0.426	0.519
Bed+57	52.6	0.435	0.328	0.831	0.020	51.6	0.426	0.506
Bed+57	52.3	0.432	0.402	0.756	0.005	51.4	0.424	0.415
Bed+57	52.9	0.437	0.369	0.772	0.005	52.3	0.432	0.421
Bed+57	53.0	0.438	0.412	0.761	0.000	53.0	0.438	0.422
Bed+57	53.6	0.442	0.427	0.802	-0.002	52.5	0.433	0.516
Bed+57	53.8	0.444	0.426	0.784	0.002	53.2	0.439	0.463
Bed+57	53.6	0.442	0.420	0.776	0.004	53.2	0.439	0.465
Bed+57	53.0	0.438	0.393	0.776	0.005	53.2	0.440	0.455

Bed+57	53.8	0.444	0.386	0.774	0.008	54.2	0.448	0.405
Bed+57	52.9	0.437	0.441	0.739	0.008	56.0	0.462	0.469
Bed+57	53.4	0.441	0.458	0.753	0.008	55.7	0.460	0.433
Bed+57	51.4	0.424	0.412	0.757	0.005	57.8	0.477	0.416
Bed+57	50.4	0.417	0.385	0.782	-0.005	56.9	0.470	0.491
Bed+57	50.8	0.420	0.482	0.766	-0.009	53.6	0.442	0.503
Bed+57	51.1	0.422	0.382	0.774	-0.006	52.1	0.430	0.310
Bed+57	52.6	0.434	0.421	0.763	-0.004	52.8	0.436	0.415
Bed+57	54.6	0.450	0.364	0.791	-0.002	52.3	0.432	0.461
Bed+57	54.1	0.447	0.402	0.781	0.001	51.0	0.421	0.377

Data from paired samples over dunes. Velocity was measured only at probe 1. y is height over the bed, d is water depth, $\overline{u}$ is average downstream velocity, $\overline{w}$ average cross-stream velocity, *z* is the distance from the flume sidewall, and *C* is the suspended sediment concentration. Position measurements are average dune height plus some distance in mm. This was used to set probe height at the beginning of the experiment.

	Probe 1 (*z*=0.33 m)					Probe 2 (*z*=0.66 m)		
Position	*y* (mm)	*y*/*d*	*C* (g/L)	$\overline{u}$	$\overline{w}$	*y* (mm)	*y*/*d*	*C* (g/L)
Dune Avg+0	52.3	0.336	1.160	0.475	-0.094	19.0	0.122	4.470
Dune Avg+0	31.7	0.204	0.300	0.321	-0.018	23.9	0.154	0.930
Dune Avg+0	44.3	0.285	1.180	0.457	-0.111	12.8	0.082	7.670
Dune Avg+0	53.1	0.341	0.160	0.277	-0.009	16.8	0.108	2.020
Dune Avg+0	11.6	0.074	5.380	0.035	0.123	45.9	0.295	0.260
Dune Avg+0	19.2	0.123	8.610	0.25	-0.111	40.2	0.258	0.220
Dune Avg+0	37.4	0.240	0.030	0.347	-0.077	50.4	0.324	0.150
Dune Avg+0	14.5	0.093	16.760	0.297	-0.011	41.3	0.265	0.250
Dune Avg+0	45.3	0.291	0.055	0.585	-0.109	20.2	0.130	0.660
Dune Avg+0	18.0	0.115	0.850	0.092	0.044	56.4	0.362	0.080
Dune Avg+0	27.1	0.174	10.710	0.14	0.031	13.5	0.087	14.760
Dune Avg+0	49.0	0.315	12.590	0.573	-0.05	19.6	0.126	1.230
Dune Avg+0	33.9	0.218	1.110	0.407	0.017	23.4	0.150	19.740
Dune Avg+0	60.8	0.391	0.130	0.237	-0.051	53.8	0.345	0.070
Dune Avg+0	61.5	0.395	0.150	0.14	0.003	19.6	0.126	0.060
Dune Avg+0	45.0	0.289	0.620	0.428	0.006	46.1	0.296	0.080
Dune Avg+10	17.4	0.119	4.785	0.379	0.009	19.0	0.129	4.950
Dune Avg+10	27.0	0.184	1.030	0.303	-0.191	15.4	0.105	4.950
Dune Avg+10	46.8	0.318	0.590	0.423	-0.112	13.2	0.090	27.060
Dune Avg+10	28.1	0.191	0.280	0.528	-0.043	18.9	0.128	1.110
Dune Avg+10	45.9	0.312	0.060	0.524	0.031	12.5	0.085	23.590

Dune Avg+10	62.1	0.422	0.190	0.603	0.021	34.2	0.232	0.720
Dune Avg+10	50.1	0.341	0.160	0.554	0.082	19.1	0.130	1.180
Dune Avg+10	69.7	0.474	0.080	0.545	0.074	46.7	0.317	0.190
Dune Avg+10	22.5	0.153	0.250	0.284	0.12	40.8	0.277	0.290
Dune Avg+10	29.5	0.200	0.840	0.461	0.015	17.2	0.117	0.180
Dune Avg+10	22.9	0.156	1.400	0.224	0.128	21.4	0.145	0.550
Dune Avg+10	40.2	0.273	0.340	0.128	0.108	40.9	0.278	0.140
Dune Avg+10	25.1	0.171	1.130	0.203	-0.077	44.5	0.303	0.150
Dune Avg+10	7.7	0.052	31.230	0.071	0.095	29.9	0.204	2.040
Dune Avg+10	11.1	0.075	16.220	0.19	0.041	21.8	0.148	1.650
Dune Avg+10	41.2	0.280	0.540	0.318	0.079	37.3	0.254	0.570
Dune Avg+10	20.8	0.141	1.120	0.107	0.041	48.4	0.329	0.740
Dune Avg+10	9.7	0.066	4.270	0.031	0.034	48.1	0.327	0.090
Dune Avg+10	21.2	0.144	1.560	0.083	-0.129	55.6	0.378	0.080
Dune Avg+10	39.3	0.267	1.270	0.451	-0.069	34.4	0.234	0.280
Dune Avg+10	47.9	0.326	0.250	0.319	-0.062	17.3	0.118	1.860
Dune Avg+10	17.1	0.117	0.800	0.237	-0.062	24.7	0.168	2.110
Dune Avg+10	36.4	0.247	0.270	0.583	-0.019	13.6	0.093	0.170
Dune Avg+10	31.9	0.217	0.230	0.511	0.144	16.3	0.111	20.770
Dune Avg+10	36.8	0.250	0.150	0.498	0.181	14.0	0.095	0.980
Dune Avg+10	74.2	0.505	0.210	0.359	0.059	15.3	0.104	1.110
Dune Avg+10	61.8	0.420	0.110	0.547	0.046	31.7	0.216	0.390
Dune Avg+10	30.2	0.205	0.080	0.558	-0.019	79.1	0.537	0.130
Dune Avg+10	65.1	0.443	0.050	0.51	0	44.9	0.305	0.440
Dune Avg+10	28.5	0.194	0.120	0.633	0.098	17.8	0.121	1.730
Dune Avg+10	47.3	0.321	0.020	0.232	-0.026	29.3	0.199	0.070
Dune Avg+30	46.5	0.320	0.303	0.668	-0.029	55.0	0.378	0.231
Dune Avg+30	42.7	0.294	0.072	0.723	0.026	68.3	0.469	0.283
Dune Avg+30	104.0	0.715	0.145	0.515	-0.017	54.7	0.376	0.036
Dune Avg+30	104.7	0.719	0.040	0.561	-0.023	45.2	0.311	1.194
Dune Avg+30	88.2	0.606	0.017	0.736	-0.036	36.1	0.248	0.788
Dune Avg+30	40.9	0.281	0.005	0.693	0.139	24.3	0.167	12.007
Dune Avg+30	58.0	0.398	0.089	0.716	0.106	28.7	0.197	1.149
Dune Avg+30	66.2	0.454	0.062	0.594	0.023	46.8	0.321	0.130
Dune Avg+30	38.9	0.267	0.099	0.298	-0.003	72.6	0.498	0.072
Dune Avg+30	29.7	0.204	3.819	0.539	0.005	52.3	0.359	0.228
Dune Avg+30	44.0	0.302	1.292	0.588	0.089	30.5	0.209	0.314
Dune Avg+30	21.7	0.149	0.106	0.423	0.142	27.0	0.186	0.494
Dune Avg+30	19.6	0.135	0.714	0.397	0.112	27.6	0.190	1.334

Dune Avg+30	22.6	0.155	1.994	0.322	0.108	51.1	0.351	1.499
Dune Avg+30	32.1	0.220	0.368	0.669	-0.015	75.1	0.516	0.071
Dune Avg+30	43.9	0.302	0.124	0.745	-0.07	83.3	0.572	0.141
Dune Avg+30	105.1	0.722	0.187	0.58	-0.021	64.7	0.444	0.216
Dune Avg+30	75.9	0.522	0.562	0.693	-0.012	17.2	0.118	0.311
Dune Avg+30	49.1	0.337	0.197	0.807	-0.019	19.6	0.135	3.534
Dune Avg+30	55.7	0.382	0.009	0.756	-0.029	26.5	0.182	15.980
Dune Avg+30	41.7	0.287	0.015	0.707	0.011	26.9	0.185	0.591
Dune Avg+30	40.5	0.278	0.021	0.777	-0.001	25.7	0.177	0.138
Dune Avg+30	43.3	0.298	0.003	0.818	0.054	33.1	0.227	0.423
Dune Avg+30	117.0	0.803	0.022	0.657	0.01	31.3	0.215	0.708
Dune Avg+30	125.8	0.864	0.009	0.741	0.008	20.2	0.138	0.254
Dune Avg+30	103.4	0.710	0.027	0.754	0.042	28.3	0.194	0.245
Dune Avg+30	98.9	0.679	0.345	0.65	0.041	25.1	0.172	0.692
Dune Avg+30	49.7	0.341	0.683	0.629	0.052	40.9	0.281	0.036
Dune Avg+30	41.4	0.284	0.456	0.662	-0.098	58.2	0.400	0.041
Dune Avg+30	39.1	0.269	0.806	0.523	-0.091	64.6	0.444	0.016
Dune Avg+30	45.2	0.311	0.362	0.578	-0.021	76.8	0.527	0.040
Dune Avg+30	75.7	0.520	0.061	0.632	0.011	97.8	0.671	0.045
Dune Avg+30	63.9	0.439	0.012	0.655	0.048	67.1	0.461	0.019
Dune Avg+30	77.0	0.529	0.008	0.539	0.003	60.9	0.418	0.126
Dune Avg+30	44.1	0.303	0.047	0.625	0.006	98.1	0.674	0.040
Dune Avg+30	34.4	0.236	0.281	0.595	0.001	67.8	0.466	0.804
Dune Avg+30	87.9	0.604	0.031	0.677	-0.022	63.1	0.434	0.213
Dune Avg+30	50.3	0.346	0.016	0.68	-0.061	77.5	0.532	0.068
Dune Avg+30	72.5	0.498	0.016	0.668	-0.016	26.6	0.183	6.694
Dune Avg+30	70.7	0.486	0.035	0.605	0.014	56.0	0.384	1.021
Dune Avg+30	80.6	0.554	0.017	0.564	0.019	57.8	0.397	0.156
Dune Avg+30	78.4	0.539	0.074	0.701	0.056	39.7	0.272	0.780
Dune Avg+30	26.9	0.185	4.159	0.611	0.13	38.1	0.261	0.127
Dune Avg+30	42.5	0.292	0.196	0.548	0.093	62.1	0.426	0.125
Dune Avg+30	67.6	0.464	0.039	0.5	0.02	52.8	0.363	0.130
Dune Avg+50	56.2	0.378	0.170	0.854	0.103	45.9	0.309	0.030
Dune Avg+50	45.2	0.304	0.040	0.737	-0.014	95.4	0.641	0.010
Dune Avg+50	30.6	0.205	0.040	0.725	-0.021	85.6	0.576	0.060
Dune Avg+50	30.9	0.208	0.060	0.75	-0.045	55.2	0.371	0.080
Dune Avg+50	27.7	0.187	0.090	0.718	0.01	58.7	0.394	0.180
Dune Avg+50	60.4	0.406	0.070	0.769	-0.017	73.4	0.493	0.100
Dune Avg+50	51.8	0.348	0.060	0.749	-0.041	50.9	0.342	0.070

Dune Avg+50	60.1	0.404	0.010	0.753	0.014	58.6	0.394	0.010
Dune Avg+50	57.9	0.389	0.010	0.74	0.01	63.9	0.430	0.010
Dune Avg+50	70.5	0.474	0.040	0.645	-0.029	79.0	0.531	0.020
Dune Avg+50	64.2	0.432	0.050	0.678	-0.053	88.0	0.592	0.080
Dune Avg+50	71.4	0.480	0.060	0.76	-0.079	96.2	0.647	0.230
Dune Avg+50	74.7	0.502	0.030	0.767	-0.033	50.0	0.336	0.690
Dune Avg+50	91.5	0.615	0.020	0.823	-0.007	71.4	0.480	0.510
Dune Avg+50	38.5	0.259	0.020	0.854	0.022	39.2	0.264	0.030
Dune Avg+50	47.9	0.322	0.040	0.816	0.01	43.5	0.292	0.040
Dune Avg+50	51.7	0.348	0.050	0.737	0.014	49.7	0.334	0.030
Dune Avg+50	63.0	0.424	0.030	0.697	0.025	71.4	0.480	0.050
Dune Avg+50	73.2	0.492	0.010	0.71	0.011	66.2	0.445	0.370
Dune Avg+50	111.2	0.748	0.030	0.646	0.025	65.4	0.440	0.030
Dune Avg+50	72.4	0.487	0.020	0.846	0.034	55.0	0.370	0.020
Dune Avg+50	45.7	0.307	0.070	0.871	-0.022	50.3	0.338	0.030
Dune Avg+50	58.2	0.392	0.130	0.687	0.049	48.8	0.328	0.150
Dune Avg+50	47.4	0.319	0.080	0.73	0.019	65.2	0.439	0.410
Dune Avg+50	46.5	0.313	0.040	0.746	0.084	51.7	0.348	0.110
Dune Avg+50	41.7	0.280	0.140	0.688	-0.021	97.0	0.652	0.010
Dune Avg+50	42.5	0.286	0.020	0.847	-0.003	65.3	0.439	0.100
Dune Avg+50	85.7	0.577	0.010	0.743	-0.052	76.4	0.514	0.070
Dune Avg+50	130.6	0.879	0.020	0.659	-0.034	83.5	0.561	0.050
Dune Avg+50	125.1	0.842	0.060	0.563	-0.019	103.6	0.697	0.030
Dune Avg+50	57.5	0.386	0.010	0.74	-0.01	41.6	0.280	0.040
Dune Avg+50	64.4	0.433	0.010	0.744	0.027	61.3	0.412	0.120
Dune Avg+50	88.7	0.597	0.010	0.664	0.043	58.6	0.394	0.010
Dune Avg+50	110.6	0.744	0.010	0.574	0.016	79.1	0.532	0.040
Dune Avg+50	126.5	0.851	0.010	0.602	0.017	101.6	0.683	0.020
Dune Avg+50	142.8	0.960	0.050	0.682	-0.001	59.7	0.402	0.050
Dune Avg+50	89.5	0.602	0.210	0.691	0.028	100.9	0.679	0.060
Dune Avg+50	86.9	0.585	0.040	0.704	0.063	85.7	0.577	0.030
Dune Avg+50	60.4	0.406	0.040	0.74	0.045	75.4	0.507	0.030
Dune Avg+50	63.9	0.429	0.050	0.705	-0.025	96.4	0.648	0.160
Dune Avg+50	52.9	0.355	0.090	0.769	-0.018	96.2	0.647	0.360
Dune Avg+50	55.1	0.371	0.110	0.713	0.01	50.7	0.341	0.290
Dune Avg+50	64.1	0.431	0.190	0.619	0.037	77.4	0.521	0.120
Dune Avg+50	88.7	0.596	0.610	0.607	-0.031	106.9	0.719	0.280
Dune Avg+50	55.1	0.371	0.140	0.69	-0.05	104.2	0.701	0.060
Dune Avg+50	41.006	0.276	0.07	0.731	-0.028	84.248	0.567	0.01

Dune Avg+70	129.8	0.867	0.097	0.696	-0.033	56.9	0.380	0.002
Dune Avg+70	85.1	0.568	0.005	0.698	0.022	68.0	0.454	0.007
Dune Avg+70	72.8	0.486	0.018	0.702	0.066	79.2	0.529	0.007
Dune Avg+70	91.3	0.610	0.099	0.658	0.049	74.6	0.498	0.007
Dune Avg+70	128.2	0.856	0.029	0.617	-0.022	77.5	0.517	0.010
Dune Avg+70	121.3	0.810	0.072	0.722	0.021	85.0	0.568	0.014
Dune Avg+70	118.8	0.793	0.005	0.7	0.014	88.1	0.588	0.012
Dune Avg+70	82.3	0.549	0.063	0.773	0.017	95.1	0.635	0.017
Dune Avg+70	97.0	0.648	0.043	0.788	-0.01	117.3	0.783	0.007
Dune Avg+70	57.1	0.381	0.012	0.838	-0.111	100.1	0.669	0.076
Dune Avg+70	56.9	0.380	0.025	0.88	-0.081	72.2	0.482	0.202
Dune Avg+70	64.9	0.434	0.015	0.87	-0.098	76.6	0.511	0.367
Dune Avg+70	110.8	0.740	0.007	0.808	-0.08	37.4	0.250	0.133
Dune Avg+70	99.6	0.665	0.038	0.691	0.002	49.0	0.328	0.051
Dune Avg+70	87.6	0.585	0.141	0.68	0.067	59.2	0.395	0.010
Dune Avg+70	92.4	0.617	0.003	0.767	0.019	72.7	0.486	0.063
Dune Avg+70	101.0	0.675	0.005	0.735	-0.023	86.0	0.574	0.376
Dune Avg+70	84.3	0.563	0.010	0.731	-0.05	69.1	0.462	0.346
Dune Avg+70	98.3	0.657	0.015	0.735	-0.043	77.6	0.518	0.529
Dune Avg+70	132.8	0.887	0.036	0.681	-0.028	86.8	0.580	0.362
Dune Avg+70	112.2	0.750	0.038	0.611	-0.024	90.8	0.606	0.008
Dune Avg+70	77.0	0.515	0.057	0.764	-0.035	130.7	0.873	0.010
Dune Avg+70	75.9	0.507	0.088	0.707	-0.03	71.6	0.478	0.014
Dune Avg+70	72.9	0.487	0.120	0.665	-0.01	62.2	0.415	0.007
Dune Avg+70	77.5	0.518	0.212	0.666	0.01	75.8	0.506	0.028
Dune Avg+70	80.8	0.540	0.151	0.621	0.005	84.2	0.562	0.021
Dune Avg+70	82.8	0.553	0.103	0.646	0.033	100.8	0.673	0.005
Dune Avg+70	87.0	0.581	0.085	0.682	0.03	121.6	0.812	0.014
Dune Avg+70	76.3	0.509	0.031	0.766	0.045	128.4	0.858	0.010
Dune Avg+70	51.7	0.345	0.005	0.883	0.008	89.6	0.599	0.010
Dune Avg+70	56.9	0.380	0.013	0.841	-0.043	91.0	0.608	0.002
Dune Avg+70	63.2	0.422	0.008	0.881	-0.04	78.7	0.526	0.007
Dune Avg+70	67.7	0.452	0.019	0.86	-0.064	87.8	0.587	0.036
Dune Avg+70	70.6	0.471	0.008	0.822	-0.057	109.0	0.728	0.019
Dune Avg+70	73.2	0.489	0.160	0.76	-0.099	106.9	0.714	0.044
Dune Avg+70	124.3	0.831	0.515	0.639	-0.055	115.4	0.771	0.110
Dune Avg+70	134.4	0.898	0.191	0.743	-0.057	112.1	0.749	0.057
Dune Avg+70	149.3	0.997	0.026	0.694	-0.023	134.4	0.898	0.040
Dune Avg+70	117.4	0.785	0.030	0.684	-0.012	71.5	0.478	0.026

Dune Avg+70	109.2	0.729	0.013	0.694	-0.015	68.4	0.457	0.025
Dune Avg+70	130.1	0.869	0.017	0.696	0.001	67.3	0.450	0.044
Dune Avg+70	147.5	0.985	0.003	0.754	0.026	73.5	0.491	0.326
Dune Avg+70	101.8	0.680	0.012	0.783	0.059	48.8	0.326	0.048
Dune Avg+70	78.1	0.522	0.027	0.804	0.102	49.1	0.328	0.016
Dune Avg+70	73.5	0.491	0.002	0.852	0.102	60.3	0.403	0.012

Appendix C: Flow maps

This appendix consists of maps of flow quantities collected in the experiment described in chapter 4. They were prepared using a commercially available software package. Kriging was used to create 50 by 50 grids which were used to create the contour maps shown here.

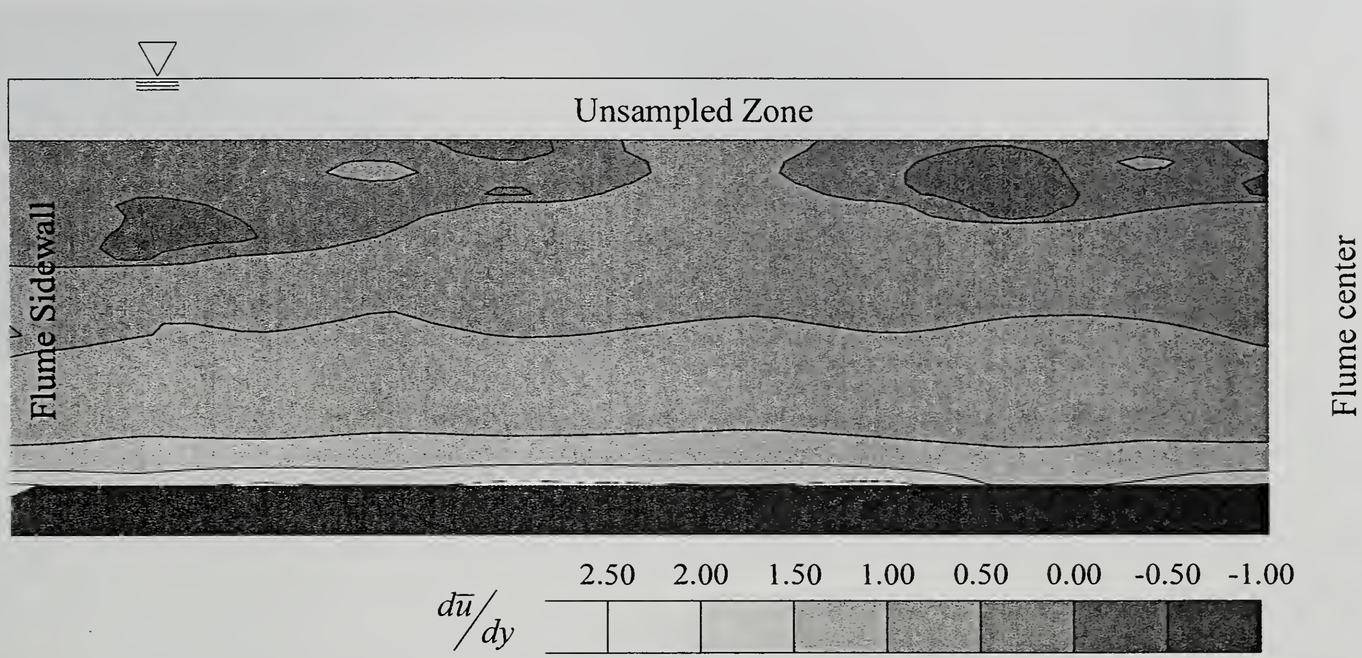

This is a map of the vertical gradient of average downstream velocity.

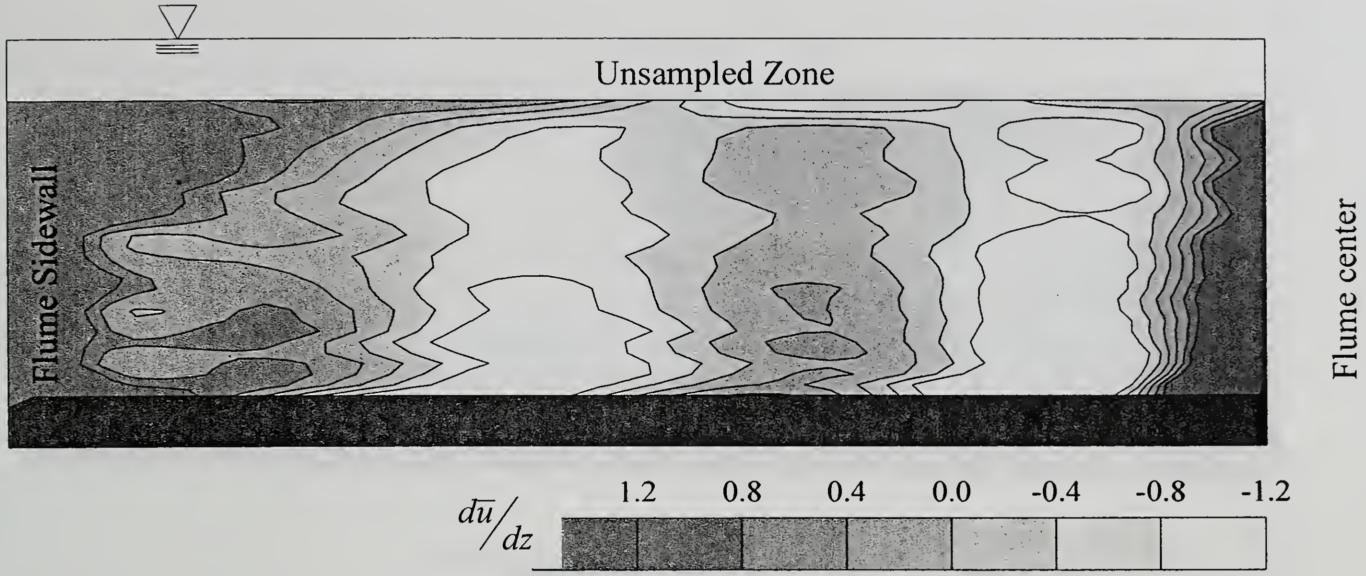

This is a map of the horizontal gradient of average downstream velocity.

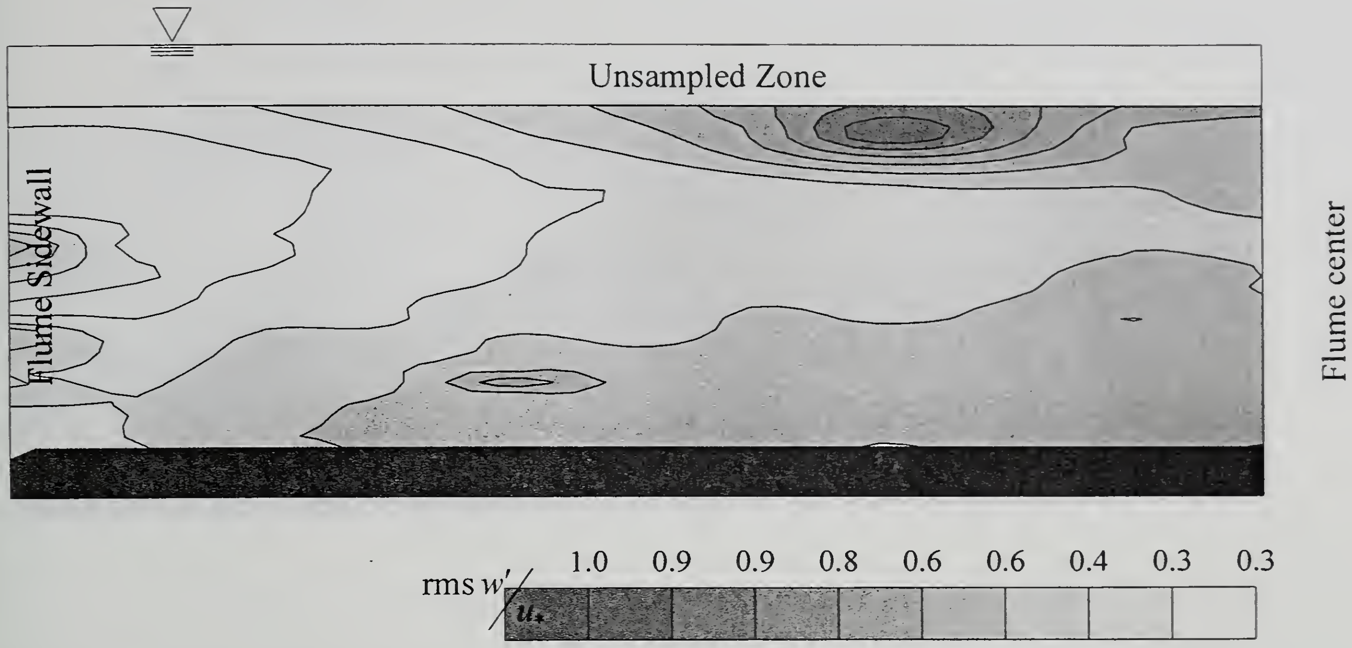

This is a map of root mean squared instantaneous cross-stream velocity scaled with shear velocity.

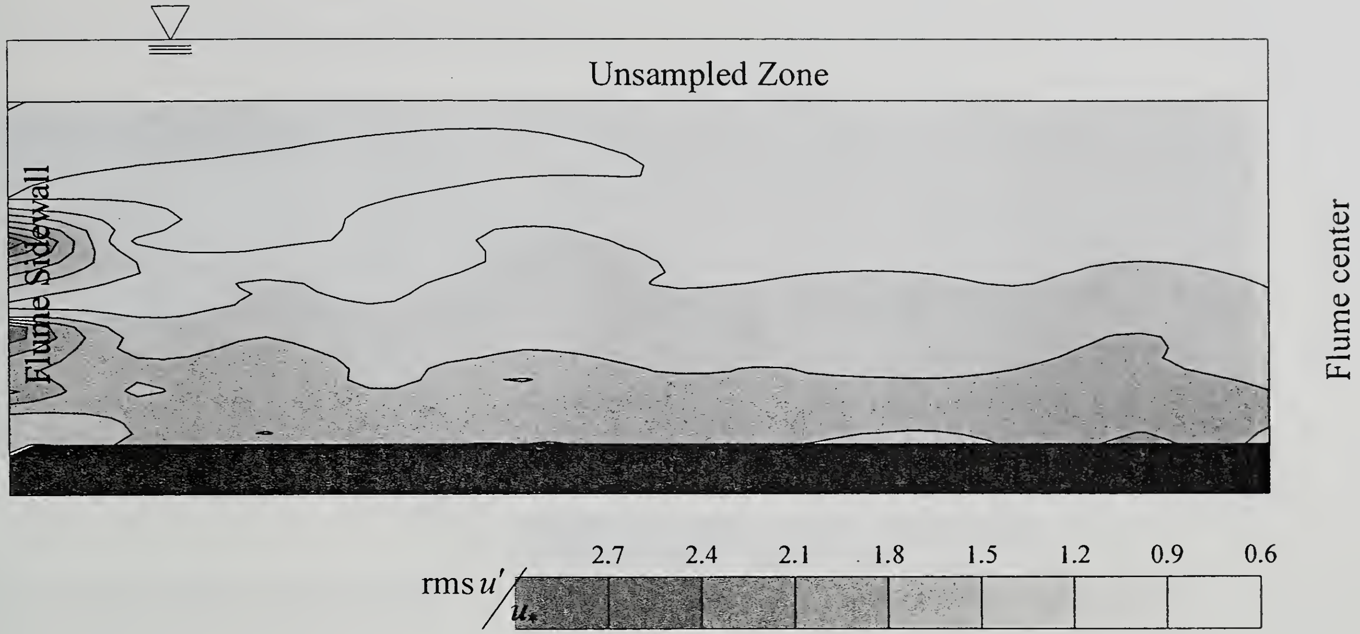

This is a map of root mean squared instantaneous down-stream velocity scaled with shear velocity.

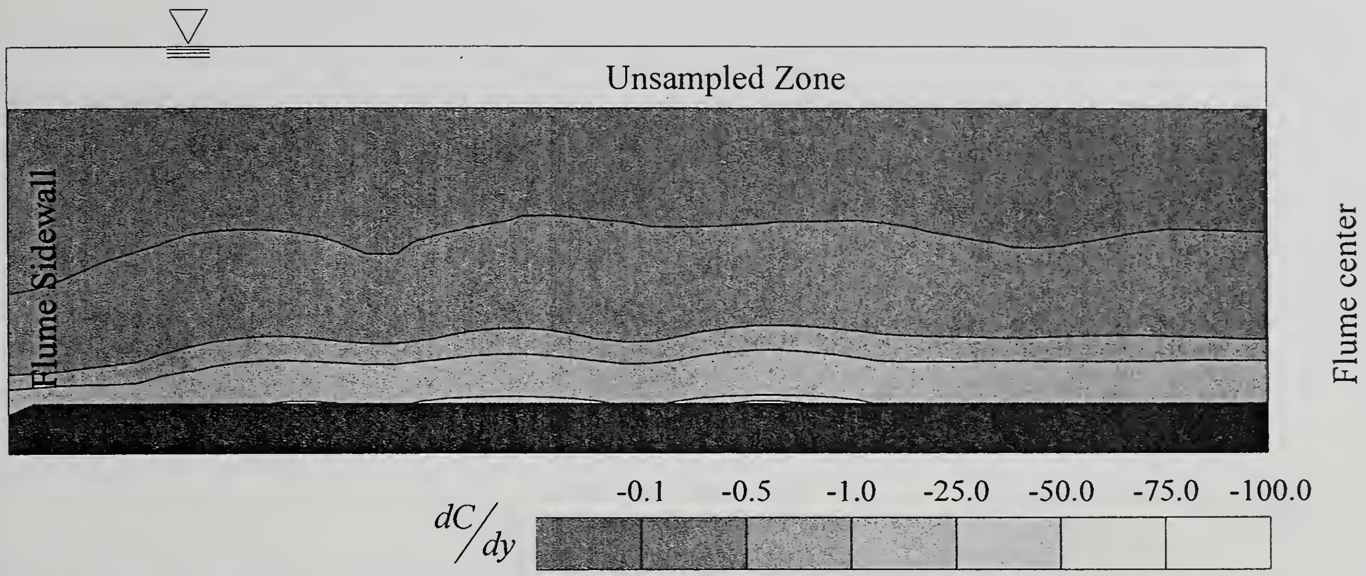

This is a map of the vertical gradient of suspended-sediment concentration.

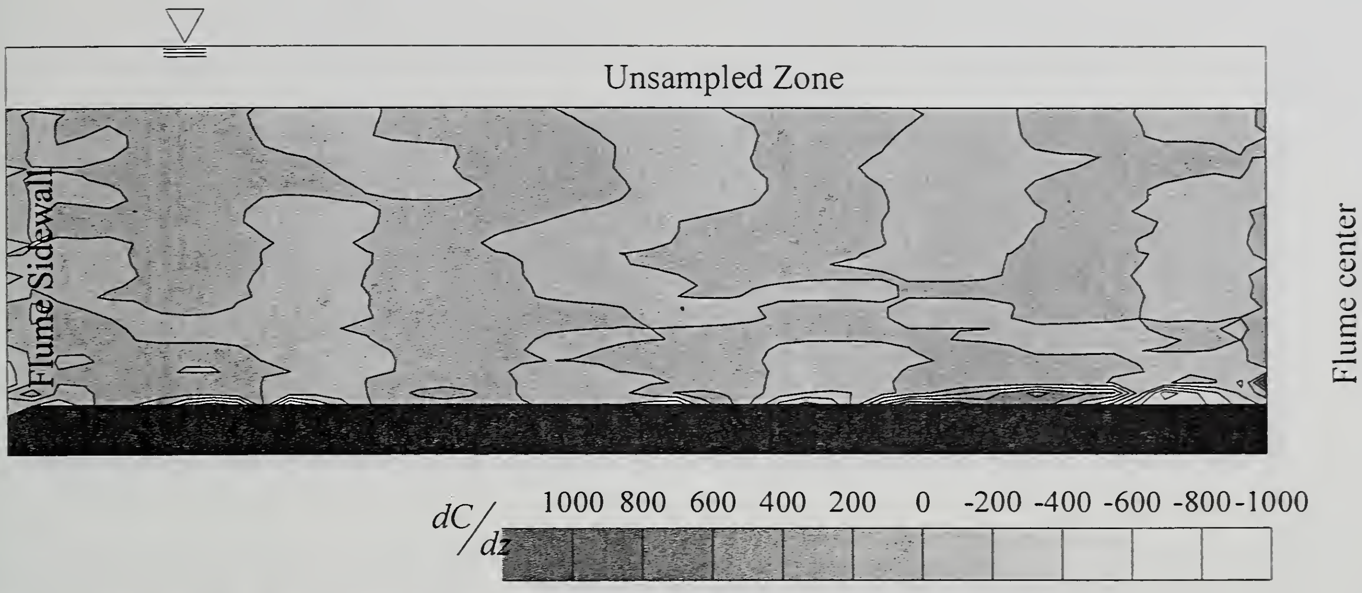

This is a map of the horizontal gradient of suspended-sediment concentration.

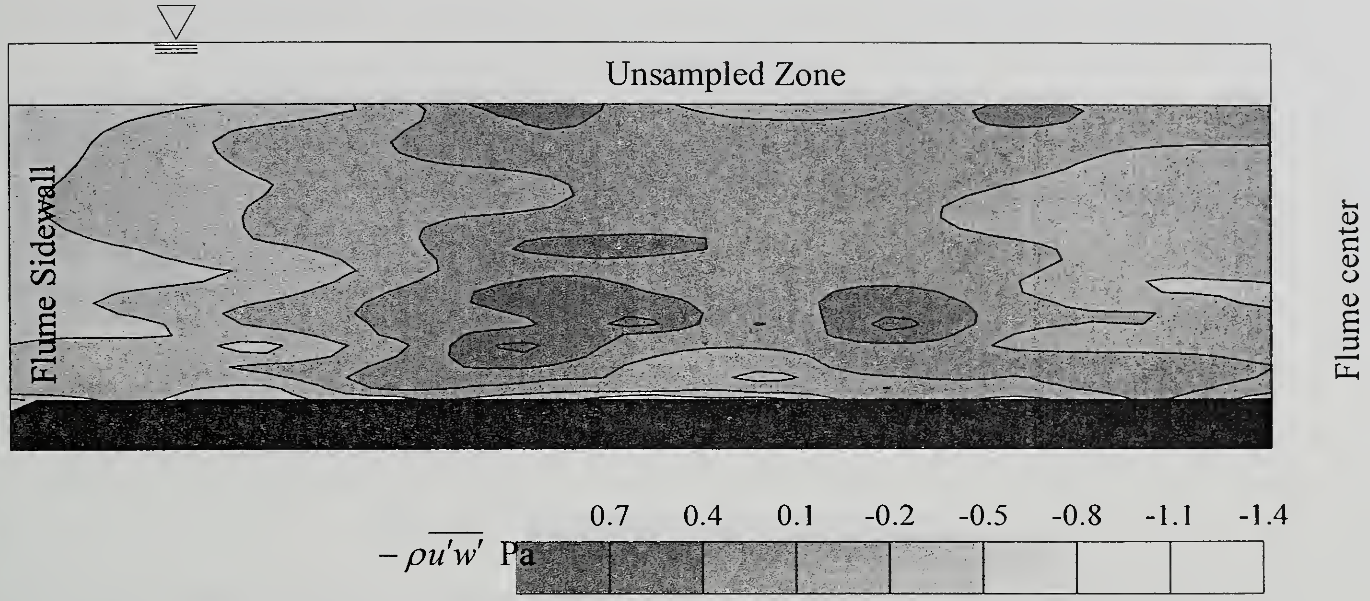

This is a map of the cross stream downstream Reynolds stress.

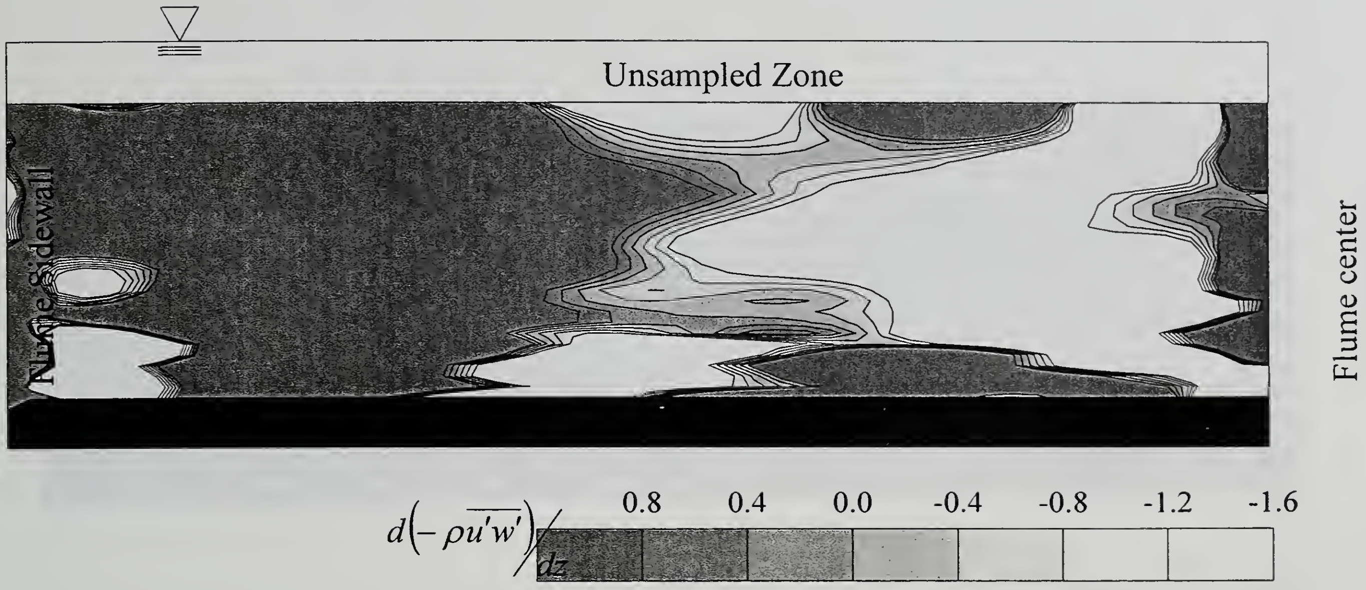

This is a map of the horizontal gradient of the cross stream downstream Reynolds stress.

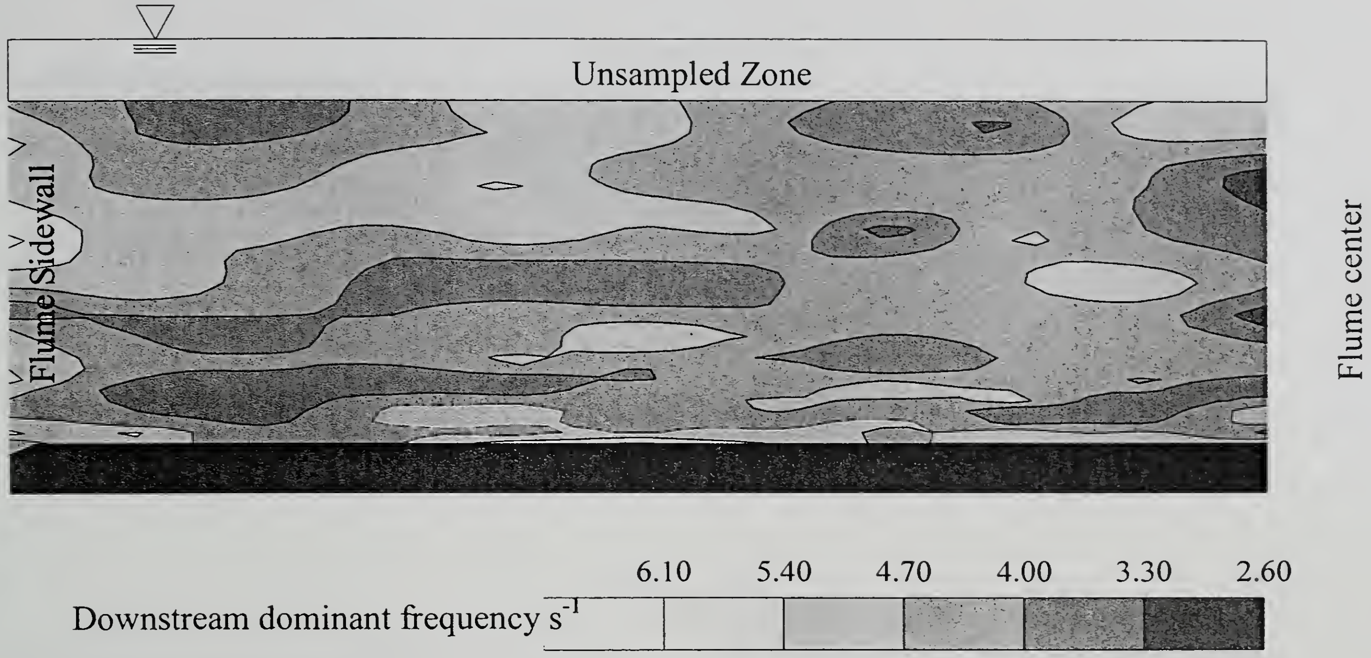

This is a map of the dominant frequency of the downstream velocity component.

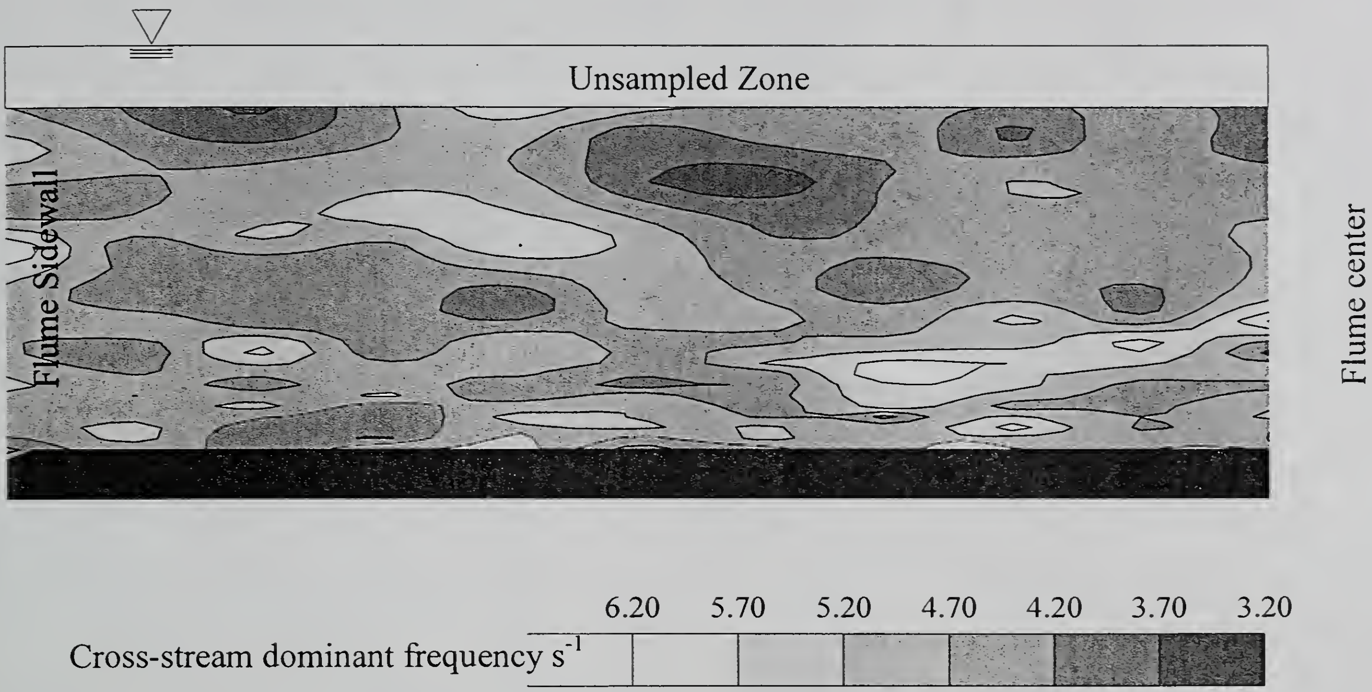

This is a map of the dominant frequency of the cross-stream velocity component.